DISSERTATION

SCFA has a preventative effect in a mouse model with relevance for age-related macular degeneration

Untersuchung zur präventiven Wirkung von SCFA in einem Mausmodell für altersbedingte Makuladegeneration

zur Erlangung des akademischen Grades
Doctor rerum medicinalium (Dr. rer. medic.)

vorgelegt der Medizinischen Fakultät
Charité – Universitätsmedizin Berlin

von

Chufan Yan

Erstbetreuung: PD Dr. Susanne Wolf

Datum der Promotion: 28. February. 2025

Table of contents

List of tables

List of figures

List of Abbreviation

AMD	Age-related macular degeneration
nAMD	Neovascular AMD
SCFAs	Short chain fatty acids
CNS	Central nerve system
CNV	Choroidal neovascularization
RPE	Retinal pigment epithelium
NFL	Nerve fiber layer
GCL	Ganglion cell layer
IPL	Inner plexiform layer
INL	Inner nuclear layer
OPL	Outer nuclear layer
ONL	Outer nuclear layer
BRB	Blood-retina barrier
oBRB	Outer blood-retina barrier
iBRB	Inner blood-retina barrier
AREDS	Age-Related Eye Disease Study
VEGF-A	Anti-vascular endothelial growth factor-A
LPS	Lipopolysaccharide
TNFα	necrosis factor-α
FFAR2	free fatty acid receptor 2

FFAR3	free fatty acid receptor 3
GPR43	G protein-coupled receptor 43
GPR41	G protein-coupled receptor 41
HDACs	histone deacetylases
DR	diabetic retinopathy
PBS	phosphate-buffered saline
TBS	tris-buffer saline
Iba1	Ionized calcium-binding adaptor molecule 1
MCC	Maximal Clique Centrality
GO	Gene ontology
OGT	O-GlcNAc transferase
AP-1	activator protein-1
CXCL10	C-X-C Motif Chemokine Ligand 10
CCL2	Chemokine (C–C motif) Ligand 2
CCL4	Chemokine (C–C motif) Ligand 4
OGA	GlcNAcase
iNOS	inducible NOS
Ca^{2+}	calcium

Zusammenfassung

Hintergrund: Die altersbedingte Makuladegeneration (AMD) ist eine der führenden Ursachen für einen Sehverlust weltweit. Die Endstadien der AMD manifestieren sich in einer chorioidalen neovaskulären (CNV) Form (nAMD) oder in der geographischen Atrophie. Gegenwärtig wird die neovaskuläre Form in der klinischen Routine mit Anti-VEGF-Medikamenten behandelt. Kurzkettige Fettsäuren (SCFAs) sind die primären Stoffwechselprodukte von Bakterien, die durch die Fermentation von Ballaststoffen entstehen. In der Literatur gibt es Belege, das SCFAs entzündlich pathologische Prozesse in der Retina und zentralen Nervensystem (ZNS) abmildern können und somit potenziell auch eine ergänzende Behandlungsmethode für die Therapie der Netzhautdegenerationen darstellen. Diese Studie zielt darauf ab, die Auswirkungen von SCFAs in einem laserinduzierten CNV-Mausmodell zu untersuchen, das Relevanz zur nAMD aufweist.

Methoden: In einer interventionellen Studie wurden die Effekte SCFAs auf die chorioidale Neovaskularisation im Mausmodell der Laser-induzierten CNV in vivo untersucht: Laserläsionen wurden mittels Fluoreszeinangiographie visualisiert und quantifiziert. Narbenbildung, zelluläre lokale Inflammation, und Müllerzellreaktion wurden mittels Immunfluoreszenzfärbung analysiert. RNAseq Technologien dienten der Beschreibung der differentiellen Genexpression. Um der Hypothese der vornehmlichen Wirkung der SCFA auf Mikrogliazellen an der lokalen zellulären Entzündung zu prüfen, wurden die Signalwege der SCFA (Ca2+Signaling, O-GlcAcylierung) unter TNFα Stimulation an primär kultivierten Mikrogliazellen und deren Konsequenzen auf die Mikrogliafunktion (Phagozytose, Sekretion, Aktivierungszustand) untersucht.

Ergebnisse: SCFAs haben in vivo eine schützende Wirkung im Modell der Laser-induzierten Neovaskularisation; sowohl bei männlichen als auch bei weiblichen Mäusen. SCFAs reduzierten SCFAs die Größe der Laserläsion, regulierten vaskulär-bezogene biologische Prozesse, verminderten die Expression entzündungsbedingter Gene und verringerten die Aktivierung [SO1] [X2] von Mikroglia, wobei der Effekt bei männlichen Tieren ausgeprägter war. Bei weiblichen Tieren verminderten SCFAs das Volumen der choroidalen Laserläsion und die Müllerzellgliose. Darüber hinaus unterdrückten SCFAs die Sekretion entzündlicher Zytokine und die Phagozytose in primären Mikrogliazellen, die

von männlichen Tieren stammten und hemmten die O-GlcNAcylierung in der entsprechenden weiblichen Kohorte.

Fazit: Der Interventionsversuch zeigte die Abschwächung vaskulärer Aktivität sowie Entzündung im Mausmodell der Laser-induzierten CNV mit Relevanz zur nAMD, was durch in vitro Untersuchungen zur zellulären Entzündung unterstützt wird.

Abstract

Background: Age-related macular degeneration (AMD) stands as a primary cause of global vision impairment, presenting in advanced stages as either neovascular AMD (nAMD) or geographic atrophy. In clinical routine, nAMD is treated by anti-VEGF drugs. Short-chain fatty acids (SCFAs) are the primary bacterial metabolites produced by the fermentation of dietary fiber. The application of SCFAs demonstrated the potential in alleviating inflammation in retina and central nerve system (CNS), suggesting a supplementary role in nAMD treatment. This study aimed to assess the impact of SCFAs in a mouse model of laser-induced choroidal neovascularization (CNV) with properties of nAMD alongside exploring SCFA effects on microglial cells *in vitro*.

Methods: An interventional study was conducted to evaluate SCFA effects in the mouse model of laser-induced CNV by means of fluorescein angiography, while volume of new blood vessels, microglia density, and GFAP expression in Müller cells were examined using immunofluorescence microscopy. RNA sequencing was employed to characterize differential gene expression. Primary microglial cells, isolated from neonatal mouse cortex, were exposed to TNFα to simulate pathological conditions and effects of SCFA on microglia function were assessed by inflammatory cytokine secretion and phagocytic activity. The underlying pathways were elucidated through quantification O-GlcNAcylation and calcium imaging.

Results: SCFAs have a protective effect in a mouse model of nAMD in both male and female. SCFAs mitigated laser lesion size, modulated vascular – related biological process, dampened inflammatory gene expression, and decreased microglial activation with a more pronounced effect in males. In females, SCFAs reduced volume of choroidal laser lesion and Müller cell gliosis. Additionally, SCFAs suppressed inflammatory cytokine secretion and microglial phagocytosis in primary microglia derived from male, and inhibited O-GlcNAcylation in the corresponding female cohort.

Conclusion: Overall, SCFA treatment demonstrated attenuation of vascularization and inflammation in a mouse model representative of nAMD.

1. Introduction

1.1 Cell population and structure of retina

Vision starts in the retina, the light-sensitive structure of the eye. It captures light and converts it into neural signals that can be interpreted by the brain. The retina consists of two parts: the retinal pigment epithelium (RPE) closely adjacent to the choroid, and the neuroretina between the vitreous body and RPE(Grossniklaus et al., 2015).

The neuroretina consists of 9 major cell types that contribute to its 6-layer structure. The axons of the ganglion cells comprise the majority of the nerve fiber layer (NFL), which is the innermost layer of the neuroretina. The ganglion cell layer (GCL) is primarily composed of ganglion cell nuclei. Synapses of ganglion cells connect with amacrine cells and bipolar cells in the inner plexiform layer (IPL). The nuclei of amacrine cells, bipolar cells and horizontal cells are in the inner nuclear layer (INL). Horizontal cells in the outer plexiform layer (OPL) modulate synaptic transmission between the rod/cone photoreceptors and bipolar cells. The outer nuclear layer (ONL) consists of the nuclei of rod and cone photoreceptors (Grigoryan, 2022, Hoon et al., 2014).

In addition to these six types of neurons, three other major types of glial cells are present in the neuroretina. The Müller glial cells (radial glia) extend across all layers of the retina from the NFL to the ONL. Astrocytes are only localized to the NFL and GCL participating in formation of the inner retinal blood/retina barrier. Microglial cells are found at varying densities in the IPL and OPL (Vecino et al., 2016).

The blood-retina barrier (BRB) is another crucial structure in the retina comprising the outer blood-retina barrier (oBRB) and inner blood-retina barrier (iBRB). The oBRB is maintained through tight junctions of RPE cells (Strauss, 2005). In contrast, the iBRB is formed by tight-junction between endothelial cells that form the blood vessels to supply the neuroretina, with the vasculature primarily penetrating the GCL, IPL, and OPL in the neuroretina (Hormel et al., 2021).

1.2 Classification of age-related macular degeneration

The macula is a small and highly specialized region situated at the central aspect of the retina with a diameter of approximately 5.5 - 6 mm, it is essential for visual acuity and

plays a pivotal role in providing detailed and sharp vision (Knupp et al., 2000, Provis et al., 2005).

Age-related macular degeneration (AMD) is a prevalent eye disease and the leading cause of permanent visual impairment among industrialized countries. A meta-analysis estimated that the number of individuals with AMD will reach approximately 200 million by 2020 and increase to 288 million by 2040. Late-stage disease prevalence increases significantly after the age of 75 years, particularly in individuals of European descent (Wong et al., 2014). Age is the strongest risk factor related to AMD, with chronic smoking being another crucial consistently risk living habits (Velilla et al., 2013). Race, iris color, dietary, obesity, and systemic factors, for instance, cardiovascular disease are also associated with an increased risk of AMD (Thomas et al., 2021, Lambert et al., 2016). While some studies have found that gender difference is not a significant risk factor for the development of AMD, other research suggest that AMD's prevalence and clinical manifestations may vary between male and female individuals (Rudnicka et al., 2012, Marin et al., 2022); epidemiological analysis reported a higher risk of AMD in females compared to males (Clemons et al., 2005, Hallak et al., 2019). This discrepancy may be attributed to sex hormones, as evidenced by the heightened risk observed in women nearing menopause (Vingerling et al., 1995), and the protective effect provided by hormone replacement therapy (Fraser-Bell et al., 2006).

The classification of AMD varies among studies and is mainly based on the size of the drusen and pigmentary abnormalities. Traditional clinical classifications, such as the Age-Related Eye Disease Study (AREDS) severity scale (Davis et al., 2005) and its simplified version (Ferris et al., 2005), have been established and used clinically, while new severity scales developed separately by Beckman (Ferris et al., 2013) and the Three-Continent AMD Consortium (Klein et al., 2014). While the definition of early and intermediate AMD may vary among studies, the definitions of late AMD remain consistent, characterized by pigment abnormalities in both eyes with large drusen sizes (>125μm), RPE pigmentary abnormalities, neovascularization and/or geographic atrophy (Ferris et al., 2013).

Late AMD can manifest as either the atrophic form (dry form) or the neovascular form (wet form). Atrophic AMD, also known as geographic atrophy, involves the progressive loss of the RPE, adjacent photoreceptors, and choriocapillaris, with non-neovascular

changes in the same eyes. Atrophic AMD can progress over the course of years(Keenan et al., 2018, Bird et al., 2014).

Neovascular age-related macular degeneration (nAMD) typically progresses more rapidly over weeks and months, and accounts for majority of blindness secondary to AMD (Bakri et al., 2019). As the name suggests, neovascularization is a key property of nAMD. Capillaries originate from the choroid, extend through the Bruch's membrane, and penetrate into the subretinal area, leading to the formation of disciform scars (Green and Enger, 1993). Anti-vascular endothelial growth factor-A (VEGF-A) therapy has been established as clinical routine to treat nAMD, given the critical role of the VEGF-VEGFR system in the angiogenesis process during AMD development (Papadopoulos, 2020, Pozarowska and Pozarowski, 2016).

1.3 Role of inflammation in nAMD

1.3.1 An overview of inflammation in nAMD

AMD is associated with local chronic inflammation. Aging and other disease risk factors disrupt the equilibrium between para-inflammation related tissue repair and stress-induced cell damage (Xu et al., 2009). Early AMD is characterized by the appearance of drusen (deposition of extracellular debris between Bruch's membrane and the RPE) and changes in pigmentation. In contrast, advanced nAMD is characterized by choroidal neovascularization (CNV) and the growth of new vessels from the choroid that infiltrate the retina, leading to hemorrhage, retinal detachment, and disciform scars, along with the damage or death of photoreceptors and retinal epithelial cells (Donoso et al., 2006, Ambati and Fowler, 2012). Thus, these observations result in the hypothesis that the inability to fully repair and restore functional tissues results in a prolonged inflammatory state that ultimately progresses to a diseased state.

AMD is associated with an overactivity of the complement system (Zipfel et al., 2010). The complement system is a crucial element of innate immunity, playing a key role in immune surveillance, neuroprotection, cellular debris removal, and organ regeneration (Zipfel and Skerka, 2009). Multiple complement components, complement activation products and inflammatory proteins have been identified in drusen, including terminal complement complexes (Anderson et al., 2002). The concentration of the terminal complement complex in the plasma of patients with nAMD was found to be five times higher

compared to healthy age-matched subjects (Busch et al., 2023), suggesting an up-regulation of the complement level during the development of AMD, potentially influenced by factors such as oxidative stress, lipid accumulation, and energy metabolism (Armento et al., 2021).

The RPE is a monolayer of cells located between the photoreceptors and choroid. It plays an important role in the formation of the oBRB (Cunha-Vaz, 1976) and secretion of inflammatory cytokines (Cao et al., 2013, Holtkamp et al., 2001, Zamiri et al., 2006). This contributes to the establishment of ocular immune privilege. Cell models that simulate inflammatory retinal conditions by stimulating the RPE cells with lipopolysaccharide (LPS) or tumor necrosis factor-α (TNFα) have shown an increase in inflammatory cytokine production and higher expression levels of cytokine receptors (Cheng et al., 2019, Leung et al., 2009), subsequently promoting the production of VEGF-A (Nagineni et al., 2012), which destabilize the choroidal endothelial cells (Ved et al., 2017, Zamiri et al., 2007), as pre-requisite for neovascularization from the choroid to the retina. This can result in blood leakage from these new undifferentiated vessels, causing dysfunction of the retina and acute vision loss (Shibuya, 2011, Kauppinen et al., 2016).

1.3.2 Role of microglial cells in retinal inflammation

In addition to the complement system and RPE cells, other immune cells also play a crucial role in the pathology of retinal inflammation and AMD. Microglial cells, represent the resident immune cells in the retina, which serve important function to maintain the structural integrity of the retina, actively participate in degenerative processes in retinal disease (Thanos, 1991). Microglial cells are primarily located in the IPL and OPL in proximity to the blood vessel plexus (Silverman and Wong, 2018). These cells play a crucial role in modulating inflammation, as evidenced by their accumulation in various regions of the retina and subretinal space in human eyes obtained from patients with AMD, particularly in close proximity to choroidal neovascularization areas (Combadiere et al., 2007, Lad et al., 2015).

Retinal microglial cells crosstalk with multiple types of retinal cells. Various soluble factors secreted by RPE cells, Müller cells or neuronal cells inhibit microglia from tissue damaging activation (Rashid et al., 2019), while the excessive secretion of pro-inflammatory cytokines by microglia under pathological conditions results in further inflammation and

worsens vascular damage (Kinuthia et al., 2020). Drusen accumulation is a prominent stimulus for retinal microglia, leading to their translocation to the subretinal area (Lyons and Brown, 2001, Indaram et al., 2015). *In vitro* experiments show that exposure to RPE cell debris (ARPE-19) induces an inflammatory response in microglia (Madeira et al., 2018). Conversely, the activation of retinal epithelial cells (ARPE-19 cell line) with supernatant from stimulated human iPS - derived microglial cells and other monocytes led to disorganization of cytoskeletal structure, lipid deposits accumulation, and increased expression of inflammatory cytokines, such as IL-6, IL-8, IL-1β, GM-CSF and CCL-2 (Nebel et al., 2017). These findings further suggest the interaction between microglial and RPE cells.

Like brain microglial cells, retinal microglial cells also perform phagocytosis as an important function. This process can lead to “phagoptosis” (microglial phagocytosis of live neurons (Brown and Neher, 2014)) in pathological conditions. In healthy retinas, phagocytosis is responsible for the clearance of dead cells to prevent the release of cellular contents that can trigger inflammation and tissue necrosis (Thanos, 1991, Schuetz and Thanos, 2004). However, this protective effect may reverse in certain pathological conditions, such as retinitis pigmentosa. In the rd10 mouse model, microglia not only phagocytosed cellular debris but also living stressed photoreceptors through the CX3CL1-CX3CR1 signaling pathway (Zhao et al., 2015, Zabel et al., 2016). Intravitreal delivery of recombinant CX3CL1 reduced microglial activation and phagocytosis, leading to improved structural and functional characteristics compared to rd10 untreated controls (Zhao et al., 2015, Zabel et al., 2016). However, in another mouse model with retinal detachment, microglial cells migrated rapidly into the photoreceptor layer within 24 hours after injury and became phagocytic, protecting the surrounding photoreceptors from further damage (Okunuki et al., 2018). Therefore, it is important to evaluate the influence of microglial phagocytosis on a case-by-case basis, considering the distinct progression and pathological characteristics of each disease.

Another important function of microglial cells is shaping the retinal vessel architecture. In a mouse model of prematurity retinopathy, a reduction in the number of microglial cells was observed, leading to a decrease in central capillary density. Pharmacological depletion of microglia resulted in reduced vessel quantity and density, which could be reversed by reintroducing microglial cells into the system (Checchin et al., 2006).

In addition to the impact on other retinal cells, retinal microglial cell itself can release inflammatory cytokines and cause damage. For instance, exposure to hypoxia increased the release of TNFα, IL-1β, and MCP-1 from primary rat microglial cells, leading to the death of primary retinal ganglion cell (Sivakumar et al., 2011). Ischemic injury also activated retinal microglial cells and induced the expression of TNFα, IL-1β, IL-6 and TGF-β *in vivo* (Wagner et al., 2021). In summary, microglial cells contribute to retinal inflammation either by directly interacting with other retinal cells, or by releasing inflammatory cytokines that indirectly act on other cells.

1.4 Laser induced-CNV mouse model

1.4.1 Introduction of the laser-induced CNV mouse model

The mouse model used in this study is the laser-induced choroidal neovascularization mouse model.

A laser trauma model was firstly developed in rat retinas in 1979 by Ryan using photocoagulation. The laser caused damage in Bruch's membrane and led to the formation of pathological choroidal vessels infiltrating into the subretinal area (Ryan, 1979). Takao Tobe further adapted this technique for mice in 1998, introducing 3 laser burns in the posterior pole using a krypton laser. This resulted in CNV formation in 87% of burns within 2 weeks (Tobe et al., 1998). Over time, this technique was refined and has become one of the most widely used rodent models with features of nAMD. The laser can be applied in both wild type and knock-in/knock-out transgenic mice, making it suitable for evaluating the efficacy of new drugs administered systemically or intraocularly, as well as the potential drug targets (Lambert et al., 2013). For example, both intravitreal injection and oral administration of brivanib have been shown to reduce CNV area and leakage (Li et al., 2020). Orally administered lenvatinib has demonstrated similar effects (Wei et al., 2018).

Other advantages of the laser induced-CNV model include its ease of establishment and assessment within a short time course (2 weeks). Additionally, this method is considered relatively straightforward and easy for obtaining many analyzable data, as typically 3-4 laser burns are applied to each retina. There are other CNV models, for instance, subretinal injection of different drugs or proteins is another commonly used CNV model(Pennesi et al., 2012). Vectors encoding VEGF-A derived from adenovirus or adeno-associ-

ated virus are directly injected into the subretinal area, and the formation of CNV is observed from 2 to 4 weeks post-injection or from 5 weeks to 20 months post-injection, respectively(Baffi et al., 2000, Wang et al., 2003). The establishment of these models is more complex, making them less commonly used compared to the laser-induced CNV model.

While the laser-induced CNV model offers numerous benefits as mentioned above, it is important to acknowledge its limitations. The laser burns introduce acute CNV lesions, therefore, it cannot replicate the chronic, progressive nature of nAMD in human. In addition, the model does not account for age effects. Nevertheless, due to the existence of inflammation in human CNV secondary to AMD(Tatar et al., 2008, Knickelbein et al., 2015), macrophages expressing VEGF-A to promote angiogenesis, as well as tissue factors creating a scaffold for the growth of CNV complex (Grossniklaus et al., 2002), it remains a reliable model for our study.

1.4.2 Studies focus on inflammation using laser-induced CNV model

The laser-induced CNV model is utilized in drug and genetic research to evaluate mechanisms of neovascularization and has led to the understanding of the role of inflammation-related cytokines and cells in AMD-comparable neovascularization.

IL-6, a pro-inflammatory cytokine primarily produced by macrophages, exhibits increased expression at CNV lesions. Studies involving IL-6 knockout mouse have shown a reduction in the size of CNV lesions compared to wild type (Droho et al., 2021). Cytokine involvement in CNV formation can be explored not only through knockout mouse models but also via intravitreal inoculation. Administration of anti-IL-27p28 antibody and recombinant IL-27 has been employed to investigate the impact of altering IL-27 levels on CNV development. Elevation of IL-27 has been associated with decreased CNV area and suppression of VEGF-A release, while inhibition of IL-27 has shown the opposite effect (Hasegawa et al., 2012).

In addition, researchers have utilized transgenic knockout mouse models to investigate the role of macrophages in CNV. Laser induction was performed on wild type and *Ccr2*$^{-/-}$ mice (that display a lack of macrophages that derived from classical monocytes), followed by single-cell sequencing of retinal samples from both groups. One of the macrophages

clusters (Spp^{1+}) was detected to enrich and express a proangiogenic transcriptome in wild type retinas but not $Ccr2^{-/-}$, $CD11c^{+}$ (the marker expressed by the Spp^{1+} cluster) macrophage depletion resulted in a 40% reduction in CNV size, indicating a potential negative impact of macrophages on AMD progression (Droho et al., 2023a). Similar findings were reported by Jawad et al, who noted a reduction in CNV volume in knockout mice lacking scavenger receptors expressed by macrophages (Jawad et al., 2013). Nevertheless, the laser-induced CNV mouse model is highly compatible with a variety of sub-processing methods, making it a valuable tool for studying inflammation in AMD.

1.5 Roles of Short-Chain Fatty Acids

1.5.1 Definitions of SCFAs

Fermentation is defined as the anaerobic breakdown of carbohydrates and proteins by bacteria. Short-chain fatty acids (SCFAs) are the primary bacterial metabolites produced by the fermentation of dietary fiber (Cummings and Macfarlane, 1991). These fatty acids contain six or fewer carbon atoms and are abundant in the intestines and colon. SCFAs belong to a subset of saturated fatty acids. The main components are acetate (C2), propionate (C3), and butyrate (C4). Their proportions in the colon are approximately 60:20:20, and in the peripheral venous circulation, it is around 90:5:5 (Cummings et al., 1987). Butyrate is primarily utilized by colonocytes, propionate reaches the liver and is metabolized by hepatocytes, while acetate is absorbed in the liver or released into the peripheral venous system (Pomare et al., 1985). Consequently, only a small amount of the colon-derived SCFAs reaches the peripheral tissues and systemic circulation, with acetate comprising 36%, propionate 9% and butyrate 2% (Boets et al., 2015). Other SCFAs components, such as formate, caproate and valerate are produced to a lesser extent during the catabolism of branched chain-amino acids (Macfarlane and Macfarlane, 2003).

SCFAs play a crucial role in improving local gut health. For instance, influencing mucous production(A. et al., 2000), gut motility (Cherbut et al., 1997) and inhibiting tumorigenesis (Encarnacao et al., 2015) in the gastrointestinal tract. Multiple cells express the receptors for SCFAs, such as free fatty acid receptor 2 (FFAR2) (Maslowski et al., 2009, Chun et al., 2019, Schlatterer et al., 2021), and FFAR3 (Mishra et al., 2024, Ang et al., 2016, Nohr et al., 2015) (formerly named as G protein-coupled receptor 43 (GPR43) and GPR41). It has been shown, that SCFAs have an inhibitory effect on histone deacetylases (HDAC)

(Schilderink et al., 2013, Silva et al., 2018, Sanford et al., 2016) and can regulate inflammation and hormone production.

SCFAs modulate inflammation by regulating immune cells, for instance, microglial cells (Correa-Oliveira et al., 2016). Butyrate has demonstrated an anti-inflammatory effect on LPS-stimulated microglial cells isolated from rat cerebral cortices and midbrain by reducing the expression of IL-6, TNFα and nitric oxide. Similar effects were observed in hippocampal slice culture and a co-culture of microglial cells, astrocytes and cerebellar granule neurons (Huuskonen et al., 2004). Germ-free mice exhibit global defects in microglia, while administration of SCFAs in their drinking water for 4 weeks restored the microglial density, morphology, and immaturity to normal levels (Erny et al., 2015).

1.5.2 SCFAs exhibits a sex specific pattern during treatment

Sex is a significant risk factor for diseases that should be considered when exploring new treatments. For instance, the concentration of SCFAs in stool has been found to decrease in patients with Parkinson's disease in a sex-specific manner (Aho et al., 2021). Sex-based differences also exist in diarrhea- predominant irritable bowel syndrome, where a propionate-producing genus is significantly increased in males, leading to higher levels of IL-12 and colorectal visceral sensitivity. However, these phenomena are not observed in females (Sun et al., 2021).

Another study that focused on primary cortical astrocytes suggests that butyrate correlated with HDAC inhibitor pathways only in females. The study found that increasing expression of Gfap and Ahr regulated by acetate and increasing IL-22 expression regulated by propionate immune modulatory pathways, were more influenced by SCFAs in males (Spichak et al., 2021).

1.5.3 Role of SCFAs in retinal function and AMD.

Retina is the extension of the CNS. Research and discussion about the gut-brain axis has led to the recognition of communication between the gut and CNS, including its extension, giving rise to the concept of the gut-retina axis (Rowan et al., 2017). Diet is considered a significant risk factor in the development of retinal diseases, such as diabetic retinopathy (DR) and AMD. Mice fed with a high-glycemic index diet generated AMD features, while

these features were either halted or reversed when switched to low-glycemic index diet. This effect is linked to gut microbiota (Rowan et al., 2017). Oral administration of Metformin reduced the size of laser - induced CNV and the recruitment of $Iba1^+$ cells mediated by the gut microbiome. In addition, the concentration of butyrate and propionate significantly increased after Metformin treatment, suggesting that oral Metformin, apart from inhibiting glucose absorption from the gut to the blood stream, provides microbiome-dependent protection against retina laser lesions, and the role of SCFAs in this process warrants further investigation (Zhang et al., 2023).

To date, only limited studies focused on the effect of SCFAs on retina diseases including AMD. The application of butyrate has been shown to suppress neovascularization in both *in vivo* and *in vitro* experiments. *In vivo* injection of butyrate reduced CNV size(Xiao et al., 2020, Lyzogubov et al., 2020), while *in vitro* application inhibited choroid sprouting, tube formation, and proliferation(Xiao et al., 2020). Besides, existing evidence suggests that SCFAs could have beneficial effects on other retinal diseases. For example, a lipid-lowing drug, Fenofibrate, was found to ameliorated retinal inflammation induced by high-fat diet in mice, simultaneously decreased the abundances of bacteria associated with SCFAs(Wang et al., 2022). Additionally, intraperitoneal injection of SCFAs suppressed intraocular inflammation, reduced immune cell migration, and decreased inflammatory cytokines secretion. In a diabetic mouse model, butyrate was found to individually alleviate retinal thinning and improve visual function as measured by electroretinography (Huang et al., 2023). These findings present an optimistic outlook, suggesting that SCFAs may have the potential to either suppress the onset of CNV or alleviate its progression.

2 Methods

2.1 Experimental animals

C57BL/6J mice were purchased from Janvier (Cedex, France) and housed in the Charité Animal Houses. 7-12-week-old male and female mice were used in this study. Mice were provided with food pellets and water *ad libitum* and were group-housed in ventilated cages under standard laboratory conditions (12:12 h light/dark cycle with light on at 6:00 h, 22 ± 2°C, 45–60% humidity). All animal experiments complied with the guidelines of the ARVO Statement for the Use of Animals in Ophthalmic and Vision Research and were approved by the local governmental authorities (Landesamt für Gesundheit und Soziales, Berlin-Germany).

2.2 Laser induction of CNV lesion

Nine-week-old mice were subcutaneously injected with ketamine (100–120 mg/kg) (100–120 mg/kg; CP-Pharma, Germany) and xylazine (10–15 mg/kg; CP-Pharma) for anesthesia, followed by pupil dilation with phenylephrine-tropicamide eye drops (Charité, Germany). A round cover glass (15 mm) was placed on the cornea with lubricating eye drops (Methocel®, OmniVision, Germany). The images of fundus were captured with an imaging camera and laser photocoagulation was induced using an image-guided laser system (Visulas 532s, Zeiss, Germany). Four laser burn-spots at equal distances from the optic nerve were induced one by one in each eye by an Argon-laser pulse with a wavelength of 532 nm, a fixed diameter of 50 µm, duration of 100 ms, and power level of 120 mW. After that, the eyes were gently rinsed with Corneregel® (Bausch+Lomb, Germany) to protect the eyes from corneal opacification owing to dehydration. The mice were then placed in their cages with hot water bottles or a red lamp to keep them warm until they recovered from the anesthetic.

Some lesions were excluded, to allow accurate evaluation of the laser induced CNV lesions. Severe hemorrhages lead to larger CNV lesions, with outcomes that cannot be compared to non-hemorrhagic eyes. Lesions with a bleeding area diameter less than that of the lesion were considered Grade 0 for analysis. Lesions with a bleeding area diameter larger than the lesion but less than two times the lesion diameter were excluded from quantification (Grade 1). All lesions in the same eye were excluded from analysis if a

lesion bleeding area diameter was more than two times the lesion diameter (Grade 2). However, lesions that were fused with another lesion were not excluded; instead, the area is measured as a whole and then divided by the original number of lesions.

2.3 Group design

A total of male and female 154 C57BL/6J mice were randomly divided into two groups. The first group was the untreated group in which the animals received only laser induction without SCFA treatment. The second group was the SCFA group (Figure 1). SCFAs mixture including 5.54 g/L sodium acetate (S2889-250g, Sigma-Aldrich, USA), 4.4 g/L sodium butyrate (303410-100g, Sigma-Aldrich, USA), and 2.48 g/L sodium propionate (P1880-500g, Sigma-Aldrich, USA) were added to the drinking water 3 weeks before the laser lesion until the mice were euthanized, and samples were collected(Smith et al., 2013). All the animals included in this study underwent the same standardized experimental procedures. The retina and choroid were collected at 3-, 7-, and 14-days post-laser induction (dpl) from both sexes and prepared for subsequent experiments, for each experiment contained 5-8 mice per group.

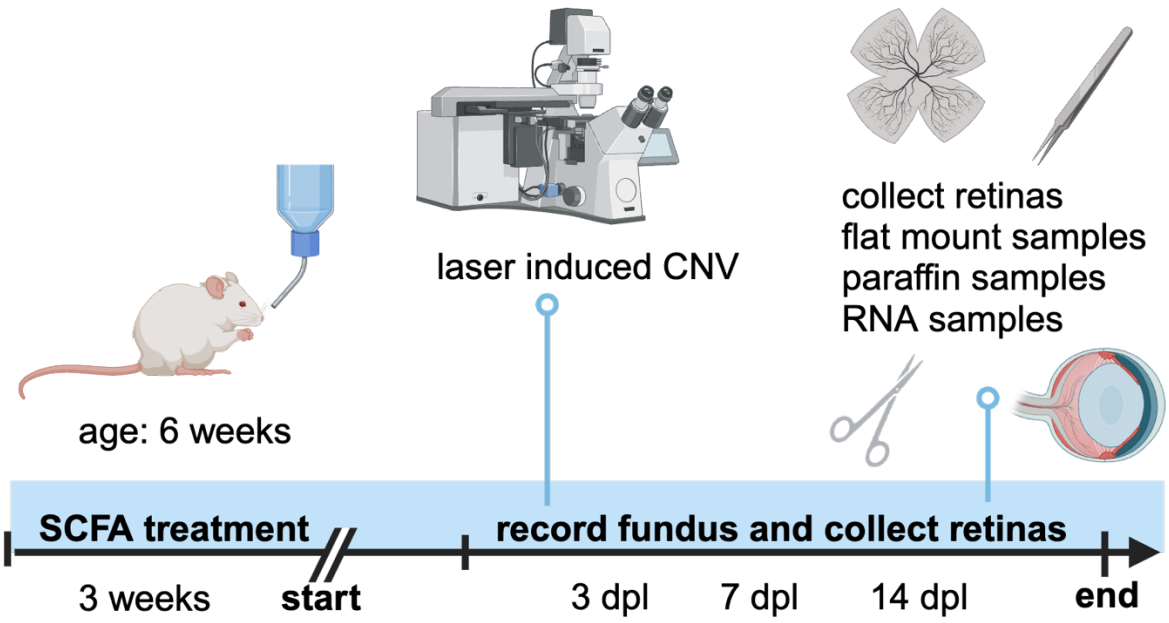

Figure 1. The experimental strategy.

2.4 Fluorescein angiography

Mice were anesthetized and their pupils dilated before being positioned horizontally on a polystyrene box attached to a head holder similar to those used in human studies. Hypofluorescence images in the infrared channel, optical coherence tomography, and blue autofluorescence images were captured using a 50º angle objective. Subsequently, mice received an intraperitoneal injection of 5 µg/g body weight of fluorescein Alcon 10% (Alcon, Germany). Fundus fluorescent angiography images were acquired 5–10 minutes post-injection using Spectralis HRA + OCT (Heidelberg Engineering, Heidelberg, Germany) and managed with Heidelberg Eye Explorer software (version 1.7.0.0). The equipment used in this experiment is designed for patients and not specific to mice. Therefore the scale only indicates the output size of the equipment and does not reflect the actual size of the mouse retina.

The extent of leakage was quantified using ImageJ software (version 2.14.0/1.54h, National Institutes of Health, USA).

2.5 Flat mount preparation

Mice were sacrificed by cervical dislocation, followed by enucleation of the eyes. The eyes were initially immersed in a 4% paraformaldehyde (PFA) solution for at least 15 min and then transferred to a phosphate-buffered saline (PBS, cat.no. 14190169, Thermo Fisher Scientific, USA) solution for further processing. The retinas and choroid were cut into four-leaf shapes under an optical microscope and gently separated from the pigmental epithelial layer. The isolated neuroretina flat mount was stored in methanol at -20°C.

2.6 Immunofluorescence staining of paraffin-embedded samples

The eyes were embedded and cut in paraffin in advance, and the paraffin section slides were stored at 25°C in the dark. A glass-rack with the paraffin section slides were introduced in a 60°C oven for at least 20min, and then the specimens were rehydrated as follows: Xylol (cat.no. CN80.1, Roche, Switzerland) 10min twice, followed by 2-propanol (cat.no.1HPH.1, Roche, Switzerland) 10min twice, after which the slides were immersed in decreasing concentrations of ethanol (96%, 90%, 70%, 50%) for 5min each. The slides were then washed in distilled water. Each paraffin section was then incubated with a drop

of proteinase K (cat.no. S3020, DAKO, Denmark) for exactly 7 min as an antigen unmasking step, followed by a 5 min wash in Tris-buffered saline (TBS). A paper towel was used to carefully remove excess liquid from the slides; a circle was drawn with a DAKO pen (DAKO, Denmark) around each section to keep them always immersed in the solution. Each section was incubated with one drop of 0.5% Triton X-100 in TBS for 10 min at 25°C for permeabilization, followed by a 10 min wash with TBS. The blocked sections were incubated with 5% bovine serum albumin (BSA, cat.no. 1ET6.3, Roche, Switzerland) in TBS for 1 h at 25°C. Next, the sections were incubated with primary antibody solution containing glial fibrillary acidic protein (GFAP) antibody (dilution 1:100, cat.no 173004, Synaptic Systems, Germany) at 4ºC overnight. On the second day, the samples were washed with TBS for 15 min, and then counterstained using AF568 goat anti-guinea pig antibody (1:4000, cat.no. A11075, Invitrogen, USA) and DAPI (3 mM, Invitrogen, USA) for 1h at 25°C. The stained sections were mounted with a DAKO mounting medium. Images were captured using a fluorescence microscope (ApoTome.2, Zeiss, Germany) and analyzed using ImageJ software (version 2.14.0/1.54h).

2.7 Immunofluorescence staining of flat-mount and choroid samples

Donkey serum 10% diluted in tris-buffer saline (TBS) was prepared as the blocking buffer and 0.5% Tween 20 in TBS as the washing buffer. The prepared retina flat mounts or choroid were transferred into 24-well plates and washed with PBS three times for 10min each at 25°C. The samples were permeabilized with 500 µl/well of 5% Triton X-100 in TBS at 25°C for 15min, followed by 1h incubation with 1% Triton X-100 in blocking buffer, in order to permeabilize and block at the same time. Subsequently, the samples were incubated with 300 µl/well anti-Iba1 antibody (dilution 1:250, cat.no. ab5076, Abcam, UK) and Isolectin GS-IB4 Alexa FluorTM 647 conjugate (dilution 1:250, cat. no. I32450, Invitrogen, USA) for 2 days at 4°C. The samples were then washed three times with washing buffer (500 µL/well) at 25°C for 10 min each. Subsequently, the samples were incubated with Alexa Fluor 488 AffiniPure™ Donkey Anti-Goat IgG (cat. no. 705-545-147, Jackson ImmunoResearch, USA), 1:200 dilution in blocking buffer, for 2 h at 4°C, followed by DAPI staining, 1:100 dilution in TBS, for 10 min at 4°C. The samples were then washed three times with TBS for 10 min each. The samples were mounted with mounting medium on glass slides, store at 4°C until the medium became dry, and then observed under a fluorescence microscope.

For choroid flat mount staining, only isolectin-AF488 (dilution 1:250, I21411, Invitrogen, USA) was used.

2.8 RNA sequencing sample preparation and data analysis.

Each RNA sample was extracted from two laser induced retinas using the RNeasy Mini kit (cat.no. 74104, Qiagen, Germany) and sent to Novogene Co, Ltd. (Munich, Germany) for RNA sequencing. Briefly, the integrity, purity and initial quantitation of RNA samples were measured using the Bioanalyzer 2100 (Agilent Technologies, USA). The Novogene NGS RNA Library Prep Set (PT042) was utilized for library construction. The constructed library was checked with Qubit 2.0 and RT-PCR for quantification. Quantified libraries were then pooled and sequenced on the Illumina Novaseq 6000 platform using a paired-end 150 strategy. The data are reported as raw read counts and fragments per kilobase of transcripts per million. DEseq2 was used to calculate the normalized read counts. Differentially expressed genes (DEGs) were identified with a fold-change >1 and adjusted p value (padj) < 0.1. Heatmaps and volcano plots were generated using the PTMCloud tools (https://www.ptm-biolab), Venn plots and bubble plots were generated using the bioinformatics platform (Tang et al., 2023). DEGs were imported into the STRING website and Cytoscape software, and hub genes were generated using the cytoHubba plugin, which was calculated using Maximal Clique Centrality (MCC). Gene Ontology (GO) terms were downloaded from the Mouse Genome Database.

2.9 RNAscope

The protocol was based on the official manual provided by ACDBio company (RNAscope™ Multiplex Fluorescent Reagent Kit v2, cat.no. 323136, ACDBio, USA). Briefly, the paraffin slides were initially baked in a 60 °C oven for 1 h, then rehydrated by immersing the slides in Xylol, 5 min twice, followed by 100% ethanol, 2 min twice at room temperature. After the sections were dried, one drop of hydrogen peroxide was added and incubated for 10 min at 25°C. The slides were washed twice with distilled water, immersed in retrieval solution provided by the kit for 15min at 99°C, and submersed in 100% ethanol for 3 min. A DAKO pen was used to create a barrier around the sections, and the sections were covered with adequate Protease Plus at 40°C for 30 min. The slides were washed twice with washing buffer for 2 min, and the sections were incubated with O-GlcNAc transferase (OGT) probe staining solution (REF. 423601, ACDBio, USA) for 2 h at 40 °C in a humid oven. A The slides were then washed twice with washing buffer

for 2 min, and immersed in 5x SSC solution at 4°C overnight. On the second day, the slides were washed with washing buffer, followed by AMP1, AMP2 and AMP3 incubations for 30 min each at 40°C. The sections were incubated with HRP-C1, followed by the addition of TSA-Fluorophor Cy3 (cat. no. SKU NEL704A001KT, Akoya Biosciences, USA) for 30 min and HRP blocker for 15 min. The slides were washed three times with TBS for 5 min each at 25°C, incubated with 1% Triton X-100+5% donkey serum in TBS for 1 h; meanwhile, the anti-Iba1 antibody solution (dilution 1:250, cat. no. ab5076, Abcam, UK) was prepared. The sections were incubated overnight at 4°C. On the third day, the slides were washed thrice with 0.5% Tween-20 in TBS for 10 min each and then incubated with the Alexa Fluor 488 AffiniPure™ Donkey Anti-Goat IgG (cat. no. 705-545-147, Jackson ImmunoResearch, USA) 1:200 dilution in blocking buffer for 2 h at 25°C. The slides were washed, dried, mounted and stored at 4°C.

2.10 Primary microglial cells isolation and culture

Cortices from male and female C57BL/6J pups (days 1–3) were collected and digested using trypsin + DNase1 to create single cell suspensions. The cells were re-suspended using 5 mL L929 supernatant + 10 mL DMEM high glucose (cat. no. 11965092, Thermo Fisher Scientific, USA), and then seeded into T75 flasks (pre-coated with poly-L-lysine for at least 30 min; cat. no. 83.3911.002, Sarstedt, Germany) for cell culture for at least 2 days. The microglial cells were shaken off using a shaker at 150 rpm, 37°C for at least 30 min, and then seeded into 12-well or 96-well plates.

Cells were divided into four groups: untreated cells; the SCFA group, with SCFAs (300 μM acetate, 20 μM propionate, and 10 μM butyrate) (Sigma-Aldrich, USA) added immediately after seeding; the TNFα group, with 10 ng/mL TNFα added 3 h after seeding; and the SCFA+TNFα group, with both SCFAs and TNFα added as described above (Figure 2).

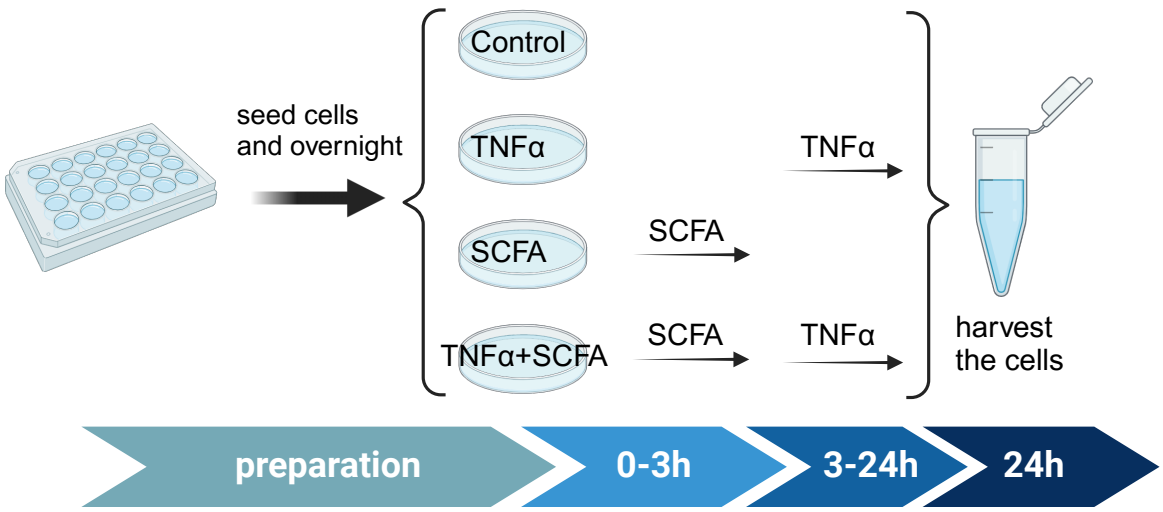

Figure 2. Group strategy of primary microglia.

2.11 ELISA

Supernatants were collected from each group of neonatal microglia that were initially seeded with 250,000 cells/well. Experiments were performed according to the manufacturer's instructions (CCL2: cat. no. DY479; CCL4: cat. no. MMB00; CXCL10: cat. no. DIP100, R&D Systems, Germany). Briefly, the 96-well plate was coated with 100 µL/well capture antibody diluted in PBS without carrier protein one day before the experiment, the plate was sealed and kept overnight at 25°C. The plate was then washed thrice with 400 µL/well wash buffer on the second day, followed by incubation with 300 µL/well reagent diluent at 25°C for at least 1 h for blocking. After washing, 100 µL of detection antibody diluted in reagent diluent was added to each well and incubated for 2 h at room temperature, followed by 20 min incubation with each of working dilution of streptavidin-HRP and substrate solution, both 100 µL/well avoiding light. Stop solution 50µL was added to each well, gently mixed and the optical density was determined immediately using a microplate reader set at 450 nm as the reader and 540 nm or 570 nm as the correction.

2.12 Calcium imaging

A total of 30,000 microglial cells were seeded in the middle of a glass coverslip and incubated in a 24-well plate one day before the experiment. E1 solution (140 mM NaCl, 5 mM KCl, 2mM $CaCl_2$, 1 mM $MgCl_2$, 10 mM HEPES and 10 mM glucose dissolved in distilled H_2O, pH=7.4) was prepared in advance, and the SCFAs mix and 10 ng/mL TNFα were

added separately. ATP 1 mM was prepared as a positive control. Then, 5.4 μg/μL Fluo-4 (cat. no. F14201, Thermo Fisher Scientific, USA) was added to cells and incubated at 37°C for at least 20 min. The activation and recording processes are outlined below:

Table 2. Calcium imaging strategy.

time	solution	concentration
0s-120s	E1	
120s-180s	TNFα or SCFA	the same concentration as primary microglial cell treatment
180s-360s	E1	
360s-420s	ATP	1mM
420s-540s	E1	

2.13 Phagocytosis monitoring using the Incucyte System.

Four groups of cells from both male and female pups were seeded into a 96-well plate. A 1:500 dilution of pHrodo™ BioParticles (1 mg/mL) (cat. no. P35361, Thermo Fisher Scientific, USA) was added 3 h after seeding. The 96-well plate was promptly placed in an incubator and monitored using the Incucyte® SX5 Live-Cell Analysis System (Sartorius, Germany). Images of each well were captured every 30 min, for 24 h, the experiments were repeated for 3 times with n=7-9.

The phase channel was utilized to identify the total cell area, while the orange channel was used to identify the phagocytosis area. The analysis was based on the percentage of phagocytosis area/ cells area.

2.14 Flow cytometry

Microglial cells were seeded in 12-well plates at 250,000 cells/well. After a 24 h incubation, the cells were dissociated using trypsin-ethylenediaminetetraacetic acid and subsequently rinsed once with PBS. Cells were stained with the LIVE/DEAD Fixable Red Dead Cell Stain Kit (L34971, Invitrogen, USA) to assess the cell viability and further stained with CD11b-PE-Cy7 (cat. no. 25-0112-82, Thermo Fisher Scientific, USA) and CD45-APC

(cat. no. 559864, BD Pharmingen, USA) antibodies to identify the microglial cells. Then, the cells were incubated in 200 µL of fixation buffer for 30 min, and the reaction was stopped by adding 150 µL of permeabilization buffer. After centrifugation, the cells were stained with O-GlcNac-fluorescein isothiocyanate (FITC) (cat. no. 53-9793-41, Invitrogen, USA) and IgG1 kappa Isotype-FITC (cat. no. 53-4714-80, Invitrogen, USA) for the experimental and negative control groups, respectively. The stained cells were re-suspended in 300 µL of FACS buffer (0.2% BSA in PBS) and maintained on ice until they were processed using flow cytometry.

2.15 Statistical analysis

All results are given as mean ± SEM. Two-way ANOVA with repeated measurement was used to analyze the leakage area. Two-way ANOVA with multiple comparison test and the unpaired t test were used for all other experimental data. Statistically significant values are indicated by asterisks in each figure.

3. Results

3.1 SCFAs treatment reduced laser leakage in retina.

In the initial phase of this study, we used a laser-induced CNV mouse model based on the C57BL/6JRj background as the Control group, and a mixture of SCFAs (5.54 g/L acetate, 4.4 g/L butyrate, and 2.48 g/L propionate) was administered in the drinking water additionally as the experimental group (SCFA group) (Smith et al., 2013). Another colleague performed the laser induction, as well as fundus fluorescein angiography (FFA) to evaluate the mean area of the laser spots.

Representative images show the area and distribution of laser spots recorded at 3-, 7- and 14 days post laser (dpl) (Figure 3). After normalized by the laser area recorded at 3 dpl, the laser area reduced gradually and significantly at 7 dpl (58%; p=0.037) and 14 dpl (51%; p=0.014) in SCFA group compared to the untreated group (Figure 4A). The leakage area in males and females were analyzed separately to further investigate potential sex differences in this shrinkage. The area decreased by approximately 60% at 7 dpl (p=0.108) and 14 dpl (p=0.037), with a statistical difference observed at 14 dpl in males. In females, the reduction was around 49% at 7 dpl (p=0.106) and 36% at 14 dpl (p=0.381), with no statistical difference noted at either timepoint (Figure 4B). The findings indicate that SCFAs treatment reduced leakage area in both sexes, with a more pronounced effect observed in males.

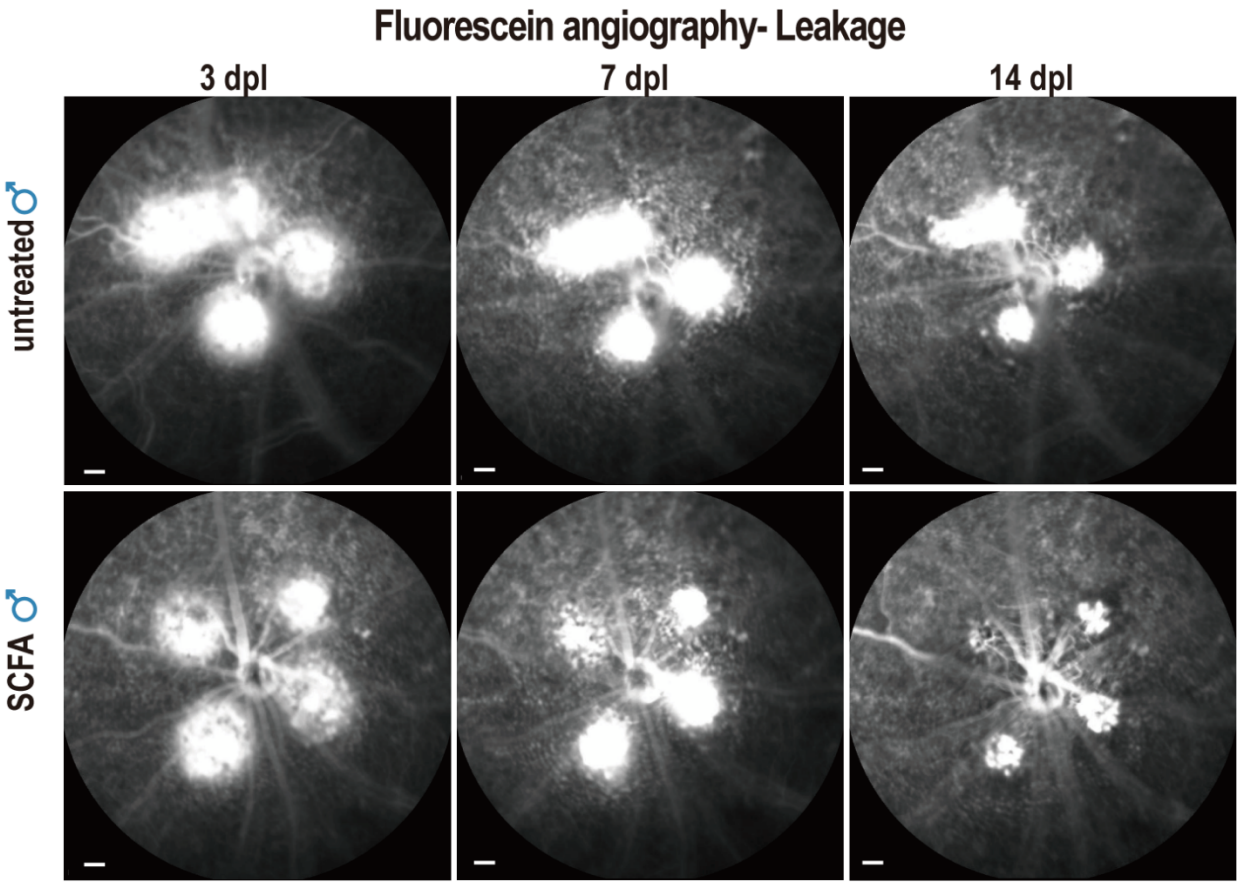

Figure 3. CNV laser-lesions from male mice, control and SCFA treated, evaluated at 3, 7, and 14 dpl. Scale bars =1mm

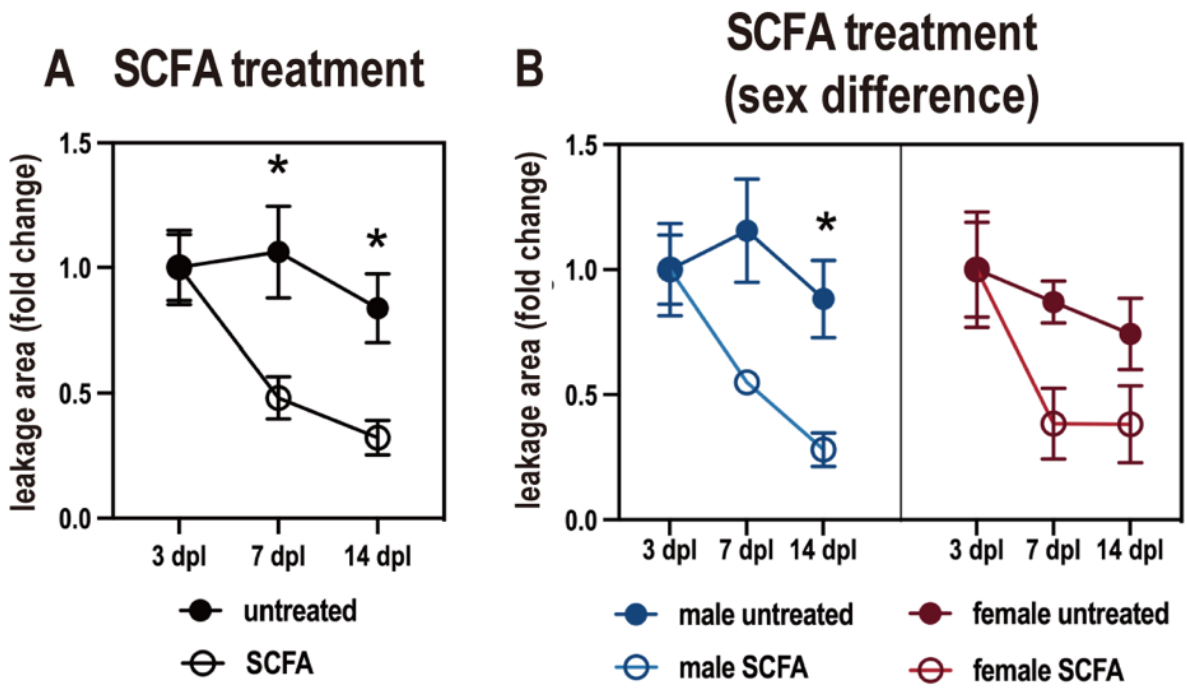

Figure 4 Quantification of laser leakage area.

(A) Time course of laser leakage area at 3dpl, 7dpl and 14 dpl normalized by 3dpl accordingly in CNV and SCFA group. Data show in mean ± SEM, n=8-12, *p<0.05 (2-way ANOVA with repeated measurements). (B). Time course of laser leakage area at 3dpl, 7dpl and 14 dpl normalized by 3dpl accordingly in CNV and SCFA group, data collected from male and female were analyzed separately. Data show in mean ± SEM, male untreated group: n=6; male SCFA group: n=4; female untreated group: n=5; female SCFA group: n=4, *p<0.05 (2-way ANOVA with repeated measurements).

3.2 SCFA treatment reduced neovascularization area in choroid.

Choroid flat mount samples were stained with isolectin B4-FITC, and the images were captured at AF-488 channel and autofluorescence channel (Figure 5). The isolectin positive area and autofluorescence area were initially calculated, with no significant difference observed between two channels. Therefore, the subsequent analysis was focused only on the autofluorescence channel. The lesion volume was defined as the sum of the autofluorescence positive area. We here focused on 14 dpl to specifically investigate the choroidal lesion at the late stage. SCFAs treatment reduced the choroidal lesion volume (Figure 6A) by around 47% (p=0.028). When considering sex as a factor, it appears that SCFAs treatment only reduced the lesion volume significantly in females by 85% (p=0.045), although the lesion volume in males appeared to reduce by 54%, there was no statistical significance (p=0.816) (Figure 6B). Our findings suggest that the effectiveness of SCFAs treatment in reducing lesion volume in choroid is stronger in females compared to males.

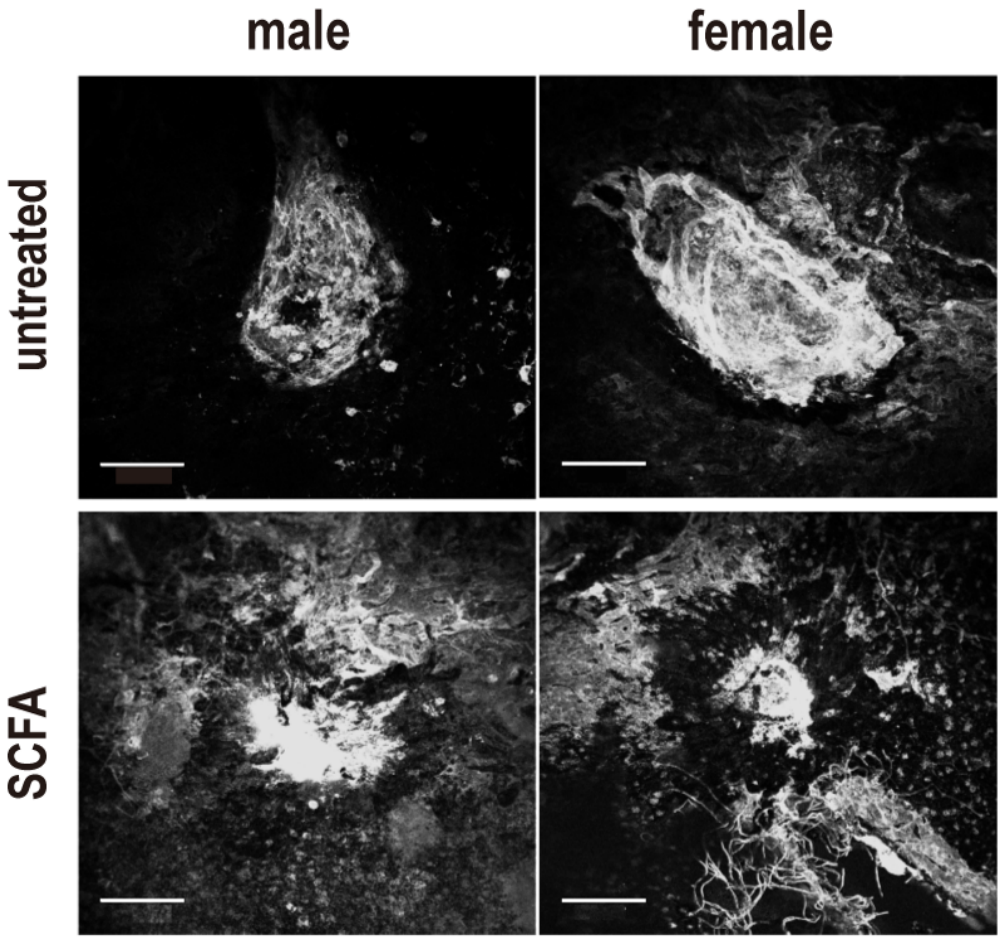

Figure 5. Representative pictures of choroidal lesions at 14dpl.

Scale bars = 100 µm.

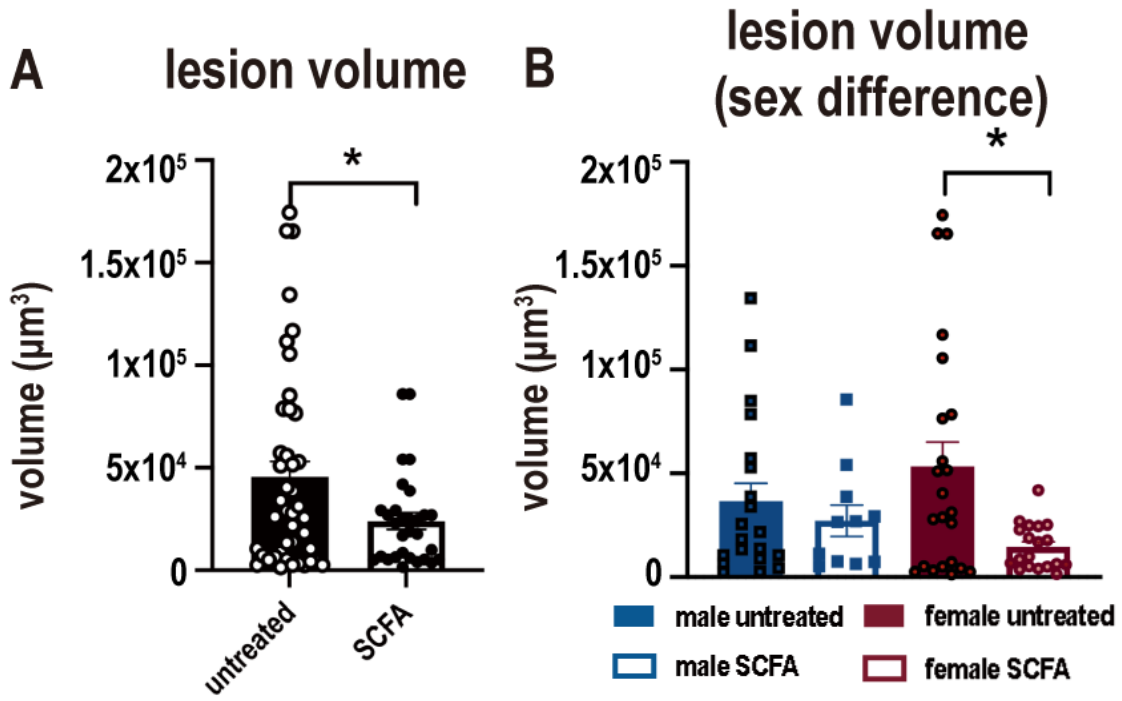

Figure 6. Quantification of choroidal lesion volume.

Lesion volume at laser spots in untreated and SCFA group. Lesion volume was assessed as volume of auto-fluorescent area of the laser spots. (A)all samples, unpaired t test (B) sex difference, 2-way ANOVA with multiple comparison. Data shown as mean ± SEM, male untreated group: n=21; male SCFA group: n=11; female untreated group: n=26; female SCFA group: n=19, *p<0.05.

3.3 SCFAs treatment reduced Müller cell gliosis in neuroretina.

Müller cells typically do not express GFAP under physiological conditions but upregulate it under pathological conditions (Eisenfeld et al., 1984, Nurnberg et al., 2018). While Astrocytes express GFAP under physiological conditions, they also upregulate the expression in pathologies. Upregulation of GFAP is often regarded as gliosis. Therefore, immunofluorescence staining was conducted to assess the impact of SCFAs treatment on GFAP expression (Figure 7). The expression of GFAP (Figure 8A) notably decreased following SCFA treatment on 14 dpl (p=0.007). When male and female subjects were analyzed separately, the expression of GFAP in the SCFA group was down regulated comparing to the untreated group statistically significant only in females (p=0.0371) while there is only a trend visible in males (Figure 8B). Taken together with the scar volume data, gliosis is prevented by SCFA in females much stronger and significant compared to males.

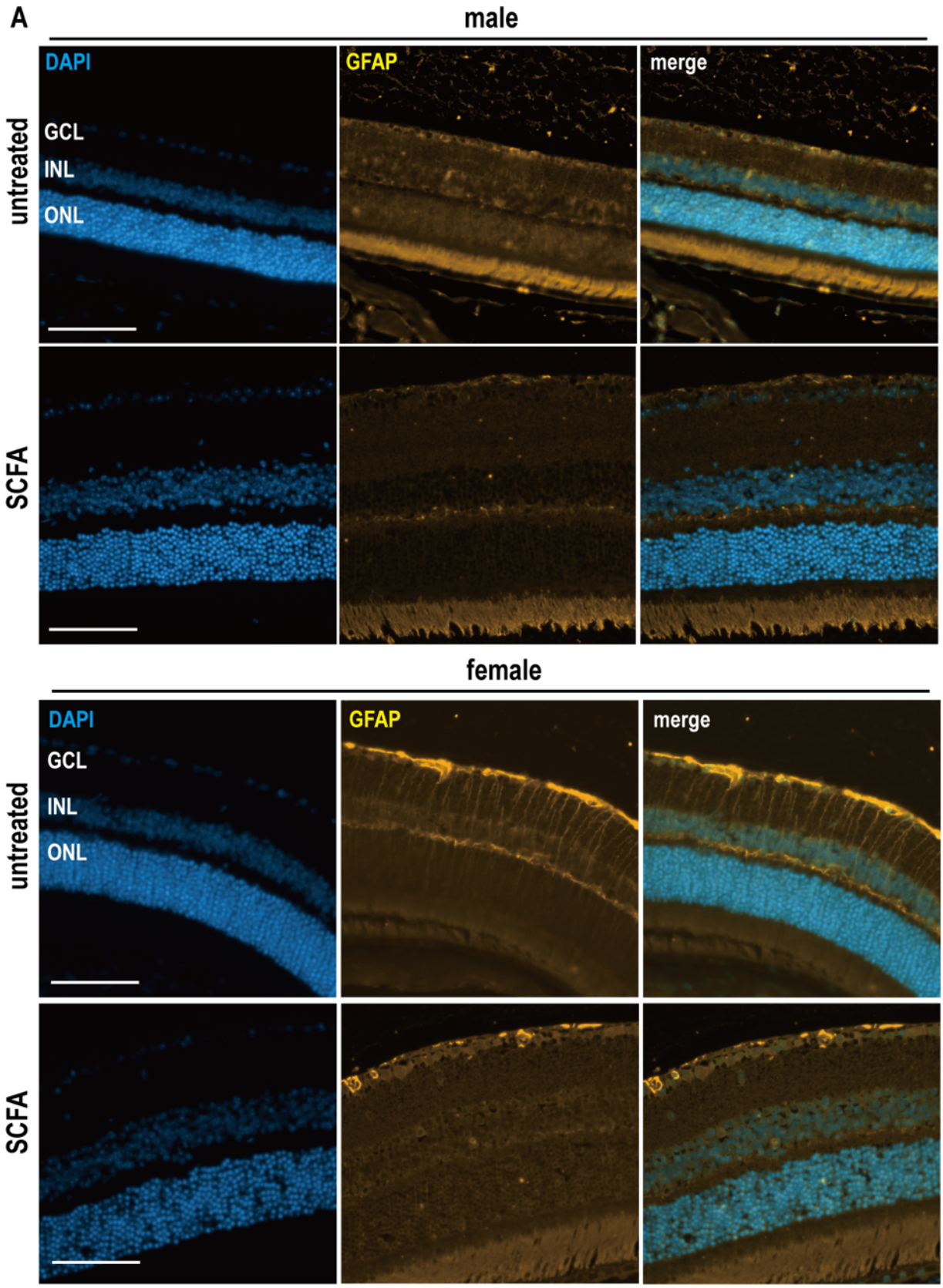

Figure 7. Representative images of GFAP and DAPI staining in retina.

Scale bars = 100 μm

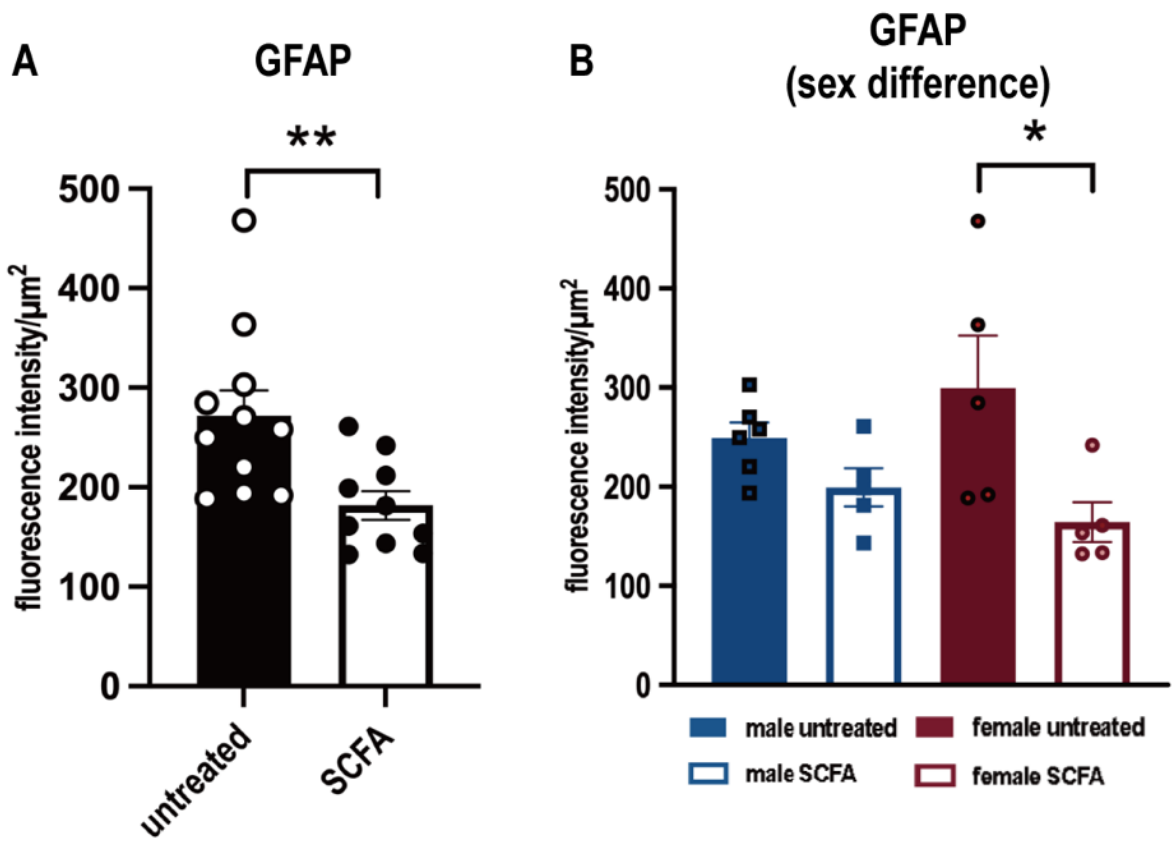

Figure 8. Quantification of GFAP expression.

Fluorescence intensity density of GFAP in CNV and SCFA group, (A) all samples, unpaired t test; (B) sex difference, 2-way ANOVA with multiple comparison. Data were shown as mean ± SEM, male untreated group: n=6; male SCFA group: n=4; female untreated group: n=5; female SCFA group: n=5. *p<0.05, **p<0.01.

3.4 SCFAs treatment reduced microglial density and activation.

3.4.1 SCFAs treatment reduced microglial density at laser spots.

Microglial cells in retina flat mount were stained with Iba1 to evaluate changes in density and morphology after SCFAs treatment. Isolectin B4 stained vessels and was utilized to identify the IPL and OPL.

Figure 9 shows representative images of microglial distribution at laser spots on day 7. Due to difficulties in identifying distinct and clear laser spots at 14 dpl in the images (scar formation stage), I analyzed the images from 3 dpl and 7 dpl in this study. At 3 dpl, no difference was detected in the density of microglia after SCFAs treatment in both sexes. At 7 dpl, the microglial density increased by CNV. This increase was prevented by SCFAs treatment at the laser spots (p<0.0001) (Figure 10A). When analyzed separately by sex,

SCFAs treatment led to a significant reduction of microglia in both males ($p<0.0001$) and females ($p=0.005$) (Figure 10B).

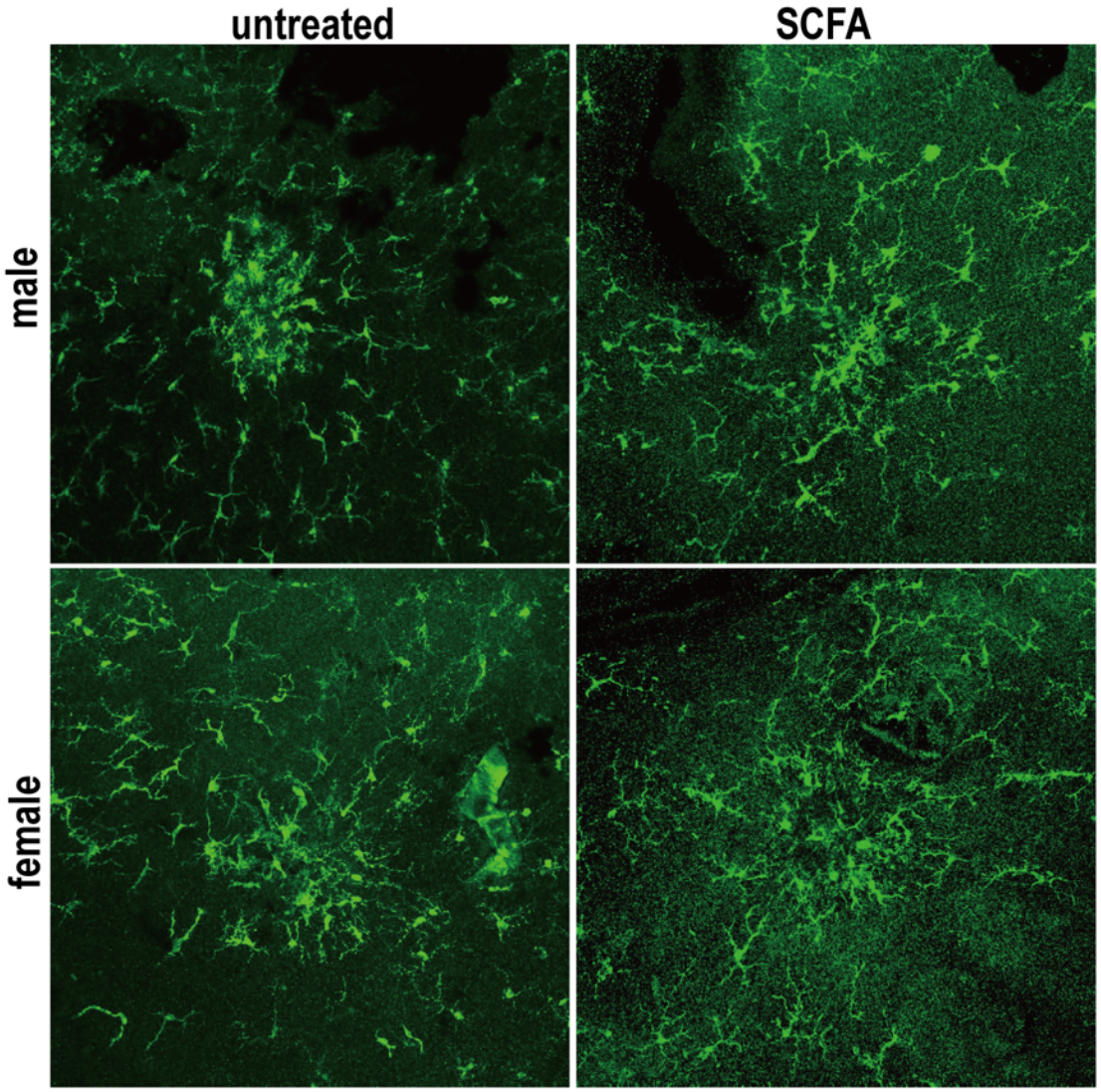

Figure 9. Representative images of Iba+ cells (green) at laser spots in CNV and SCFA group on day 7.

The images from male and female were shown separately. Scale bars = 100 μm.

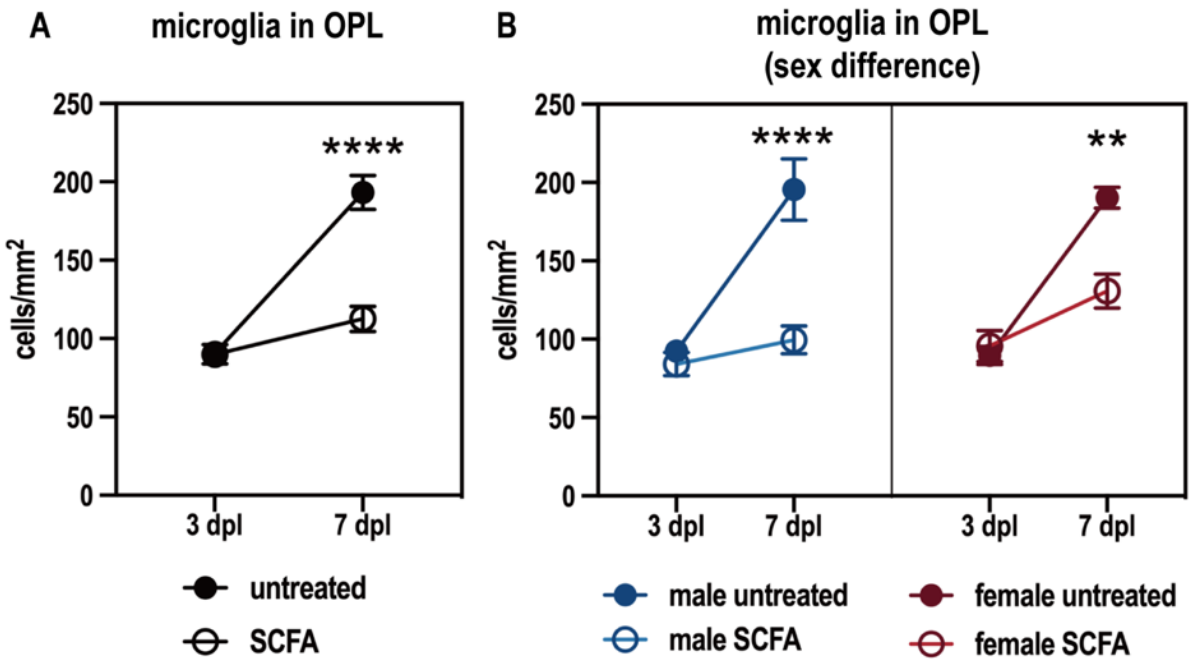

Figure 10. Statistical analysis of microglial density at laser spots on 7 days.

The density of microglia in untreated and SCFA group in OPL were analyzed, (A) all samples; (B) sex difference. Data were shown as mean ± SEM. At 3 dpl, male untreated group: n=4; male SCFA group: n=4; female untreated group: n=7; female SCFA group: n=6. At 7 dpl, male untreated group: n=5; male SCFA group: n=7; female untreated group: n=4; female SCFA group: n=5, per groups, **p*<0.05, ****p*<0.001, 2-Way ANOVA with multiple comparation.

3.4.2 SCFAs treatment reduced microglial density near laser spots.

Figure 11 displays representative images depicting the staining of microglial cells in the retina, predominantly concentrated in the IPL and OPL, corresponding to the thin vessel layer and thick vessel layer, respectively. The density of Iba1$^+$ cells increased at 3dpl and decreased at 7 dpl after SCFAs treatment in both IPL and OPL (Figure 12A and C). When analyzed separately by sex, it was observed that SCFAs treatment reduced the number of Iba1$^+$ cells at 7 dpl in both layers and OPL at 14 dpl in males. Conversely, no similar results were observed in females. SCFAs treatment increased Iba1$^+$ cells density at 3 dpl in both layers but did not have an effect on 7 dpl and 14dpl (Figure 12B and D).

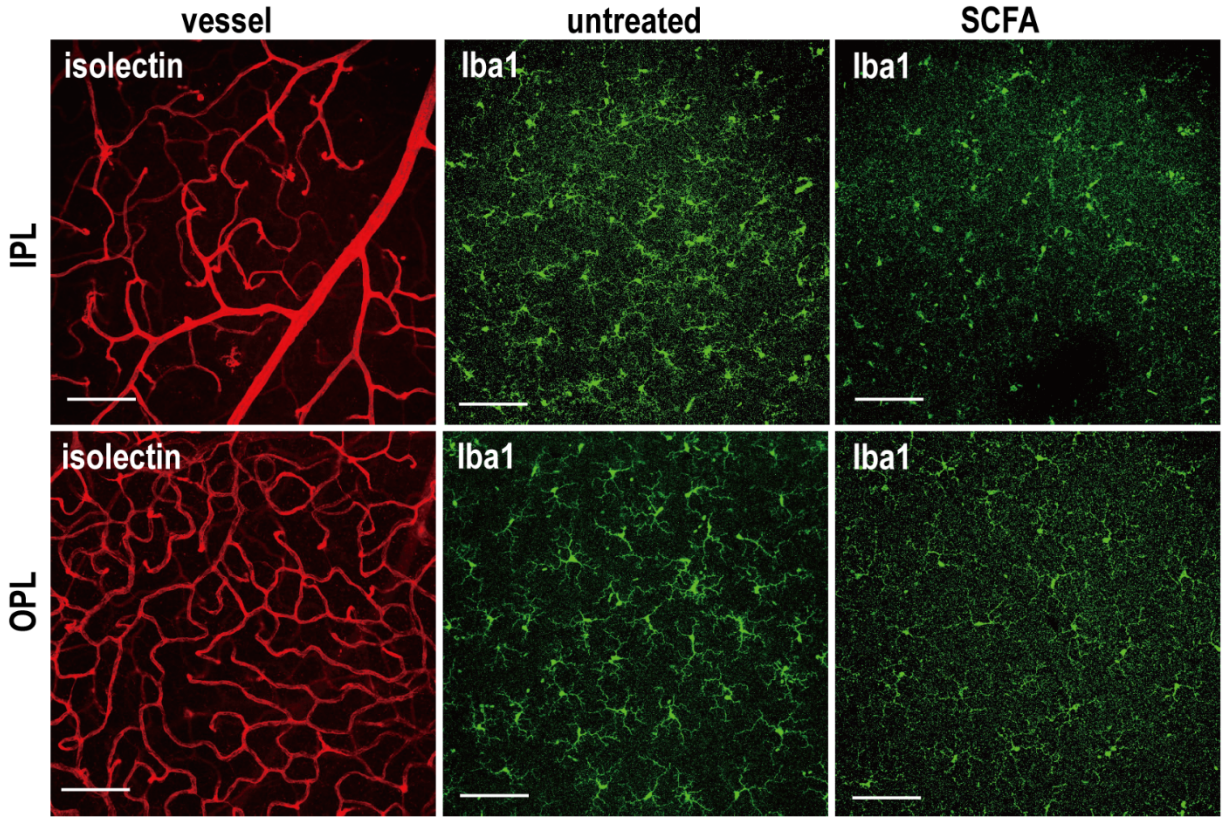

Figure 11. Graphical illustration of Iba1^{+} cells in retina.

Immunofluorescence staining of retina flat mount. Blood vessels were labeled by Isolectin (red), With thin vessels indicating IPL, thick vessels indicating the OPL). Iba1 (green) was used to stain microglial cells. The scale bar is set at 100μm.

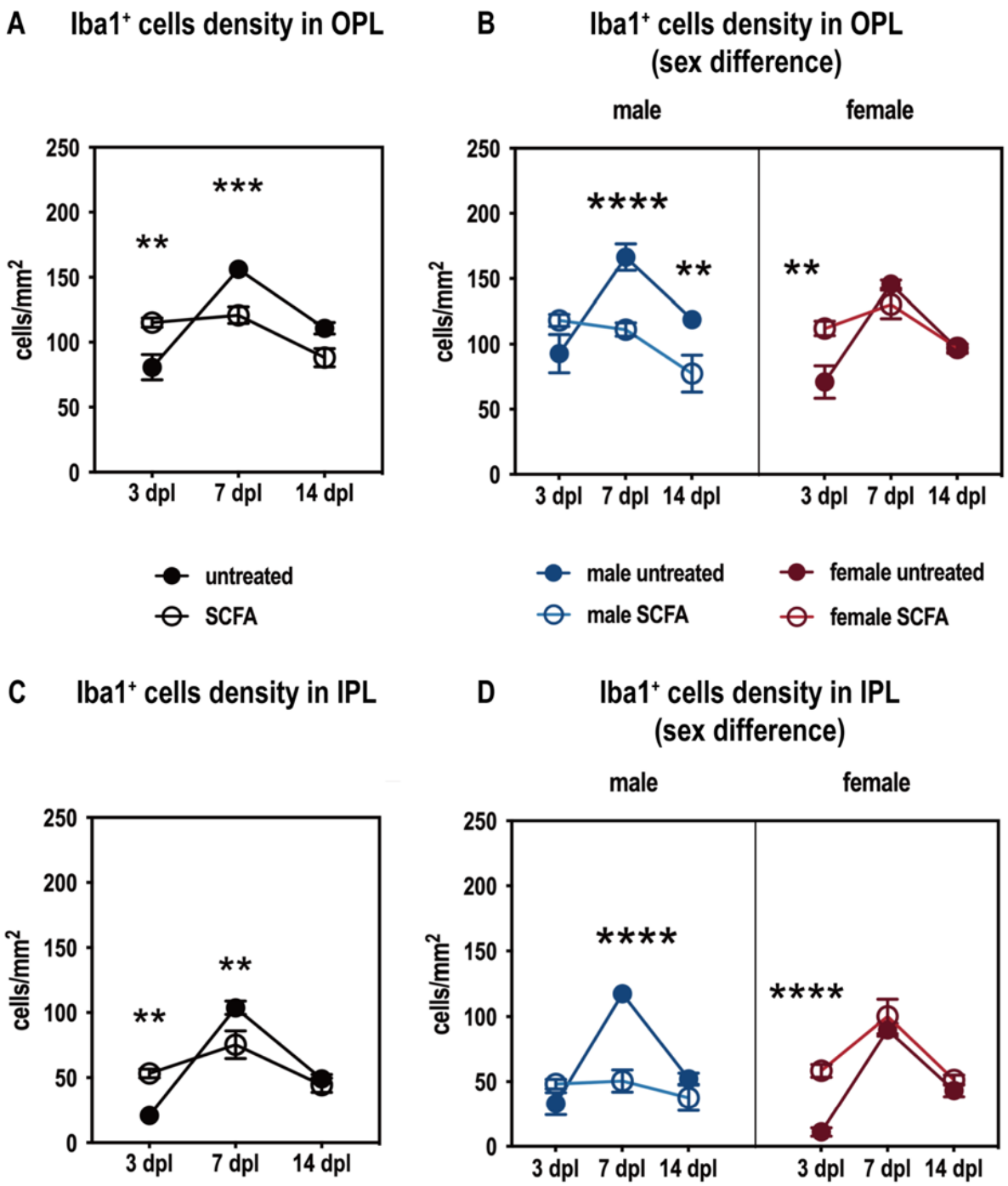

Figure 12. Statistical analysis of Iba1$^+$ cells density.

Iba1$^+$ cell density in OPL at 3 dpl, 7 dpl and 14 dpl, (A) all samples; (B) sex difference. The data were represented as mean ± SEM. At 3 dpl, male untreated group: n=5; male SCFA group: n=5; female untreated group: n=6; female SCFA group: n=5. At 7 dpl, male untreated group: n=7; male SCFA group: n=6, female untreated group: n=7; female SCFA group: n=6. At 14 dpl, male untreated group: n=7; male SCFA group: n=5, female untreated group: n=4; female SCFA group: n=6 **p< 0.01; ***p< 0.001; ****p<0.0001, 2-way ANOVA with multiple comparison test. Iba1$^+$ cell

density in IPL at 3 dpl, 7 dpl and 14 dpl, (C) all samples; (D) sex difference. The number of n and the statistical method were the same as OPL.

SCFAs treatment not only influence the microglial density, but also affects the microglial morphology. The microglial branch, soma, and branch length were defined as shown in Figure 13. Retinal microglial cells in the OPL displayed a more ramified morphology after SCFAs treatment at 7 dpl, characterized by an increase in both the average number of branches ($p=0.001$) and the length of branches ($p=0.004$) (figure 14A and C). Sex–specific analysis revealed that SCFAs treatment induced these changes in both males and females, but with different extent (Figure 14B and D). The statistically significant increase in the average number of branches observed only in males ($p=0.027$), and a statistically significant increase in branch length observed only in females ($p<0.001$).

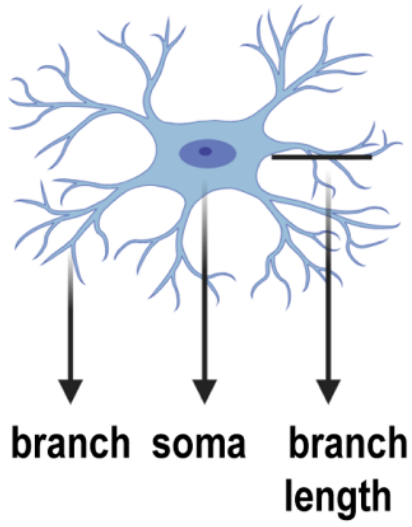

Figure 13. Morphology of microglial cells.

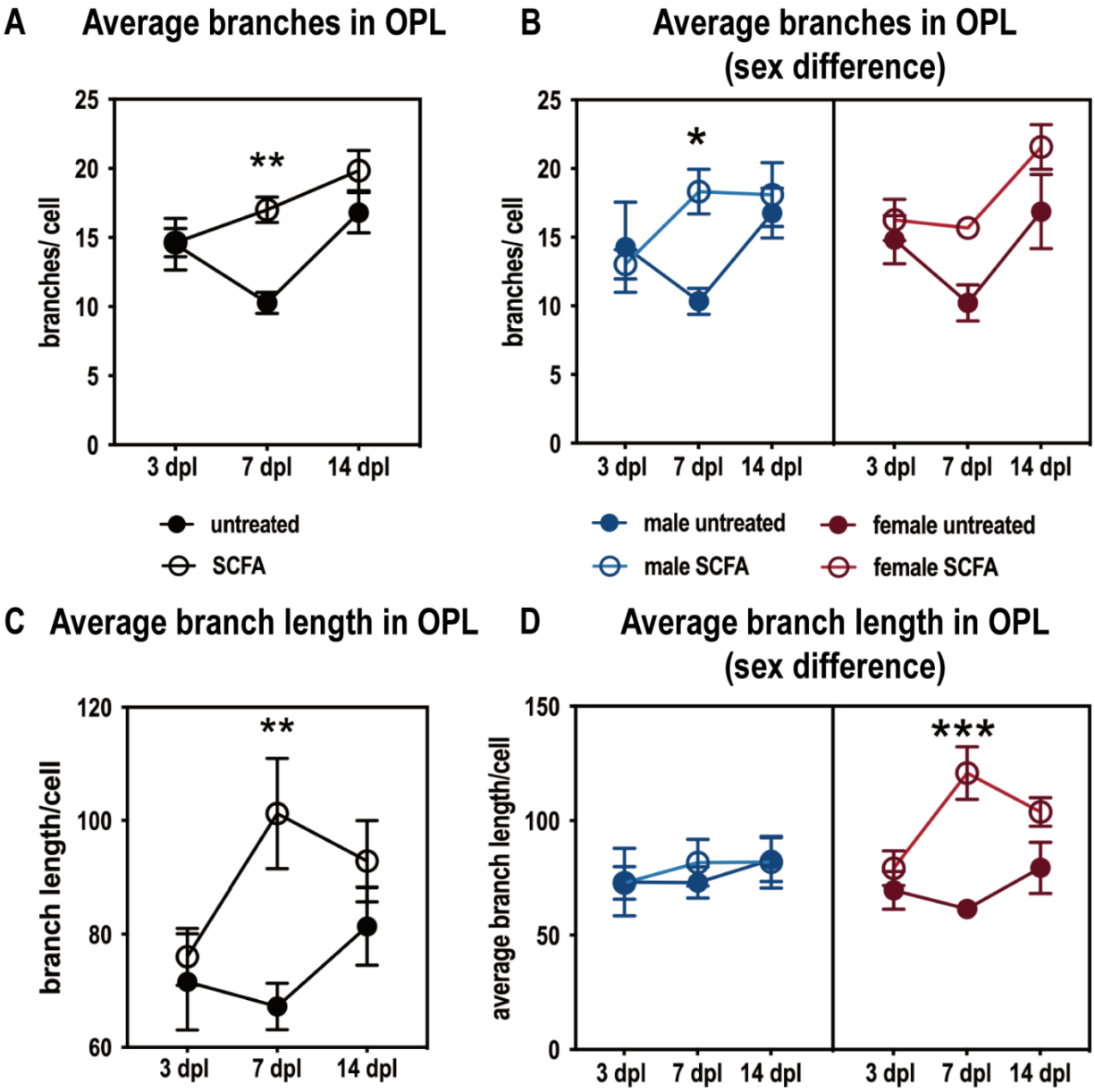

Figure 14. Morphology of retina microglial cells.

The number of branches in one cell in the OPL. (A) all samples; (B) sex difference. The data were represented as mean ± SEM. At 3 dpl, male untreated group: n=5; male SCFA group: n=5; female untreated group: n=4; female SCFA group: n=5. At 7 dpl, male untreated group: n=5; male SCFA group: n=5, female untreated group: n=5; female SCFA group: n=5. At 14 dpl, male untreated group: n=5; male SCFA group: n=5, female untreated group: n=4; female SCFA group: n=5. *p< 0.05; **p< 0.01; ***p< 0.001; 2-way ANOVA with multiple comparison test. The average branch length of $Iba1^+$ cells in OPL. (C) all samples; (D) sex difference The number of n and the statistical methods were the same as (A) and (B)

3.4 SCFAs modulate CNV development in a sex-specific manner.

Previous data in this study has shown that SCFAs treatment had a protective effect on both angiogenesis and gliosis in male and female following laser-induced CNV. While the degree of protection varied and some indicators did not reach statistical significance, there was a clear trend towards protection. Sex differences were significant in the effect of SCFAs on retina microglial cells, with a more pronounced down-regulating effect on the density and activation of microglia observed in males. To delve deeper into the sex differences at a transcriptomic level, we conducted RNA sequencing analysis.

Differentially expressed genes (DEGs) were identified between the untreated group and SCFA group based on a fold change > 1 and adjusted p-value (padj) < 0.1. Specifically, 145 DEGs in males and 45 DEGs in females were identified at 7 dpl, while 210 DEGs in males and 514 DEGs in females were identified at 14 dpl. Despite the identification of numerous DEGs across various groups, only 3 DEGs were found to be commonly regulated between males and females at 7 dpl, with 50 DEGs at 14 dpl (Figure 15A and B), suggesting that at the transcriptomic level, SCFAs treatment impact the development of laser-induced CNV in both males and females, but in a sex-specific manner. Notably, more genes were regulated in males compared to females at 7 dpl, whereas the pattern reversed at 14 dpl.

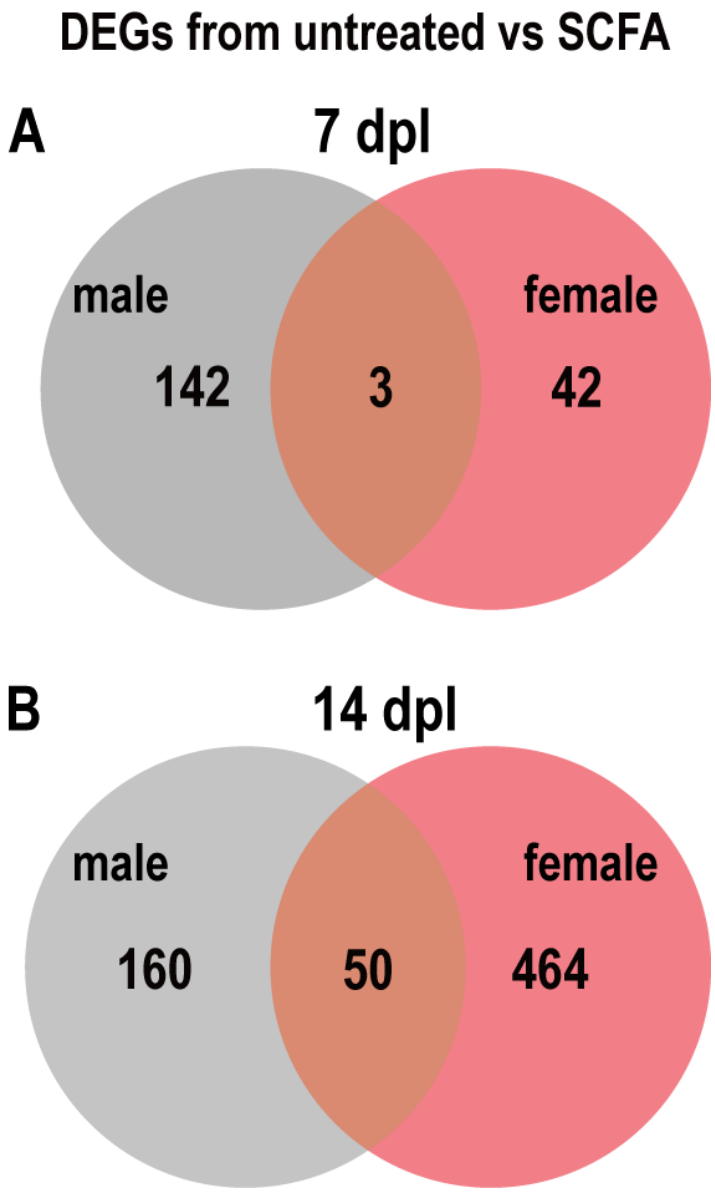

Figure 15. SCFA modulate DEGs differently between male and female.

(A) In the comparison between the untreated group and SCFA group on 7 dpl, 145 DEGs were identified in males and 45 DEGs in females, with 3 DEGs commonly expressed in both sexes. (B) On 14 dpl, 210 DEGs were found in males and 514 DEGs in females, with 50 DEGs commonly expressed in both sexes.

3.5 SCFAs modulate neovascularization and inflammation in laser-induced CNV mouse.

Heatmaps were used to visualize the pattern of DEGs regulation. The results indicated that at 7 dpl, 94 out of 145 DEGs were down-regulated with SCFAs treatment in males, while at 14 dpl, the trend reversed, with only 85 out of 210 DEGs showing down-regulation

(Figure 16A and B). In females, 37 out of 46 DEGs were up-regulated by SCFAs treatment, while 241 out of 545 DEGs were up-regulated at 14 dpl (Figure 16C and D).

Since only 45 DEGs were identified in females at 7 dpl, which was insufficient for further analysis, such as enrichment analysis, the focus of the study shifted primarily to analyzing the RNA sequencing data from males at 7 dpl and 14 dpl, as well as females at 14 dpl.

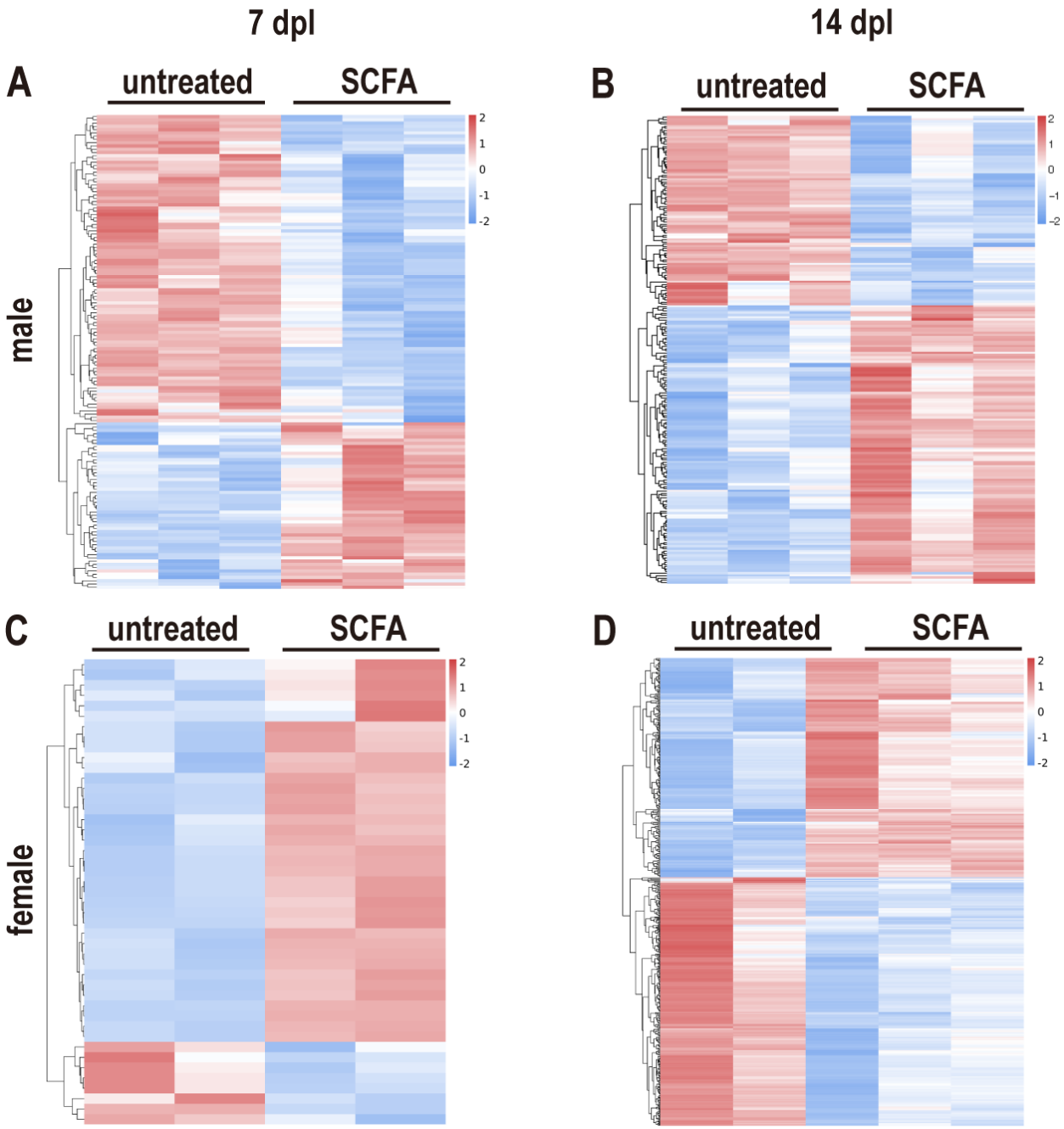

Figure 16. Heatmap of DEGs on 7 dpl and 14 dpl.

DEGs that identified between untreated group and SCFA group at (A) 7 dpl from males, (B) 14 dpl from males, (C) 7 dpl from females, (D) 14 dpl from females. each row represents a gene, and

each column represents a sample. Up-regulated genes are depicted in red while down-regulated genes are depicted in blue.

GO analysis was conducted to assess the impact of SCFAs treatment on neovascularization and inflammation. Vascular-related and inflammation-related biological process GO terms were selected and visualized by bubble plots.

Vascular-relates GO terms were significantly enriched in both males and females when comparing between the untreated and SCFA groups. In males, 10 terms, for instance, “regulation of endothelial cell proliferation”, “sprouting angiogenesis”, and “branching involved in blood vessel morphogenesis”, were enriched at 7dpl (Figure 17A), while 13 terms, including “regulation of vasculature development”, “sprouting angiogenesis”, and “blood vessel endothelial cell migration” were enriched at 14dpl (Figure 17B). Conversely, only 3 terms were enriched in females at 14dpl, which were “regulation of endothelial cell differentiation”, “regulation of vascular endothelial growth factor signaling pathway” and “venous blood vessel development” (Figure 17C).

In addition, inflammation-related GO terms were only significantly enriched at 7dpl in males. This included “inflammatory response to wounding”, “regulation of inflammatory response”, “cytokine production involved in inflammatory response” and “neuroinflammatory response”. Microglial cell activation and phagocytosis were identified at this time point as well (Figure 17A).

Since the analysis above suggested a more pronounced effect of SCFAs treatment on neovascularization and inflammation in males comparing to females at the gene expression level, our subsequent analysis focused primarily on male data.

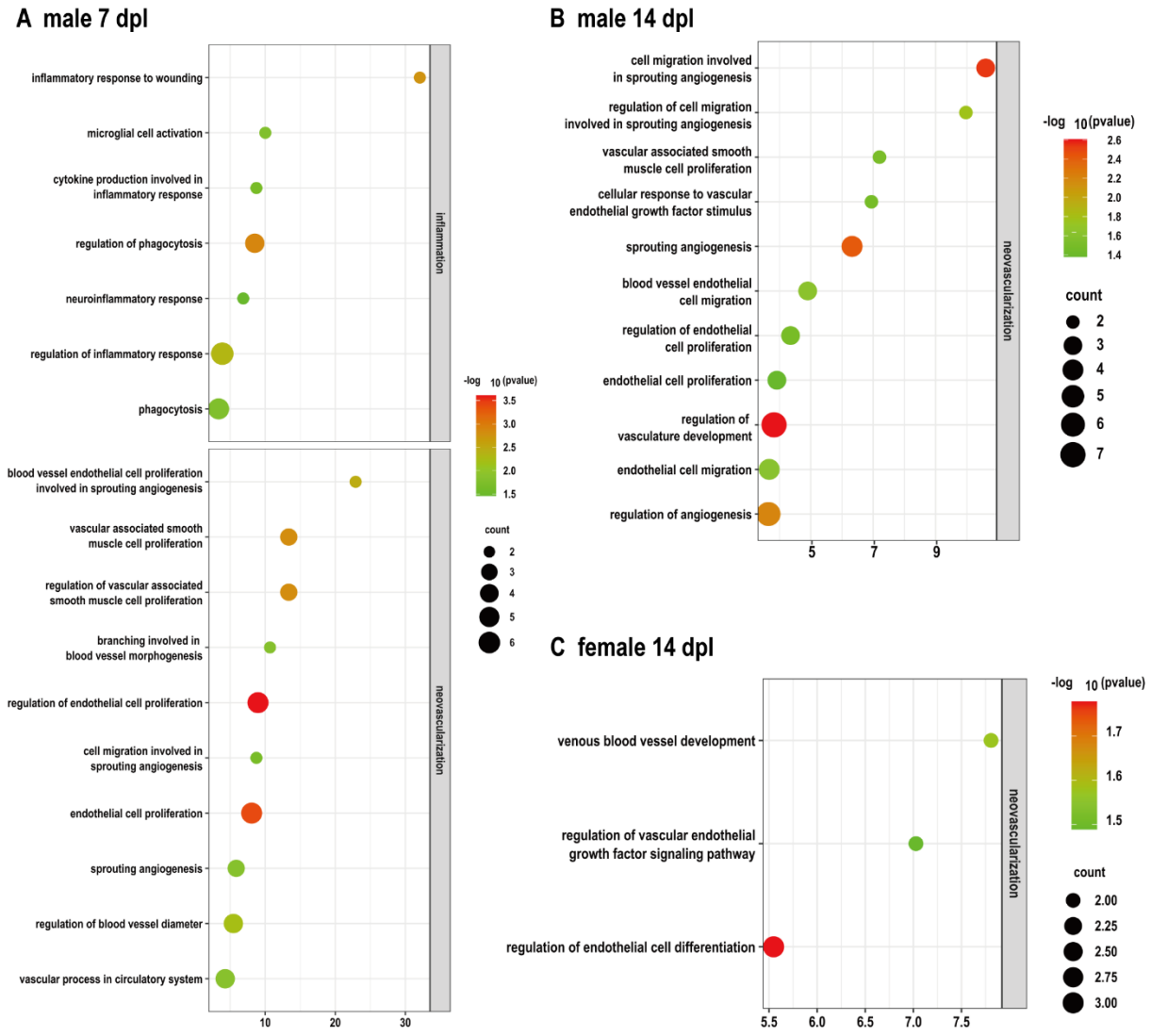

Figure 17. Bubble plots of vascular-related and inflammation-related GO term.

Bubble plots show the vascular-related and inflammation-related GO term on 7 dpl (A) and 14 dpl (B) from males and 14 dpl from females (C).

Through protein-protein analysis and cytoscape, the top 15 hub genes were identified at 7 dpl and 14 dpl in males after SCFAs treatment. These hub genes were then labeled in the corresponding volcano plots. 13 hub genes at 7 dpl and all 15 hub genes at 14 dpl were down-regulated in SCFA group (Figure 18A and C). The hub genes on 7 dpl were Junb, Fos, Erg4, Erg1, Cyr61, Nr4a1, Dcx, Pou3f2, Timp1, Gpnmb, Dct, Mlana, Mlph, Pmel, and Oca2, whereas those at 14 dpl were Junb, Fos, Erg4, Erg1, Cyr6, Nr4a1, Klf2, Dusp1, Cdkn1a, Klf4, Slk1, Maff, Nr4a3, Atf3, and Fosb. Notably, the expression of Junb, Fos, Erg4, Erg1, Cyr61, and Nr4a1 decreased at both time points (Figure 18B and D).

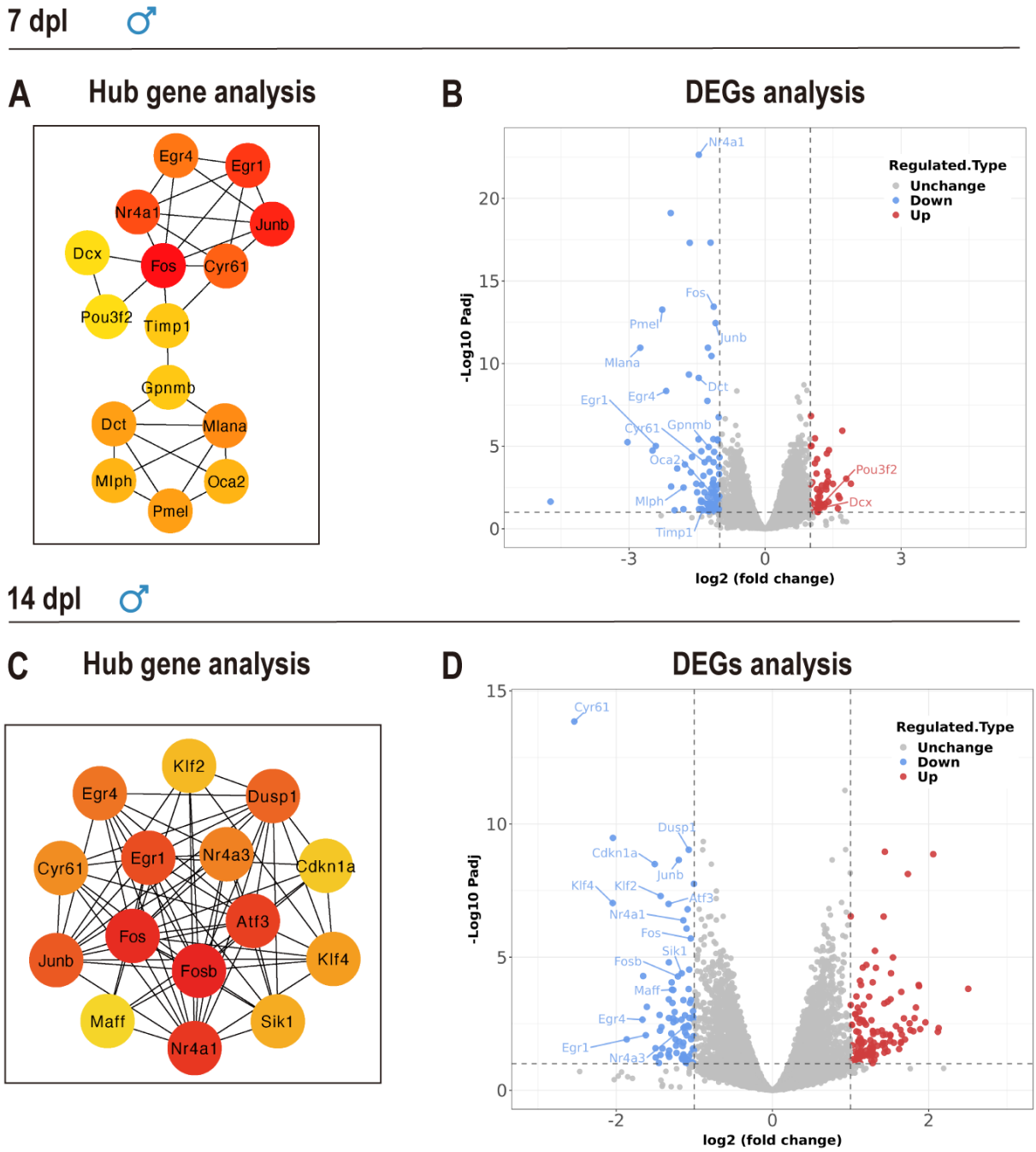

Figure 18. Hub genes identified at 7 dpl and 14 dpl in males.

The interaction network of the top 15 hub genes at 7 dpl (A) and 14 dpl (C) was analyzed using STRING and Cytoscape plugin Cytokabba, and visualized by Cytoscape. Nodes colored from yellow to red indicated the increasing strength of gene connections. Volcano plots showed DEGs with labeled top 15 hub genes at 7 dpl (B) and 14 dpl (D). Blue dots represented down-regulated genes, red dots represented up-regulated genes, and grey dots represented genes that were not differentially expressed.

To further explore the anti-inflammatory effects of SCFAs treatment, the gene list for the positive regulation of the inflammatory response GO term (GO0050729) was downloaded.

Due to inflammation-related GO terms were not enriched in 14dpl in male, to assess the impact of SCFAs treatment more accurately and comprehensively on this aspect, we broadened the range of DEGs from a fold change >1 to a fold change>0.5, this enabled us to include more genes that are associated with this biological process.

The results indicated that 8 out of 10 genes were downregulated after SCFAs treatment at both time points, suggesting that SCFAs attenuated the inflammatory response in the entire retina throughout the development of laser-induced CNV (Figure 19A and B).

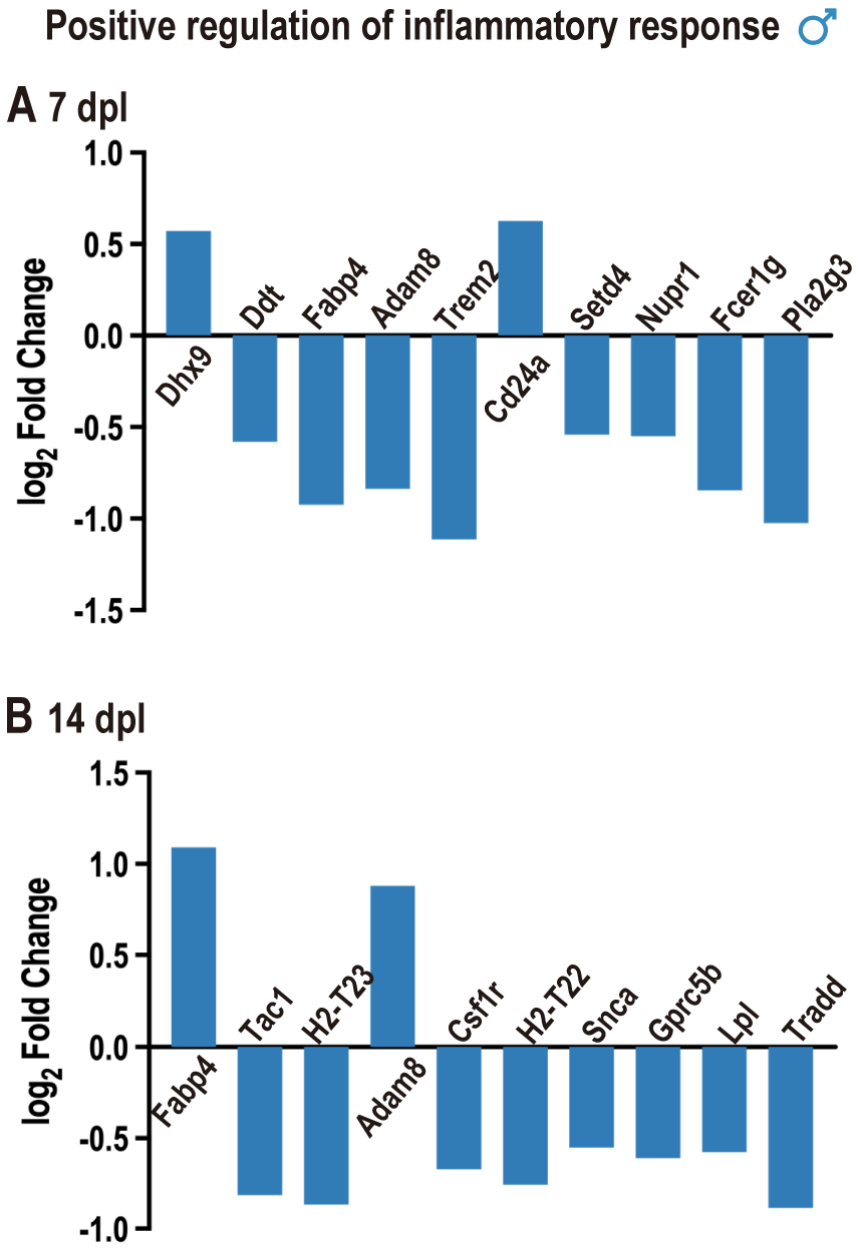

Figure 19. Gene expression related to positive regulation of inflammatory response.

The expression of the top 10 genes related to positive regulation of inflammatory response from the GO term GO0050729 (log2 fold change > 0.5 and padj < 0.1) at (A) 7 dpl and (B) 14 dpl.

3.6 SCFAs treatment attenuated the activation of microglial cells in laser-induced CNV males.

Previous findings indicated that Junb, Fos, Erg4, Erg1, Cyr61 and Nr4a1 were down-regulated following SCFAs treatment in males over time. Specifically, Junb, Fos, and Erg1 were found to be expressed at low levels in homeostatic microglia, whereas at high level in highly phagocytic disease-associated microglia (DAM-1) [31]. This highlights the necessity for further investigating the impact of SCFAs on retinal microglial cells.

Genes associated with microglial cell activation (GO0001774) and the positive regulation of phagocytosis (GO0050766) were identified. While the expression of microglial cell activation related genes was not inhibited at 7dpl, the expression of phagocytosis related genes was hindered, as 7 out of 8 phagocytosis-related genes were down-regulated in the SCFA group (Figure 20A and B). Conversely, at 14dpl, 8 out of 9 genes related to microglial cell activation showed reduced expression, but only 2 phagocytosis-related genes exhibited differential expression between the untreated and SCFA groups (Figure 20C and D). This suggested that, at the gene expression level, SCFAs initially reduced phagocytosis and subsequently attenuated microglial cell activation.

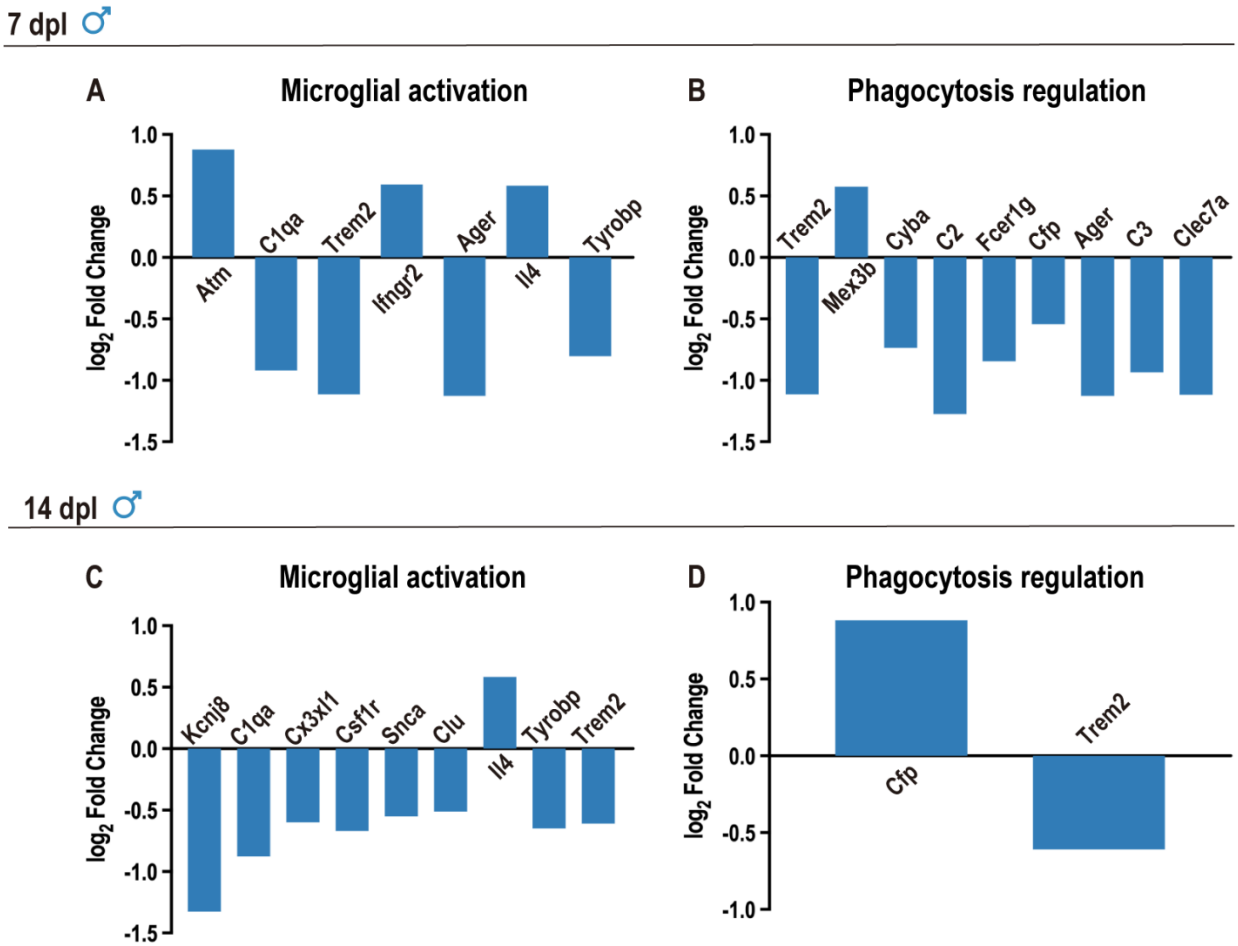

Figure 20. Gene expression that related to microglial activation and phagocytosis regulation.

The expression of microglial activation related genes (GO0001774) at (A) 7 dpl and (C) 14 dpl (log_2 fold change > 0.5 and padj < 0.1). The expression of phagocytosis related genes (GO0050766) at (B) 7 dpl and (D) 14 dpl (log2 fold change > 0.5 and padj < 0.1).

3.7 SCFAs treatment attenuated phagocytosis in microglial cells derived from males.

Considering the profound impact of SCFAs on microglia cells in *ex vivo* studies, our objective was to investigate the precise aspects through which SCFAs influence microglia *in vitro*, with a focus on measuring phagocytosis as the principal activity parameter. Neonatal microglial cells were isolated from mouse brains, divided into four groups, and seeded into 96-well plates. SCFAs were introduced to assess their direct effects. TNFα was used to create an inflammatory environment, and a combination of TNFα and SCFA was administered to assess the influence of SCFA on microglial phagocytosis under

pathological conditions. Phagocytosis was monitored and quantified using the Incucyte system.

In microglial cells derived from males, TNFα significantly increased phagocytosis between 5 and 12 hours of observation; however, pre-treatment with SCFAs notably attenuated this enhancement from 7 to 24 hours (Figure 21A), indicating that SCFAs reduced the phagocytic process in microglial cells under pathological conditions. Interestingly, this effect differed in the female cohort, in which neither TNFα nor SCFAs induced significant changes in phagocytosis (Figure 21B), supporting the sex-specific microglial responses observed ex vivo.

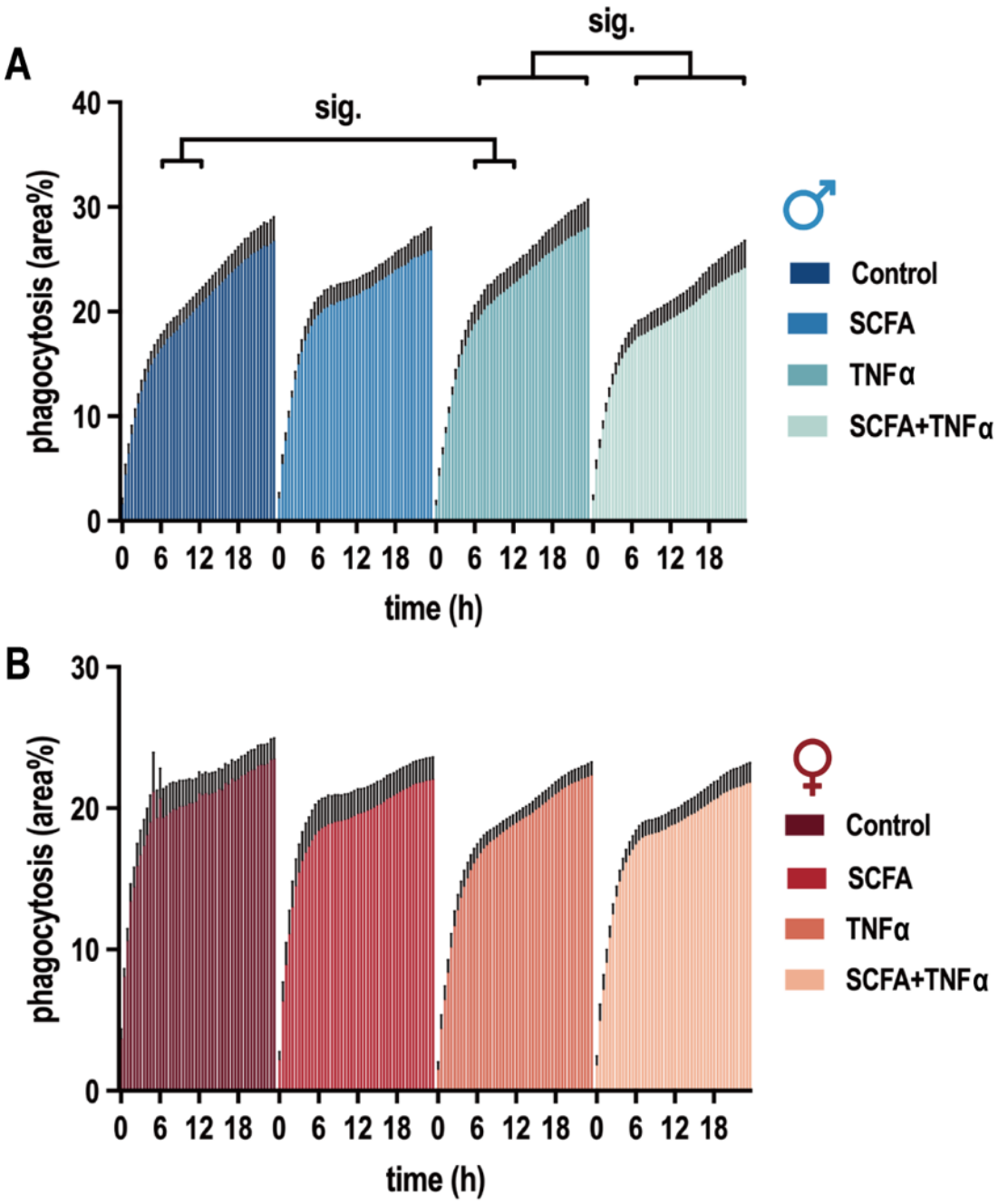

Figure 21. SCFAs reduced phagocytosis in male microglial cells.

A. The bar chart illustrated the impact of SCFAs on phagocytosis levels in male microglial cells. TNFα significantly increased phagocytosis from 5h to 12h ($p<0.05$), whereas SCFAs exhibited inhibitory effects from 7h until the end of the recording (24h) ($p<0.05$). (2-way ANOVA with repeated measurements, the data are presented as mean ± SEM with n=9). B. Neither TNFα nor SCFAs have an impact on phagocytosis in female microglial cells. (2-way ANOVA with repeated measurements, the data are presented as mean ± SEM with n=6).

3.8 SCFAs treatment suppressed TNFα-induced elevation of CXCL10 expression.

ELISA was performed to measure the effect of SCFAs treatment on the secretion of various cytokines. CXCL10, CCL2 and CCL4 were examined. Results showed that TNFα stimulation significantly increased the secretion of CXCL10 in male-derived microglial cells, while pre-incubating the cells with SCFAs inhibited this effect. However, this effect was not observed in female-derived microglial cells, as neither TNFα nor SCFAs affected the secretion of CXCL10. (Figure 22A)

Furthermore, CCL2 and CCL4 secretions were not influenced by SCFAs treatment (Figure 22B and C).

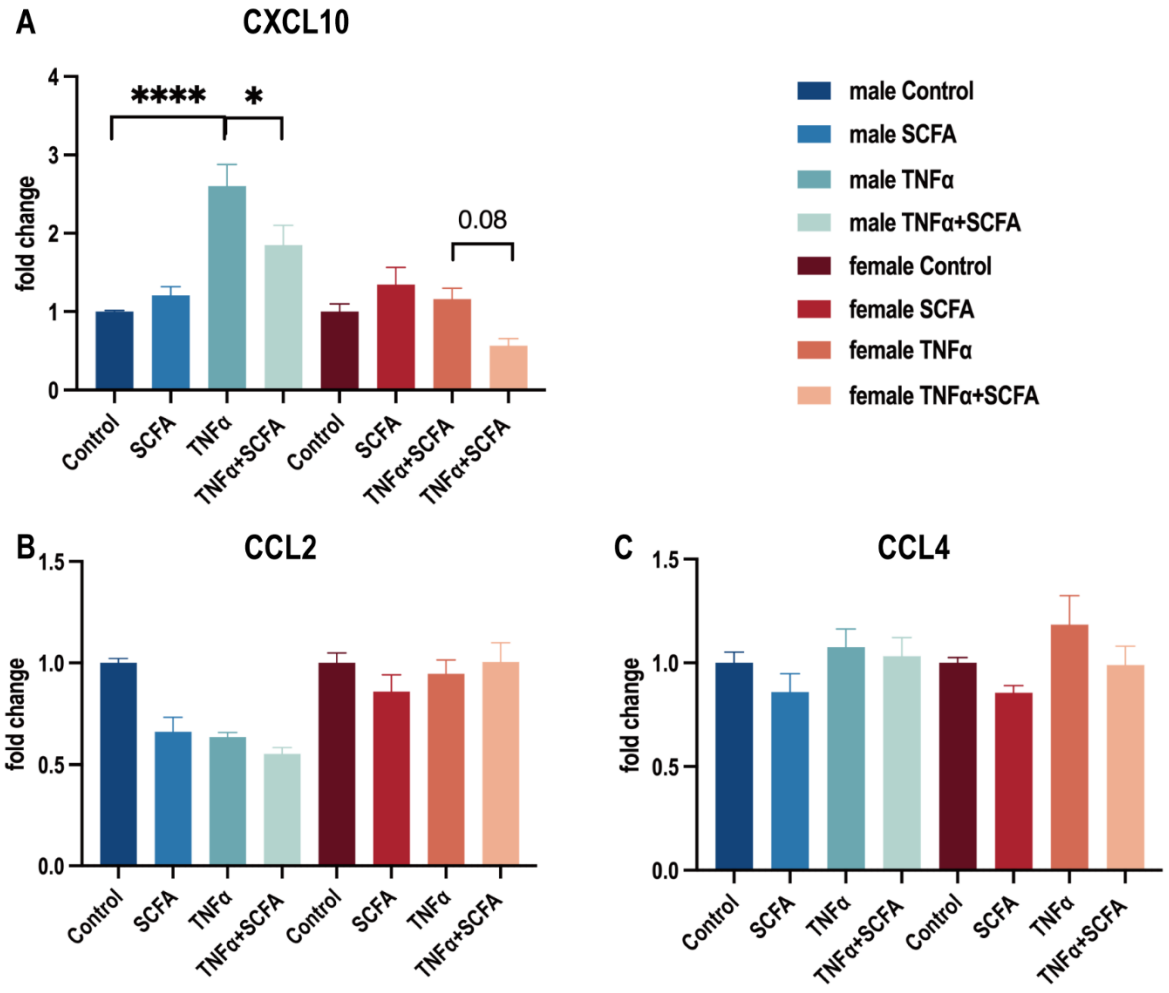

Figure 22. SCFAs inhibited the secretion of CXCL10 in male-derived microglial cells.

The relative concentration of CXCL10 (A), CCL2 (B) and CCL4 (C) in collected supernatant. The concentrations of the cytokines in each experimental groups were normalized against the corresponding Control group in male and female-derived microglial cells. 2-way ANOVA with multiple comparison was used for statistical analysis. the data were presented by mean ± SEM with the n=5. *p<0.05, *p<0.05; ****p<0.0001.

3.9 SCFAs treatment suppressed the O-GlcNAcylation in female microglial cells.

RNA sequencing demonstrated that SCFAs treatment increased OGT expression *ex vivo* (Figure 23B), however, this effect was observed only in male mice. Following SCFA treatment, OGT expression exhibited a slight upward trend at 7 dpl. Although the padj value exceeded 0.1 at this time point, the increasing in OGT expression became statistically significant at 14 dpl, showing a higher level of regulation compared to the 7 dpl. In contrast, there was no significant change in OGT expression observed in females over the same period. High level of O-GlcNAcylation has detrimental effects on retinal cells. RNAscope showed that OGT was widely expressed in among almost all retinal layers (Figure 23A), it also co-localized with retinal microglia (Figure 23C). To ascertain whether SCFAs induce the O-GlcNAcylation in microglial cells, we quantified the expression of intracellular O-GlcNAc using flow cytometry to explore its association with microglial cells.

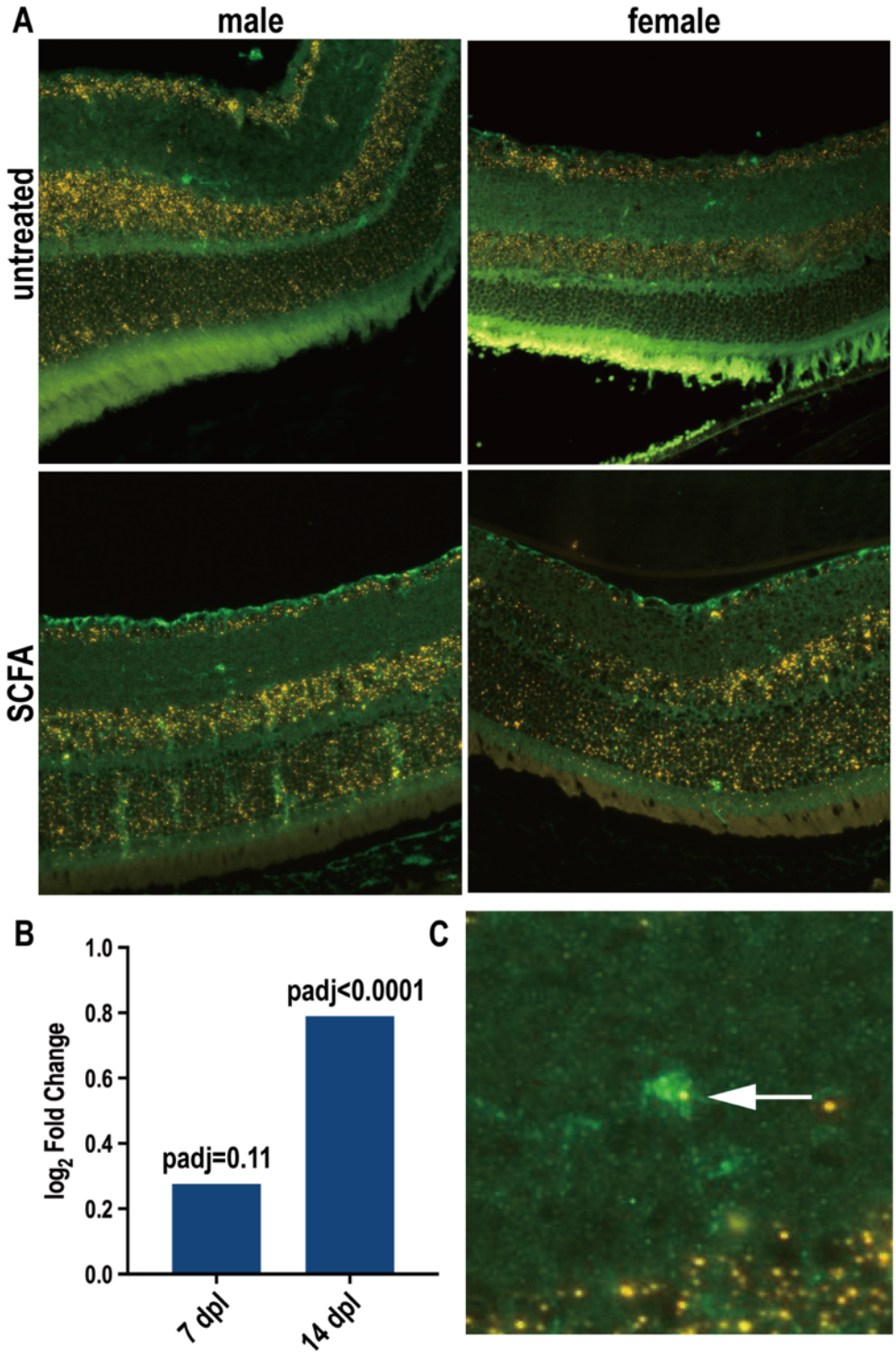

Figure 23. OGT expression in retina.

(A) Representative images of OGT and Iba1$^+$ staining using RNAscope. Scale bars = 100 μm. (B) The fold change of expression of OGT between untreated group and SCFA group. (C) Amplified image to observe the expression of OGT in Iba1$^+$ cells.

After gating live microglial cells (live/dead cell dye$^-$, CD45$^+$/CD11b$^+$) in BD Diva (Figure 24), we analyzed the median fluorescence intensity (MFI) of intracellular O-GlcNAc. Surprisingly, TNFα stimulation led to increased O-GlcNAc expression in male microglial cells, while SCFAs did not mitigate this increase (p=0.24) (Figure 25A and C). On the other hand, a notable inhibition was observed in female microglial cells, irrespective of TNFα stimulation (Figure 25B and C). These findings suggested that, contrary to ex vivo findings, SCFAs did not enhance O-GlcNAc secretion in microglial cells and actually exerted an inhibitory effect on female- derived cells. Given that the effect of SCFAs on microglial cells does not explain the observed increase in OGT expression ex vivo, further investigations are warranted.

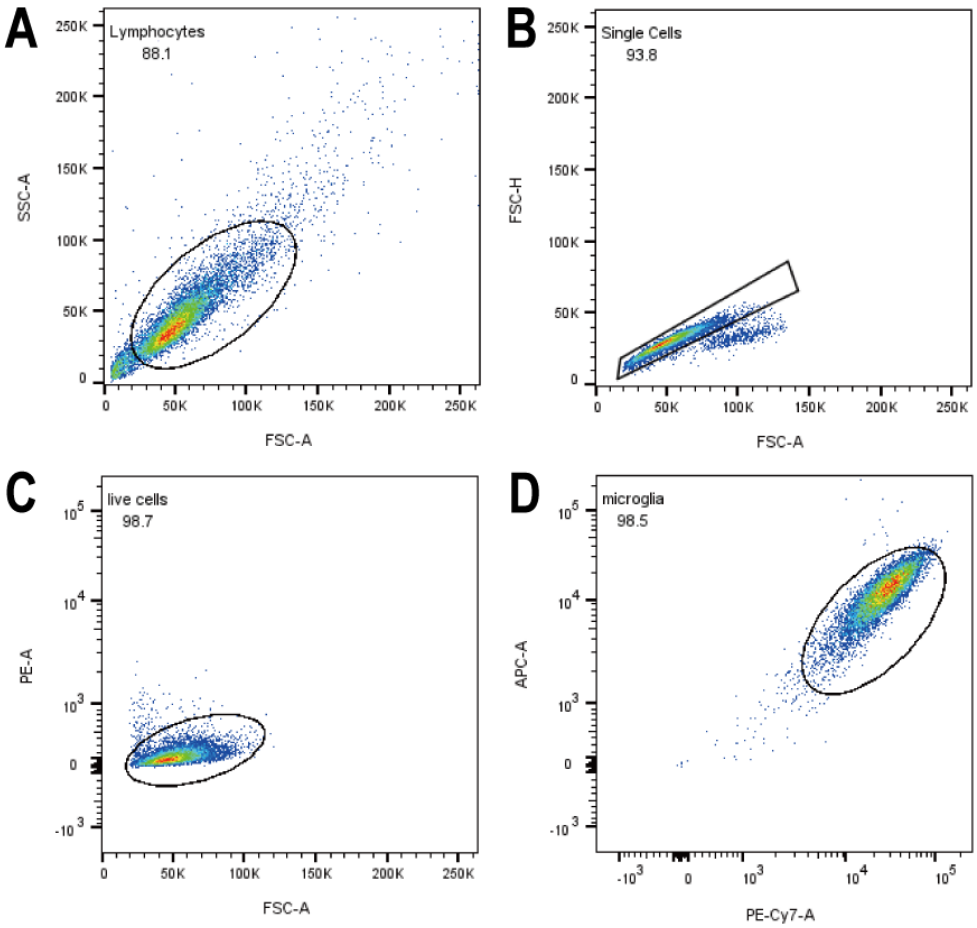

Figure 24. Gating strategy of microglial cells.

Gating strategy of primary microglial cells isolated from mice cortex. A. Gating of all the recording cells. B. Gating of all the single cells, excluding duplicates. C. Gating of all the live cells using live/dead cell dye (red). D. Gating of the microglial cells, stained by CD11b (PE-Cy7) and CD45 (APC).

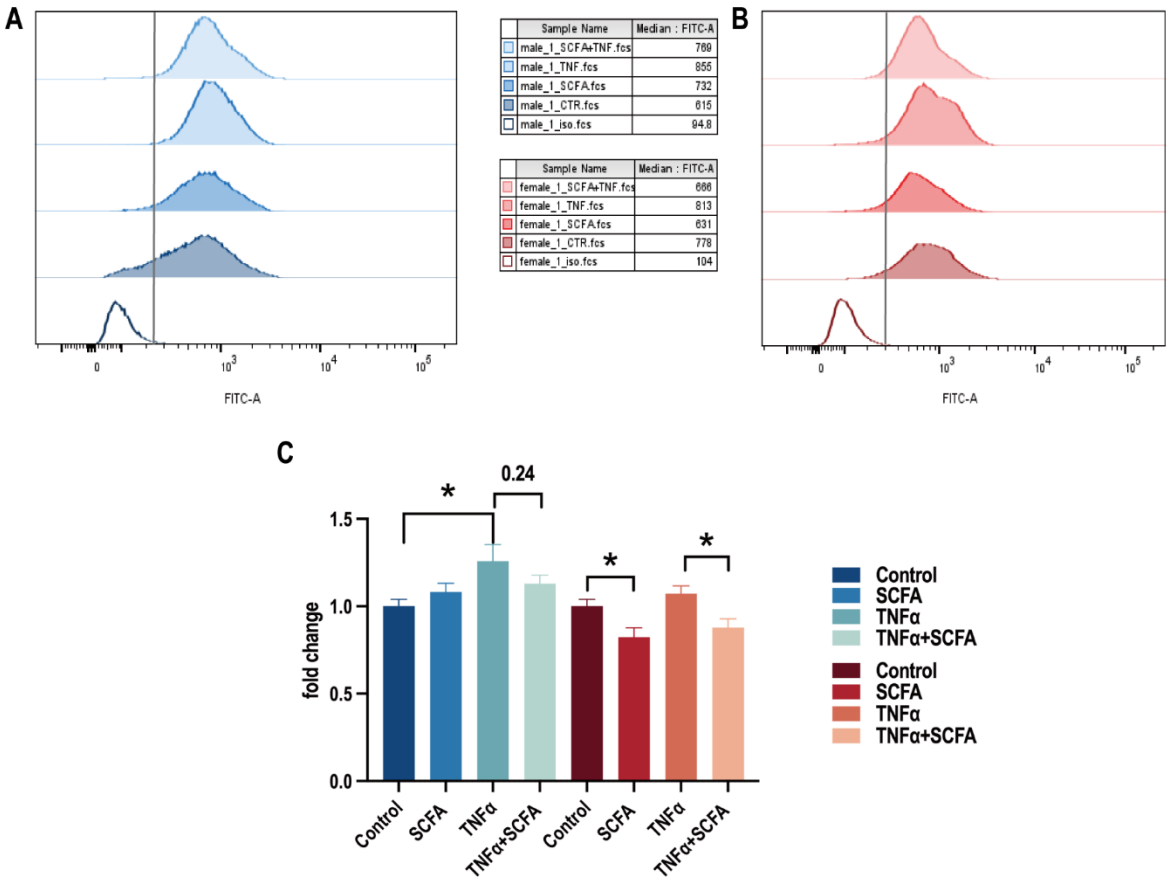

Figure 25. SCFAs inhibited O-GlcNAcylation in microglial cells derived from females.

Representative histograms indicating the O-GlcNAc signal in microglial cells of Control, SCFA, TNFα and SCFA+TNFα group including male (A) and female (B) mice. IgG kappa Isotype was used as a negative control for each experiment. At least 10K cells were recorded per sample with a n=6. C. Bar chart showed the median fluorescence intensity that recorded by BD FACS Diva and collected using FlowJo™ 10.8.1. Data were analysis using unpaired t test, the data were presented as mean ± SEM, *p<0.05.

3.10 SCFAs had no impact on calcium pathway in microglial cells.

Calcium (Ca^{2+}) signals has been considered a common signal transduction mechanism in microglial cells in recent years. We performed calcium imaging on microglial cells derived from males (Figure 26A) and females (Figure 26B) to investigate whether SCFAs affected the Ca^{2+} pathway.

Only a small percentage of the cells derived from males (less than 5%) and females (less than 10%) responded to Fluo-4 stimulation (Figure 26C). Although the proportion of re-

active cells derived from females was higher than that derived from males, both responses were less than 10% when compared to the positive control stimulated by ATP, this suggesting that SCFAs had no influence on the Ca^{2+} pathway in microglial cells regardless of sexes.

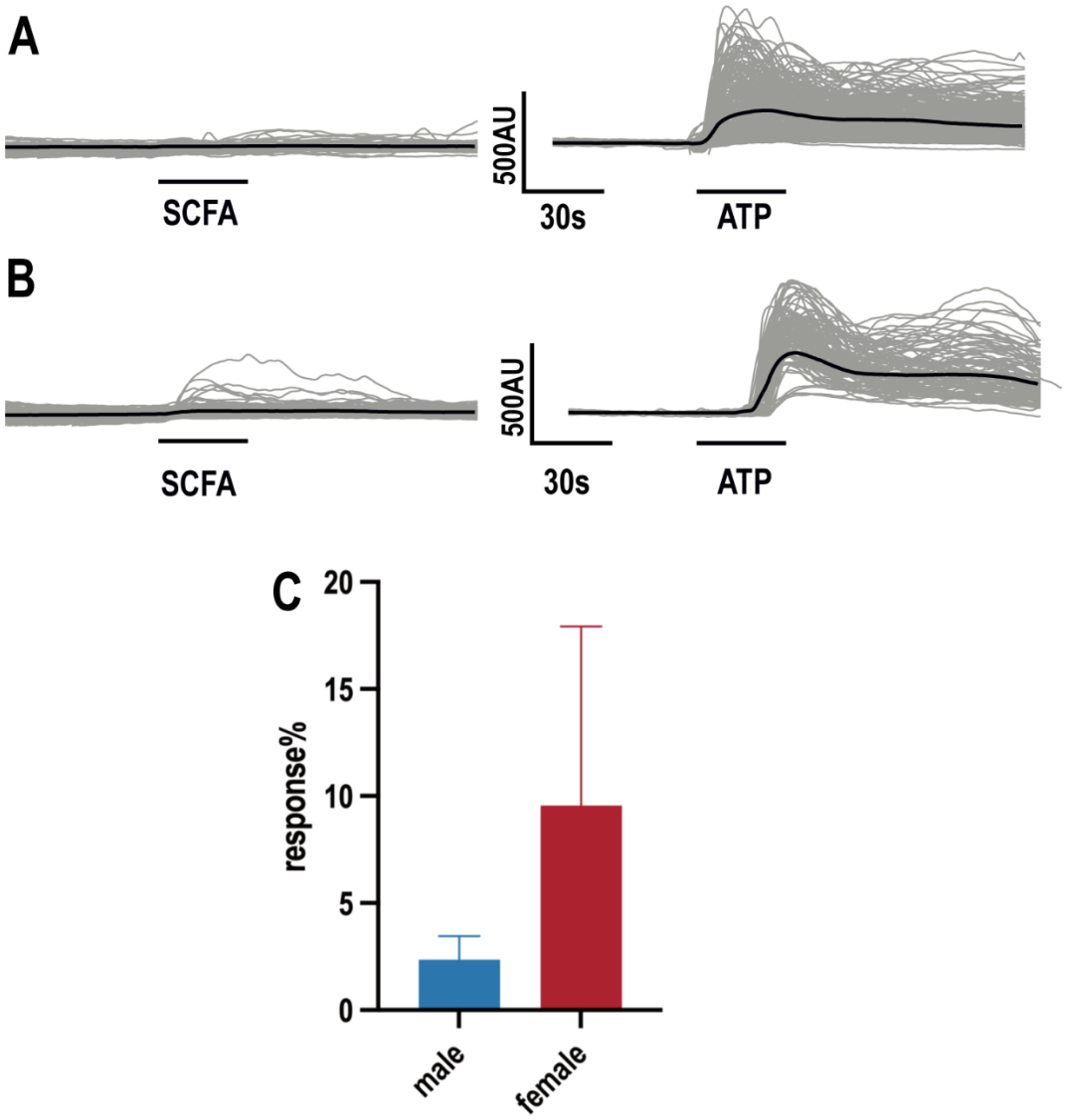

Figure 26. SCFAs did not activate calcium pathway.

Graphical illustration of time course of signal after application of SCFAs for 60s as a stimulation reagent following by 1mM ATP for 60s as a positive control in males (A) and females (B) derived microglial cells. C. Bar chart demonstrates the percentage of microglial cells that can be activated by SCFAs. The data were presented as mean ± SEM, in male group: n=3; in female group: n=5.

4. Discussion

AMD is a neurodegenerative disease that significantly affects vision, potentially leading to vision loss. While anti-VEGF-A therapy is currently the most widely used treatment in clinic, many nAMD patients suffer persistent or experience decline responses over time with anti-VEGF-A treatment (Fu et al., 2024). Therefore, there is a need to explore complementary treatments and preventive measures for nAMD. The concept of the gut-retina axis has brought attention to the potential influence of gut health on retinal diseases (Zhang and Mo, 2023). SCFAs, which are produced through bacterial fermentation of dietary fiber in the colon, have been linked to retinal diseases like diabetic retinopathy (Huang et al., 2023). This study aims to investigate SCFAs potential to inhibit the chain of pathogenic events in nAMD.

4.1 SCFAs treatment suppresses lesion formation in laser induced CNV mouse model.

Our study found that treatment with SCFAs resulted in a reduction of lesion formation on retina from 7dpl to 14 dpl, and on the choroid at 14 dpl. This was evidenced by a decrease in leakage size in the retina and lesion volume in the choroid. Furthermore, the alleviation of neovascularization-dependent gene expression was also observed by RNA sequencing. Previous studies suggested that butyrate alleviates CNV individually in retina by reduced CNV size (Xiao et al., 2020, Lyzogubov et al., 2020), while our study revealed that the mixture of SCFAs has the same effect.

According to a study by Anna Salas, it was found that in the initial stage up to 7 dpl, there was an acute inflammatory response with increased expression of inflammatory factors observed within the first 3 days, the size of CNV lesions reaches its peak at 7 dpl. In the second stage from 7 dpl to 14 dpl, they observed stabilization of the CNV lesions and the formation of fibrosis(Salas et al., 2023). Our findings demonstrated that treatment with SCFAs modulates several vascular - related biological processes from RNA sequencing. Through RNA sequencing and morphological observations of laser lesions, we speculate that SCFAs exhibit protective effects during the progress of laser induced CNV. Additionally, the effects above also vary by sex, with a greater reduction in CNV size observed in males, and a greater reduction in choroidal lesion observed in females.

A sex-specific effect of SCFA on the CNV was observed at the transcriptomic level. Specifically, at 7 dpl, SCFAs targeted more genes in males than in females, with nearly three times more DEGs identified in males. Conversely, DEGs identified in females were nearly three times more than those in males at 14dpl. Enrichment analysis reveals that SCFAs regulate many vascular-related biological processes at 7 dpl and 14 dpl in males. However, the number of processes regulated in corresponding female cohort is relatively lower, suggesting that the modulation may not be as strong in females as males. Among all the DEGs identified from bulk RNA sequencing, Junb, Fos, Cyr61, Erg4, Erg1, and Nr4a1 were recognized as hub genes at both 7 dpl and 14 dpl.

Junb, a member of the activator protein-1 (AP-1) transcription factor family, closely related to neovascularization. Research on Junb in ocular diseases has primarily focused on its function in retinal endothelial cells. It is found in nuclei of endothelial cells at the vascular front and in blind-ended vascular sprouts in the retina, as well as in endothelial cells that vertically invade the deep layer. Additionally, its expression can be induced by VEGF-A, suggesting a promotion of angiogenesis (Yanagida et al., 2020, Yoshitomi et al., 2021), the expression of Junb increases after stimulating the freshly isolated endothelial cells with TNFα (Ma et al., 2023).

Fos, also known as c-Fos, is another member of the AP-1 family, and closely interacts with Junb. It binds to the AP-1 complex to promote cell death. C-fos is positive correlated with light-induced photoreceptor apoptosis (Hafezi et al., 1997). Its expression has been observed to increase in a N-methyl-D-aspartate-induced retina neuronal apoptosis model (Lambuk et al., 2021). In another pathological angiogenesis mouse model, Fos's expression significantly rises in all retina layers, along with inflammation-related cytokines, such as IL6, IL1 beta and TNF. Pharmacologic inhibition of Fos alleviates the retinal neovascularization and reduce the expression of IL6, IL1 beta and TNFα (Sun et al., 2017).

Cyr61 is an angiogenic factor whose expression is increased in a hypoxia-induced retinal vascular endothelial cell model through modulation by c-Jun/AP-1 (You et al., 2010). A recent study using a similar laser injury-induced CNV mice model demonstrated that Cyr61 is strongly upregulated by endothelial cells in CNV lesions. The produced Cyr61 then recruits and activates monocyte-derived macrophages. Furthermore, many of the

genes responsive to Cyr61 treatment in macrophages are related to inflammation and angiogenesis, such as Saa3, Mmp9, Mmp14, Ccl4, etc(Lin et al., 2024).

Erg4 and Erg1, which are part of the E-26 gene family, are expressed in endothelial cells and play a crucial role in regulating endothelial homeostasis and angiogenesis in the retinal vasculature (Birdsey et al., 2015, Shah et al., 2016). While there is limited knowledge about the impact of Erg4 on retina diseases or cells, a study revealed that the expression of Erg1, along with the inflammatory-related gene TXNIP, increases in UV-B induced human retinal endothelial cells. Conversely, silencing Erg1 results in a decrease of TXNIP, indicating that Erg1 is involved in mediating inflammation in endothelial cells (Shi et al., 2021a).

The downregulation of these hub genes suggested that SCFAs treatment decreases the expression of neovascular-associated genes expression *ex vivo*, indicating that SCFAs treatment may have the ability to suppress neovascularization.

4.2 SCFAs treatment suppress inflammation in retina.

4.2.1 SCFAs treatment ameliorate inflammation *in vivo*.

SCFAs possess anti-inflammatory properties in ocular diseases. One study has demonstrated that SCFAs decrease the secretion of cytokines and chemokines in LPS-stimulated retinal astrocytes (Chen et al., 2021). Although the amount of research on the anti-inflammatory effects of SCFA in ocular diseases is limited, some studies have indicated that the systematic administration of butyrate alone inhibits inflammation in ocular surface and fundus diseases. Butyrate has been shown to mitigate retinal thinning and reduce blood glucose levels in a type 1 diabetic mouse model induced by intraperitoneal injection of streptozotocin(Huang et al., 2023). Administration of tributyrin (a stable and rapidly absorbed form of butyrate) protects against corneal barrier disruption and restores conjunctival goblet cells(Schaefer et al., 2022). Butyrate treatment also reduces the secretion of IL-6 and TNFα in corneal explants induced by TLR ligands (such as LPS) *in vitro*, as well as the secretion of IL-8 in corneal epithelial cells under the same stimulation (Wu et al., 2024).

Our study elucidated the protective effect of SCFAs against inflammation in laser-induced CNV mice, as evidenced by the decrease of $Iba1^+$ cells (including microglial cells and monocytes) density at and near the laser spots with a more ramified morphology, the reduction of GFAP at a protein level, and the gene expression related to inflammatory response throughout the entire pathological wound healing process following laser induction.

GFAP is typically expressed exclusively in retinal astrocytes, however, it was also found to express in Müller cells under pathological conditions, for instance, in experimental mouse model of photoreceptor degeneration (constant light exposure) and oxygen-induced retinopathy (Eisenfeld et al., 1984, Nurnberg et al., 2018), GFAP is used to assess subretinal fibrotic tissue on choroidal flat mounts (Jo et al., 2011) and the extent of gliosis in retina diseases, such as proliferative vitreoretinopathy(Lee et al., 2020) and retinal detachment(Luna et al., 2010). Downregulation of GFAP represents a low gliosis and damage of Müller cells and astrocytes, indicating a low level of inflammation and better wound healing.

The downregulation of inflammatory response was only detected in male retina after SCFA treatment at both 7 dpl and 14 dpl. Studies have demonstrated that SCFAs may have anti-inflammatory effects in both sexes through independent mechanisms(Shah et al., 2021, Spichak et al., 2021). For example, one study demonstrated that butyrate activates HDACi activity specifically in primary cortical astrocytes derived from females, while acetate and propionate are implicated in the anti-inflammatory response solely in astrocytes derived from corresponding males (Spichak et al., 2021). Our study underscores the beneficial effect of SCFAs treatment on inflammation in nAMD-featured model and indicates potential sex-specific regulation in this aspect.

4.2.2 SCFAs treatment suppress microglial activation *in vivo*.

Butyrate has been shown to promote neuroprotection by modulating the inflammatory response of microglia in a mouse model of middle cerebral artery occlusion. It reduces the expression of pro-inflammatory cytokines like TNFα and increases the expression of anti-inflammatory cytokines like IL-10 (Patnala et al., 2017). One of the hub gene that was mentioned above, Nr4a1 has been linked to microglial activation. A study reported an

increase in microglial cell density and recruitment of pro-angiogenic macrophages in CNV Nr4a1$^{se2/se2}$ mice(Droho et al., 2023b). Additionally, targeted deletion of Bace-1 in microglial cells enhanced the expression of Junb, Fos, and Egr1(Singh et al., 2022), which are three of the hub genes that regulated by SCFAs. Therefore, we hypothesized that SCFAs may potentially alleviate the inflammation of retina by influencing, among other cells, the activation of retinal microglial cells.

The density of Iba1$^+$ cells at the laser spots in the OPL decreased at 7 dpl, the density of ramified Iba1$^+$ cells also decreased in both the IPL and OPL near the laser spots, with a more ramified morphology, indicating that SCFAs treatment suppress both the migration and activation of Iba1$^+$ cells in the laser-induced neuroretina. Analysis of sex differences revealed that SCFAs treatment had a more pronounced effect on Iba1$^+$ cells in males compared to females, because of a significant reduction in Iba1$^+$ cell numbers at and near the laser spots was only observed in males. Need to mention that a significant increase of the density of Iba1$^+$ cells was observed at 3dpl, especially in females, this may be due to a higher inflammatory response induced by SCFAs at the acute phase, but the underlying mechanism remains unclear.

Iba1$^+$ cells in the retina consist of monocytes and microglial cells. To investigate whether SCFAs treatment has a specific impact on microglial cells, the expression of genes related to microglial cell activation from RNA sequencing was analyzed at 7 dpl and 14 dpl. Results show that microglial cell activation-related genes such as Trem2 and C1qa were modulated by SCFAs treatment at both timepoints. Although there was no clear regulation pattern of genes at 7 dpl, mostly of them were down-regulated at 14 dpl. Notably, no differential expression of microglial activation-related genes was observed in the female cohort.

While limited studies have investigated the impact of SCFAs on retinal microglial cells, Wang et al. demonstrated that fenofibrate prevented retinal microglial cell accumulation in high-fat diet mouse and restored SCFAs levels in the retina, serum, and feces(Wang et al., 2022). Furthermore, individually administration of sodium butyrate inhibited both the number and activation of microglial cells in diabetic mouse, highlighting a direct influence of SCFAs on retinal microglia(Huang et al., 2023).

4.3 The impact of SCFAs on microglial cells.

4.3.1 SCFAs may have a protective effect against inflammation *in vitro* only in males.

Microglial cells are present in both the brain and retina, originating from primitive yolk sac progenitors(Alliot et al., 1999). In mouse, microglial cells can be earliest identified in the brain at embryonic day 7.5 - 8.5 (E7.5 - E8.5)(Ginhoux et al., 2010), and in the retina at E11.5(Santos et al., 2008). Various studies have analyzed the sequencing profile of microglial cells during development in both the brain(Hammond et al., 2019, Matcovitch-Natan et al., 2016) and the retina(Anderson et al., 2019). A comparison of these profiles suggests that while some genes are similarly expressed in both the retina and brain, the cluster patterns are distinct during development (Anderson et al., 2019). While brain and retina microglia exhibit differences in RNA expression, they both perform similar fundamental functions, including phagocytosis and debris clearance. Due to the technical challenge of obtaining a large quantity of retinal microglia from mice, we chose to use microglial cells isolated from neonatal mouse cortex for our initial investigation.

C-X-C Motif Chemokine Ligand 10 (CXCL10) is a 10kDa protein known for its “inflammatory”(Taub et al., 1993) and “angiostatic”(Strieter et al., 1995) properties. The mRNA expression of CXCL10 increases in microglial cells derived from hippocampus in hyperglycemia rats.(Satrom et al., 2018). The mRNA and protein expression of CXCL10 both increases in LPS induced BV2 cells (Shen et al., 2006). Chemokine (C–C motif) Ligand 2 (CCL2) and chemokine (C–C motif) Ligand 4 (CCL4) belong to a group of chemotactic cytokines(Zlotnik and Yoshie, 2000). The concentrations of CCL2 in cortex and serum are upregulated after intraperitoneal injection of thioacetamide, led to an increase in microglial activation. Moreover, inhibiting the CCL2 receptor could suppress microglial activation induced by supernatant collected from TNFα-treated neurons(Zhang et al., 2017). Both CCL2 and CCL4 expression levels were elevated in primary microglia and the microglial cell line (Ra2 cells) after stimulation with amyloid - β peptide in vitro(Ito et al., 2006), indicating a close association in CCL2/CCL4 and microglia.

ELISA was used to measure the secretion levels of CXCL10, CCL2 and CCL4 in microglial supernatant in this study. The findings showed that pretreatment of primary microglial

cells with SCFAs did not affect the secretion of these cytokines. Moreover, TNFα was observed to notably enhance the secretion of CXCL10, which was attenuated by SCFAs pretreatment, suggesting an anti-inflammatory effect of SCFAs on microglial cells.

Interestingly, TNFα did not impact the secretion of CCL2 and CCL4, regardless of SCFAs pretreatment. Previous studies have suggested an upregulation of CCL2 and CCL4 in TNFα-induced microglial cells (Human microglial cell line HMC3)(Wang et al., 2021), which contrasts with the results of this study. Possible reasons could be variations between primary microglial cells and cell lines, as well as differences in TNFα concentrations (10ng/ml vs 300ng/ml(Wang et al., 2021)). However, the exact underlying causes remain unknown.

4.3.2 SCFAs inhibit phagocytosis in microglial cells *in vitro*.

Phagocytosis is one of the main functions of microglial cells. Activated microglia may kill degenerated photoreceptors and neurons through phagocytosis and exacerbate retinal injury by releasing proinflammatory mediators(Fan et al., 2022). Our RNA sequencing results indicate that SCFAs treatment led to a decrease in the expression of a majority of phagocytosis – related genes in the retina at 7 dpl. Hence, further exploration is warranted to determine the impact of SCFAs treatment on the phagocytic activity of microglial cells. While the impact of SCFAs on phagocytosis in retinal microglial cells is not well understood, supplementation with SCFAs was found to inhibit microglia from phagocytosing the synapse in male hippocampus(Shi et al., 2021b). Our data indicates that the phagocytic activity was reduced by SCFAs in the male retina, as well as the reduction of microglial cell activation and $Iba1^+$ density. Since microglia are not the only type of cells capable of phagocytosis in the retina, and $Iba1^+$ cells include monocytes and microglia, whether this reduction of phagocytosis is directly associated with SCFAs remains unclear.

Our study then aimed to explore the potential direct impact of SCFAs on phagocytosis in vitro, beginning with neonatal microglial cells. In contrast to a previous study that suggested SCFAs had no direct effect on the phagocytic capacity of primary microglia derived from wildtype mice(Colombo et al., 2021), our study demonstrated that SCFAs directly inhibit phagocytosis in microglial cells derived from male mouse under pathological conditions (TNFα stimulation) *in vitro*, with no such inhibition observed in the corresponding

female group. Limited information exists regarding the direct effects of SCFAs on phagocytosis. Specifically, two other SCFA components, valerate and formate, were found to inhibit phagocytosis in human THP-1 microglia-like cells stimulated with LPS and IFN-γ(Wenzel et al., 2020). Our study shows that a mixture of SCFAs directly alleviates microglial phagocytosis, additionally highlighting a sex-specific response.

4.4 SCFAs suppress O-GlcNAcylation in microglia derived from female.

O-GlcNAcylation, short for O-linked-N-acetylglucosaminylation, is a post-translational modification where a GlcNAc molecule is attached to serine/ threonine sites on proteins by O-GlcNAc transferase (OGT), and can be removed by GlcNAcase (OGA)(Holt et al., 1987, Chang et al., 2020). The role of O-GlcNAcylation varies in different conditions and organs(Baudoin and Issad, 2014). In the retina, O-GlcNAcylation is significantly up-regulated under pathological conditions like aging in rats(Zhao et al., 2014) and in db/db mice (type 2 diabetic mice model)(Xu et al., 2014). Enhanced O-GlcNAcylation can protect against oxidative stress by reducing reactive oxygen species in ARPE cells(Zhao et al., 2014), while inhibiting it in endothelial cells decrease VEGF-A expression and protect the blood-retina barrier(Xu et al., 2014).

Our data demonstrated that the expression of OGT existed in almost all type of retina cells including microglial cells and was increased after SCFAs treatment but only in males, yet the inflammatory state was attenuated under this condition. Although the up-regulation of OGT does not necessarily indicate an increase in O-GlcNAcylation, further investigation is needed to understand how SCFAs modulate O-GlcNAcylation in the retina.

While research in this area is limited, current studies suggest an interaction between SCFAs and O-GlcNAcylation. SCFAs up regulate O-GlcNAcylation levels in several diseases and cells, such as in colonic epithelial cells (Zhao et al., 2020) and in a hepatocellular carcinoma mouse model(Zhou et al., 2023).

We then shifted our focus to O-GlcNAcylation in microglial cells. Strikingly different from the results observed *in vivo*, the protein level of O-GlcNAc did not respond to SCFAs in microglial cells derived from males. However, it was significantly downregulated with or without TNFα stimulation in microglial cells derived from females. O-GlcNAcylation was

found to be dramatically up-regulated in the LPS-induced BV2 cells (a mouse microglial cell line). LPS stimulation increased the O-GlcNAcylation of c-Rel via NF-κB, while glucosamine (GlcN) attenuated the effect caused by LPS. NF-κB serves as the principal regulator of pro-inflammatory genes, such as inducible NOS (iNOS). The O-GlcNAcylation of total nucleocytoplasmic proteins was suppressed by GlcN, along with the level of iNOS and NF-κB, indicating that the promotion of O-GlcNAcylation was observed in microglial cells under pathological conditions, while inhibition of these conditions resulted in a decrease in O-GlcNAcylation(Hwang et al., 2013), Our data further verified this finding in primary isolated microglial cells.

Although, we revealed that SCFAs might affect O-GlcNAcylation pathways in the retina of laser-induced CNV males, this was not specific to microglial cells. Additionally, although SCFAs treatment did not exhibit any modulation to O-GlcNAcylation in female retina overall, the inhibitory effect was found in female microglial cells.

Our study provides initial insights into the correlation between SCFAs and O-GlcNAcylation in the retina. Nevertheless, the precise regulatory effects and underlying mechanisms remain unclear, and it is uncertain whether different effects may exist in various types of retinal cells. Further research is essential to fully understand these relationships.

4.5 SCFAs has no impact on calcium ($Ca2^{+}$) pathway in microglia

Many functions of microglia have been found to be associated with intracellular calcium pathway (Farber and Kettenmann, 2006). For instance, the administration of a specific Ca^{2+} - ATPase inhibitor of endoplasmic reticulum, thapsigargin have been shown to prevent LPS-induced microglial activation and migration *ex vivo* (Sunkaria et al., 2016). In vitro experiments demonstrated that thapsigargin significantly inhibits the phagocytosis in both microglial cell line and isolated primary microglial cells (Morales-Ropero et al., 2021). Furthermore, microglial activation leads to a persistent elevation of intracellular calcium levels (Farber and Kettenmann, 2006).

SCFAs were found to raise intracellular calcium levels in the intestinal secretin tumor cell-1 cell line *in vitro* (Kumar et al., 2021) and enhance cecal calcium fluxes *in vivo* (Thammayon et al., 2024), this may due to the specifically activation of SCFAs receptor

GPR43(Xu et al., 2019). This study aimed to investigate the impact of SCFAs on calcium signaling in microglia. The results indicated that SCFAs did not affect the binding of Ca^{2+} to the membrane of microglia derived from both male and female, possibly due to the lower presence of GPR43 on the microglia membrane. Additionally, given the large deviation in this experiment and the use of only one experimental method for detection, further investigation is needed to determine whether SCFA acts on Ca^{2+} pathway in microglia.

4.6 Limitations and outlook

This study primarily investigated the impact of SCFAs on the CNV mouse model and primary microglial cells. However, there are limitations to consider.

While RNA sequencing analysis revealed that SCFAs treatment modulates the expression of genes that associated with vascularization and inflammatory response, the specific target genes within different retinal cell types or the activation of pathways could not be further elucidated through this method. Additionally, regulation at the RNA level can serve as a valuable reference for understanding the effects of SCFAs, but it cannot capture changes in protein levels or elucidate specific mechanisms.

Hub genes analysis aims to identify a set of genes that exhibit the strongest correlation among DEGs, serving as initial targets for further investigation. It is important to note that the identification of these 15 genes does not imply that they are the most critical, nor does it render other DEGs irrelevant. Rather, they will be utilized as a starting point for subsequent discussions within this study. Future plans involve utilizing experimental methods to assess the impact of SCFAs treatment on the protein expression of these hub genes in retinal cells, as well as exploring the upstream and downstream pathways to delve deeper into the mechanism of action of SCFAs.

SCFAs have been shown to impact various types of retinal cells during treatment. Specifically, it regulates genes associated with inflammatory responses and microglial cell activation at the RNA level, as well as decrease the density of $Iba1^{+}$ cells in the retina. Given the challenges in obtaining retinal microglia and their limited quantity, we initiated our in vitro studies using neonatal microglia which possess similar functions and are more

readily available in larger quantities. Through a series of experiments, we aimed to identify the most promising direction for further investigation, ultimately discovering that SCFAs can directly influence the phagocytic activity of microglia. Further investigation is warranted to understand the direct effects of SCFAs on adult retina microglial cells.

Furthermore, our study revealed that SCFAs treatment elicits different responses in males and females, both in vivo and in vitro. Whether it be attributed to sample size limitations or distinct underlying mechanisms remain unclear and needed to be further investigated.

Lastly, the research specifically focused on one mixture of SCFAs including acetate, butyrate, and propionate. Future studies will explore whether individual components of SCFAs can provide protection against laser-induced retinal damage.

5. Summary

Age-related macular degeneration (AMD) is a leading cause of blindness worldwide. Choroidal neovascularization (CNV) in late AMD, known as neovascular AMD, results in retinal degeneration and exudation. Retinal microglial cells play a crucial role in local inflammation, potentially impacting vision in nAMD. SCFAs have emerged as potential treatments due to their anti-neovascularization and anti-inflammatory properties. Using a laser-induced CNV mouse model, we investigated the effects of SCFA treatment.

We found that SCFAs treatment suppresses both neovascularization and inflammation in a nAMD-featured mouse model. SCFA reduced CNV area in retina and lesion volume in choroid, attenuated retinal inflammation, and decreased retinal Iba^+ cells density and microglial activation *in vivo*. When considering sex differences, the effect of SCFAs on microglial cells was more pronounced in males comparing with females. SCFAs suppressed phagocytosis in male microglial cells and O-GlcNAcylation in female microglial cells *in vitro*.

Our findings highlight the beneficial effect of SCFA treatment on the progression of retinal neovascularization and inflammation, suggesting a promising avenue for targeted therapeutic intervention.

Reference

A., B., J., C., F., M., J-A., C., J-C., C. & P., P. 2000. Mucin secretion is modulated by luminal factors in the isolated vascularly perfused rat colon. *Gut,* 46**,** 6.

AHO, V. T. E., HOUSER, M. C., PEREIRA, P. A. B., CHANG, J., RUDI, K., PAULIN, L., HERTZBERG, V., AUVINEN, P., TANSEY, M. G. & SCHEPERJANS, F. 2021. Relationships of gut microbiota, short-chain fatty acids, inflammation, and the gut barrier in Parkinson's disease. *Mol Neurodegener,* 16**,** 6.

ALLIOT, F., GODIN, I. & PESSAC, B. 1999. Microglia derive from progenitors, originating from the yolk sac, and which proliferate in the brain. *Brain Res Dev Brain Res,* 117**,** 145-52.

AMBATI, J. & FOWLER, B. J. 2012. Mechanisms of age-related macular degeneration. *Neuron,* 75**,** 26-39.

ANDERSON, D. H., MULLINS, R. F., HAGEMAN, G. S. & JOHNSON, L. V. 2002. A role for local inflammation in the formation of drusen in the aging eye. *Am J Ophthalmol,* 134**,** 411-31.

ANDERSON, S. R., ROBERTS, J. M., ZHANG, J., STEELE, M. R., ROMERO, C. O., BOSCO, A. & VETTER, M. L. 2019. Developmental Apoptosis Promotes a Disease-Related Gene Signature and Independence from CSF1R Signaling in Retinal Microglia. *Cell Rep,* 27**,** 2002-2013 e5.

ANG, Z., ER, J. Z., TAN, N. S., LU, J., LIOU, Y. C., GROSSE, J. & DING, J. L. 2016. Human and mouse monocytes display distinct signalling and cytokine profiles upon stimulation with FFAR2/FFAR3 short-chain fatty acid receptor agonists. *Sci Rep,* 6**,** 34145.

ARMENTO, A., UEFFING, M. & CLARK, S. J. 2021. The complement system in age-related macular degeneration. *Cell Mol Life Sci,* 78**,** 4487-4505.

BAFFI, J., BYRNES, G., CHAN, C. C. & CSAKY, K. G. 2000. Choroidal neovascularization in the rat induced by adenovirus mediated expression of vascular endothelial growth factor. *Invest Ophthalmol Vis Sci,* 41**,** 3582-9.

BAKRI, S. J., THORNE, J. E., HO, A. C., EHLERS, J. P., SCHOENBERGER, S. D., YEH, S. & KIM, S. J. 2019. Safety and Efficacy of Anti-Vascular Endothelial Growth Factor Therapies for Neovascular Age-Related Macular Degeneration: A Report by the American Academy of Ophthalmology. *Ophthalmology,* 126**,** 55-63.

BAUDOIN, L. & ISSAD, T. 2014. O-GlcNAcylation and Inflammation: A Vast Territory to Explore. *Front Endocrinol (Lausanne),* 5**,** 235.

BIRD, A. C., PHILLIPS, R. L. & HAGEMAN, G. S. 2014. Geographic atrophy: a histopathological assessment. *JAMA Ophthalmol,* 132**,** 338-45.

BIRDSEY, G. M., SHAH, A. V., DUFTON, N., REYNOLDS, L. E., OSUNA ALMAGRO, L., YANG, Y., ASPALTER, I. M., KHAN, S. T., MASON, J. C., DEJANA, E., GOTTGENS, B., HODIVALA-DILKE, K., GERHARDT, H., ADAMS, R. H. & RANDI, A. M. 2015. The endothelial transcription factor ERG promotes vascular stability and growth through Wnt/beta-catenin signaling. *Dev Cell,* 32**,** 82-96.

BOETS, E., DEROOVER, L., HOUBEN, E., VERMEULEN, K., GOMAND, S. V., DELCOUR, J. A. & VERBEKE, K. 2015. Quantification of in Vivo Colonic Short Chain Fatty Acid Production from Inulin. *Nutrients,* 7**,** 8916-29.

BROWN, G. C. & NEHER, J. J. 2014. Microglial phagocytosis of live neurons. *Nat Rev Neurosci,* 15**,** 209-16.

BUSCH, C., RAU, S., SEKULIC, A., PERIE, L., HUBER, C., GEHRKE, M., JOUSSEN, A. M., ZIPFEL, P. F., WILDNER, G., SKERKA, C. & STRAUSS, O. 2023. Increased plasma level of terminal complement complex in AMD patients: potential functional consequences for RPE cells. *Front Immunol,* 14**,** 1200725.

CAO, S., WALKER, G. B., WANG, X., CUI, J. Z. & MATSUBARA, J. A. 2013. Altered cytokine profiles of human retinal pigment epithelium: oxidant injury and replicative senescence. *Mol Vis,* 19**,** 718-28.

CHANG, Y. H., WENG, C. L. & LIN, K. I. 2020. O-GlcNAcylation and its role in the immune system. *J Biomed Sci,* 27**,** 57.

CHECCHIN, D., SENNLAUB, F., LEVAVASSEUR, E., LEDUC, M. & CHEMTOB, S. 2006. Potential role of microglia in retinal blood vessel formation. *Invest Ophthalmol Vis Sci,* 47**,** 3595-602.

CHEN, N., WU, J., WANG, J., PIRI, N., CHEN, F., XIAO, T., ZHAO, Y., SUN, D., KAPLAN, H. J. & SHAO, H. 2021. Short chain fatty acids inhibit endotoxin-induced uveitis and inflammatory responses of retinal astrocytes. *Exp Eye Res,* 206**,** 108520.

CHENG, S. C., HUANG, W. C., JH, S. P., WU, Y. H. & CHENG, C. Y. 2019. Quercetin Inhibits the Production of IL-1beta-Induced Inflammatory Cytokines and Chemokines in ARPE-19 Cells via the MAPK and NF-kappaB Signaling Pathways. *Int J Mol Sci,* 20.

CHERBUT, C., AUBE, A. C., BLOTTIERE, H. M. & GALMICHE, J. P. 1997. Effects of short-chain fatty acids on gastrointestinal motility. *Scand J Gastroenterol Suppl,* 222**,** 58-61.

CHUN, E., LAVOIE, S., FONSECA-PEREIRA, D., BAE, S., MICHAUD, M., HOVEYDA, H. R., FRASER, G. L., GALLINI COMEAU, C. A., GLICKMAN, J. N., FULLER, M. H., LAYDEN, B. T. & GARRETT, W. S. 2019. Metabolite-Sensing Receptor Ffar2 Regulates Colonic Group 3 Innate Lymphoid Cells and Gut Immunity. *Immunity,* 51**,** 871-884 e6.

CLEMONS, T. E., MILTON, R. C., KLEIN, R., SEDDON, J. M., FERRIS, F. L., 3RD & AGE-RELATED EYE DISEASE STUDY RESEARCH, G. 2005. Risk factors for the incidence of Advanced Age-Related Macular Degeneration in the Age-Related Eye Disease Study (AREDS) AREDS report no. 19. *Ophthalmology,* 112**,** 533-9.

COLOMBO, A. V., SADLER, R. K., LLOVERA, G., SINGH, V., ROTH, S., HEINDL, S., SEBASTIAN MONASOR, L., VERHOEVEN, A., PETERS, F., PARHIZKAR, S., KAMP, F., GOMEZ DE AGUERO, M., MACPHERSON, A. J., WINKLER, E., HERMS, J., BENAKIS, C., DICHGANS, M., STEINER, H., GIERA, M., HAASS, C., TAHIROVIC, S. & LIESZ, A. 2021. Microbiota-derived short chain fatty acids modulate microglia and promote Abeta plaque deposition. *Elife,* 10.

COMBADIERE, C., FEUMI, C., RAOUL, W., KELLER, N., RODERO, M., PEZARD, A., LAVALETTE, S., HOUSSIER, M., JONET, L., PICARD, E., DEBRE, P., SIRINYAN,

M., DETERRE, P., FERROUKHI, T., COHEN, S. Y., CHAUVAUD, D., JEANNY, J. C., CHEMTOB, S., BEHAR-COHEN, F. & SENNLAUB, F. 2007. CX3CR1-dependent subretinal microglia cell accumulation is associated with cardinal features of age-related macular degeneration. *J Clin Invest,* 117**,** 2920-8.

CORREA-OLIVEIRA, R., FACHI, J. L., VIEIRA, A., SATO, F. T. & VINOLO, M. A. 2016. Regulation of immune cell function by short-chain fatty acids. *Clin Transl Immunology,* 5**,** e73.

CUMMINGS, J. H. & MACFARLANE, G. T. 1991. The control and consequences of bacterial fermentation in the human colon. *J Appl Bacteriol,* 70**,** 443-59.

CUMMINGS, J. H., POMARE, E. W., BRANCH, W. J., NAYLOR, C. P. & MACFARLANE, G. T. 1987. Short chain fatty acids in human large intestine, portal, hepatic and venous blood. *Gut,* 28**,** 1221-7.

CUNHA-VAZ, J. G. 1976. The blood-retinal barriers. *Doc Ophthalmol,* 41**,** 287-327.

DAVIS, M. D., GANGNON, R. E., LEE, L. Y., HUBBARD, L. D., KLEIN, B. E., KLEIN, R., FERRIS, F. L., BRESSLER, S. B., MILTON, R. C. & AGE-RELATED EYE DISEASE STUDY, G. 2005. The Age-Related Eye Disease Study severity scale for age-related macular degeneration: AREDS Report No. 17. *Arch Ophthalmol,* 123**,** 1484-98.

DONOSO, L. A., KIM, D., FROST, A., CALLAHAN, A. & HAGEMAN, G. 2006. The role of inflammation in the pathogenesis of age-related macular degeneration. *Surv Ophthalmol,* 51**,** 137-52.

DROHO, S., CUDA, C. M., PERLMAN, H. & LAVINE, J. A. 2021. Macrophage-derived interleukin-6 is necessary and sufficient for choroidal angiogenesis. *Sci Rep,* 11**,** 18084.

DROHO, S., RAJESH, A., CUDA, C. M., PERLMAN, H. & LAVINE, J. A. 2023a. CD11c+ macrophages are proangiogenic and necessary for experimental choroidal neovascularization. *JCI Insight,* 8.

DROHO, S., VOIGT, A. P., STERLING, J. K., RAJESH, A., CHAN, K. S., CUDA, C. M., PERLMAN, H. & LAVINE, J. A. 2023b. NR4A1 deletion promotes pro-angiogenic polarization of macrophages derived from classical monocytes in a mouse model of neovascular age-related macular degeneration. *J Neuroinflammation,* 20**,** 238.

EISENFELD, A. J., BUNT-MILAM, A. H. & SARTHY, P. V. 1984. Muller cell expression of glial fibrillary acidic protein after genetic and experimental photoreceptor degeneration in the rat retina. *Invest Ophthalmol Vis Sci,* 25**,** 1321-8.

ENCARNACAO, J. C., ABRANTES, A. M., PIRES, A. S. & BOTELHO, M. F. 2015. Revisit dietary fiber on colorectal cancer: butyrate and its role on prevention and treatment. *Cancer Metastasis Rev,* 34**,** 465-78.

ERNY, D., HRABE DE ANGELIS, A. L., JAITIN, D., WIEGHOFER, P., STASZEWSKI, O., DAVID, E., KEREN-SHAUL, H., MAHLAKOIV, T., JAKOBSHAGEN, K., BUCH, T., SCHWIERZECK, V., UTERMOHLEN, O., CHUN, E., GARRETT, W. S., MCCOY, K. D., DIEFENBACH, A., STAEHELI, P., STECHER, B., AMIT, I. & PRINZ, M. 2015. Host microbiota constantly control maturation and function of microglia in the CNS. *Nat Neurosci,* 18**,** 965-77.

FAN, W., HUANG, W., CHEN, J., LI, N., MAO, L. & HOU, S. 2022. Retinal microglia: Functions and diseases. *Immunology,* 166**,** 268-286.

FARBER, K. & KETTENMANN, H. 2006. Functional role of calcium signals for microglial function. *Glia,* 54**,** 656-665.

FERRIS, F. L., 3RD, WILKINSON, C. P., BIRD, A., CHAKRAVARTHY, U., CHEW, E., CSAKY, K., SADDA, S. R. & BECKMAN INITIATIVE FOR MACULAR RESEARCH CLASSIFICATION, C. 2013. Clinical classification of age-related macular degeneration. *Ophthalmology,* 120**,** 844-51.

FERRIS, F. L., DAVIS, M. D., CLEMONS, T. E., LEE, L. Y., CHEW, E. Y., LINDBLAD, A. S., MILTON, R. C., BRESSLER, S. B., KLEIN, R. & AGE-RELATED EYE DISEASE STUDY RESEARCH, G. 2005. A simplified severity scale for age-related macular degeneration: AREDS Report No. 18. *Arch Ophthalmol,* 123**,** 1570-4.

FRASER-BELL, S., WU, J., KLEIN, R., AZEN, S. P. & VARMA, R. 2006. Smoking, alcohol intake, estrogen use, and age-related macular degeneration in Latinos: the Los Angeles Latino Eye Study. *Am J Ophthalmol,* 141**,** 79-87.

FU, Y., ZHANG, Z., WEBSTER, K. A. & PAULUS, Y. M. 2024. Treatment Strategies for Anti-VEGF Resistance in Neovascular Age-Related Macular Degeneration by Targeting Arteriolar Choroidal Neovascularization. *Biomolecules,* 14.

GINHOUX, F., GRETER, M., LEBOEUF, M., NANDI, S., SEE, P., GOKHAN, S., MEHLER, M. F., CONWAY, S. J., NG, L. G., STANLEY, E. R., SAMOKHVALOV, I. M. & MERAD, M. 2010. Fate mapping analysis reveals that adult microglia derive from primitive macrophages. *Science,* 330**,** 841-5.

GREEN, W. R. & ENGER, C. 1993. Age-related macular degeneration histopathologic studies. The 1992 Lorenz E. Zimmerman Lecture. *Ophthalmology,* 100**,** 1519-35.

GRIGORYAN, E. N. 2022. Self-Organization of the Retina during Eye Development, Retinal Regeneration In Vivo, and in Retinal 3D Organoids In Vitro. *Biomedicines,* 10.

GROSSNIKLAUS, H. E., GEISERT, E. E. & NICKERSON, J. M. 2015. Introduction to the Retina. *Prog Mol Biol Transl Sci,* 134**,** 383-96.

GROSSNIKLAUS, H. E., LING, J. X., WALLACE, T. M., DITHMAR, S., LAWSON, D. H., COHEN, C., ELNER, V. M., ELNER, S. G. & STERNBERG, P., JR. 2002. Macrophage and retinal pigment epithelium expression of angiogenic cytokines in choroidal neovascularization. *Mol Vis,* 8**,** 119-26.

HAFEZI, F., STEINBACH, J. P., MARTI, A., MUNZ, K., WANG, Z. Q., WAGNER, E. F., AGUZZI, A. & REME, C. E. 1997. The absence of c-fos prevents light-induced apoptotic cell death of photoreceptors in retinal degeneration in vivo. *Nat Med,* 3**,** 346-9.

HALLAK, J. A., DE SISTERNES, L., OSBORNE, A., YASPAN, B., RUBIN, D. L. & LENG, T. 2019. Imaging, Genetic, and Demographic Factors Associated With Conversion to Neovascular Age-Related Macular Degeneration: Secondary Analysis of a Randomized Clinical Trial. *JAMA Ophthalmol,* 137**,** 738-744.

HAMMOND, T. R., DUFORT, C., DISSING-OLESEN, L., GIERA, S., YOUNG, A., WYSOKER, A., WALKER, A. J., GERGITS, F., SEGEL, M., NEMESH, J., MARSH, S. E., SAUNDERS, A., MACOSKO, E., GINHOUX, F., CHEN, J., FRANKLIN, R. J. M., PIAO, X., MCCARROLL, S. A. & STEVENS, B. 2019. Single-Cell RNA Sequencing of Microglia throughout the Mouse Lifespan and in the Injured Brain Reveals Complex Cell-State Changes. *Immunity,* 50**,** 253-271 e6.

HASEGAWA, E., OSHIMA, Y., TAKEDA, A., SAEKI, K., YOSHIDA, H., SONODA, K. H. & ISHIBASHI, T. 2012. IL-27 inhibits pathophysiological intraocular neovascularization due to laser burn. *J Leukoc Biol,* 91**,** 267-73.

HOLT, G. D., SNOW, C. M., SENIOR, A., HALTIWANGER, R. S., GERACE, L. & HART, G. W. 1987. Nuclear pore complex glycoproteins contain cytoplasmically disposed O-linked N-acetylglucosamine. *J Cell Biol,* 104**,** 1157-64.

HOLTKAMP, G. M., KIJLSTRA, A., PEEK, R. & DE VOS, A. F. 2001. Retinal pigment epithelium-immune system interactions: cytokine production and cytokine-induced changes. *Prog Retin Eye Res,* 20**,** 29-48.

HOON, M., OKAWA, H., DELLA SANTINA, L. & WONG, R. O. 2014. Functional architecture of the retina: development and disease. *Prog Retin Eye Res,* 42**,** 44-84.

HORMEL, T. T., JIA, Y., JIAN, Y., HWANG, T. S., BAILEY, S. T., PENNESI, M. E., WILSON, D. J., MORRISON, J. C. & HUANG, D. 2021. Plexus-specific retinal vascular anatomy and pathologies as seen by projection-resolved optical coherence tomographic angiography. *Prog Retin Eye Res,* 80**,** 100878.

HUANG, Y., WANG, Z., YE, B., MA, J. H., JI, S., SHENG, W., YE, S., OU, Y., PENG, Y., YANG, X., CHEN, J. & TANG, S. 2023. Sodium butyrate ameliorates diabetic retinopathy in mice via the regulation of gut microbiota and related short-chain fatty acids. *J Transl Med,* 21**,** 451.

HUUSKONEN, J., SUURONEN, T., NUUTINEN, T., KYRYLENKO, S. & SALMINEN, A. 2004. Regulation of microglial inflammatory response by sodium butyrate and short-chain fatty acids. *Br J Pharmacol,* 141**,** 874-80.

HWANG, S. Y., HWANG, J. S., KIM, S. Y. & HAN, I. O. 2013. O-GlcNAcylation and p50/p105 binding of c-Rel are dynamically regulated by LPS and glucosamine in BV2 microglia cells. *Br J Pharmacol,* 169**,** 1551-60.

INDARAM, M., MA, W., ZHAO, L., FARISS, R. N., RODRIGUEZ, I. R. & WONG, W. T. 2015. 7-Ketocholesterol increases retinal microglial migration, activation, and angiogenicity: a potential pathogenic mechanism underlying age-related macular degeneration. *Sci Rep,* 5**,** 9144.

ITO, S., SAWADA, M., HANEDA, M., ISHIDA, Y. & ISOBE, K. 2006. Amyloid-beta peptides induce several chemokine mRNA expressions in the primary microglia and Ra2 cell line via the PI3K/Akt and/or ERK pathway. *Neurosci Res,* 56**,** 294-9.

JAWAD, S., LIU, B., LI, Z., KATAMAY, R., CAMPOS, M., WEI, L., SEN, H. N., LING, D., MARTINEZ ESTRADA, F., AMARAL, J., CHAN, C. C., FARISS, R., GORDON, S. & NUSSENBLATT, R. B. 2013. The role of macrophage class a scavenger receptors in a laser-induced murine choroidal neovascularization model. *Invest Ophthalmol Vis Sci,* 54**,** 5959-70.

JO, Y. J., SONODA, K. H., OSHIMA, Y., TAKEDA, A., KOHNO, R., YAMADA, J., HAMURO, J., YANG, Y., NOTOMI, S., HISATOMI, T. & ISHIBASHI, T. 2011. Establishment of a new animal model of focal subretinal fibrosis that resembles disciform lesion in advanced age-related macular degeneration. *Invest Ophthalmol Vis Sci,* 52**,** 6089-95.

KAUPPINEN, A., PATERNO, J. J., BLASIAK, J., SALMINEN, A. & KAARNIRANTA, K. 2016. Inflammation and its role in age-related macular degeneration. *Cell Mol Life Sci,* 73**,** 1765-86.

KEENAN, T. D., AGRON, E., DOMALPALLY, A., CLEMONS, T. E., VAN ASTEN, F., WONG, W. T., DANIS, R. G., SADDA, S., ROSENFELD, P. J., KLEIN, M. L., RATNAPRIYA, R., SWAROOP, A., FERRIS, F. L., 3RD, CHEW, E. Y. & GROUP, A. R. 2018. Progression of Geographic Atrophy in Age-related Macular Degeneration: AREDS2 Report Number 16. *Ophthalmology,* 125**,** 1913-1928.

KINUTHIA, U. M., WOLF, A. & LANGMANN, T. 2020. Microglia and Inflammatory Responses in Diabetic Retinopathy. *Front Immunol,* 11**,** 564077.

KLEIN, R., MEUER, S. M., MYERS, C. E., BUITENDIJK, G. H., ROCHTCHINA, E., CHOUDHURY, F., DE JONG, P. T., MCKEAN-COWDIN, R., IYENGAR, S. K., GAO, X., LEE, K. E., VINGERLING, J. R., MITCHELL, P., KLAVER, C. C., WANG, J. J. & KLEIN, B. E. 2014. Harmonizing the classification of age-related macular degeneration in the three-continent AMD consortium. *Ophthalmic Epidemiol,* 21**,** 14-23.

KNICKELBEIN, J. E., CHAN, C. C., SEN, H. N., FERRIS, F. L. & NUSSENBLATT, R. B. 2015. Inflammatory Mechanisms of Age-related Macular Degeneration. *Int Ophthalmol Clin,* 55**,** 63-78.

KNUPP, C., MUNRO, P. M., LUTHER, P. K., EZRA, E. & SQUIRE, J. M. 2000. Structure of abnormal molecular assemblies (collagen VI) associated with human full thickness macular holes. *J Struct Biol,* 129**,** 38-47.

KUMAR, V., KHARE, P., DEVI, K., KAUR, J., KUMAR, V., KIRAN KONDEPUDI, K., CHOPRA, K. & BISHNOI, M. 2021. Short-chain fatty acids increase intracellular calcium levels and enhance gut hormone release from STC-1 cells via transient receptor potential Ankyrin1. *Fundam Clin Pharmacol,* 35**,** 1004-1017.

LAD, E. M., COUSINS, S. W., VAN ARNAM, J. S. & PROIA, A. D. 2015. Abundance of infiltrating CD163+ cells in the retina of postmortem eyes with dry and neovascular age-related macular degeneration. *Graefes Arch Clin Exp Ophthalmol,* 253**,** 1941-5.

LAMBERT, N. G., ELSHELMANI, H., SINGH, M. K., MANSERGH, F. C., WRIDE, M. A., PADILLA, M., KEEGAN, D., HOGG, R. E. & AMBATI, B. K. 2016. Risk factors and biomarkers of age-related macular degeneration. *Prog Retin Eye Res,* 54**,** 64-102.

LAMBERT, V., LECOMTE, J., HANSEN, S., BLACHER, S., GONZALEZ, M. L., STRUMAN, I., SOUNNI, N. E., ROZET, E., DE TULLIO, P., FOIDART, J. M., RAKIC, J. M. & NOEL, A. 2013. Laser-induced choroidal neovascularization model to study age-related macular degeneration in mice. *Nat Protoc,* 8**,** 2197-211.

LAMBUK, L., IEZHITSA, I., AGARWAL, R., AGARWAL, P., PERESYPKINA, A., POBEDA, A. & ISMAIL, N. M. 2021. Magnesium acetyltaurate prevents retinal damage and visual impairment in rats through suppression of NMDA-induced

upregulation of NF-kappaB, p53 and AP-1 (c-Jun/c-Fos). *Neural Regen Res,* 16**,** 2330-2344.

LEE, S. Y., SURBECK, J. W., DRAKE, M., SAUNDERS, A., JIN, H. D., SHAH, V. A. & RAJALA, R. V. 2020. Increased Glial Fibrillary Acid Protein and Vimentin in Vitreous Fluid as a Biomarker for Proliferative Vitreoretinopathy. *Invest Ophthalmol Vis Sci,* 61**,** 22.

LEUNG, K. W., BARNSTABLE, C. J. & TOMBRAN-TINK, J. 2009. Bacterial endotoxin activates retinal pigment epithelial cells and induces their degeneration through IL-6 and IL-8 autocrine signaling. *Mol Immunol,* 46**,** 1374-86.

LI, L., ZHU, M., WU, W., QIN, B., GU, J., TU, Y., CHEN, J., LIU, D., SHI, Y., LIU, X., SANG, A. & DING, D. 2020. Brivanib, a multitargeted small-molecule tyrosine kinase inhibitor, suppresses laser-induced CNV in a mouse model of neovascular AMD. *J Cell Physiol,* 235**,** 1259-1273.

LIN, J. B., SANTEFORD, A., COLASANTI, J. J., LEE, Y., SHAH, A. V., WANG, T. J., RUZYCKI, P. A. & APTE, R. S. 2024. Targeting cell-type-specific, choroid-peripheral immune signaling to treat age-related macular degeneration. *Cell Rep Med,* 5**,** 101353.

LUNA, G., LEWIS, G. P., BANNA, C. D., SKALLI, O. & FISHER, S. K. 2010. Expression profiles of nestin and synemin in reactive astrocytes and Muller cells following retinal injury: a comparison with glial fibrillar acidic protein and vimentin. *Mol Vis,* 16**,** 2511-23.

LYONS, M. A. & BROWN, A. J. 2001. 7-Ketocholesterol delivered to mice in chylomicron remnant-like particles is rapidly metabolised, excreted and does not accumulate in aorta. *Biochim Biophys Acta,* 1530**,** 209-18.

LYZOGUBOV, V., DASSO, M., BORA, N. & BORA, P. S. 2020. Role of thalidomide, senicapoc, and sodium butyrate in choroidal neovascularization. *Biochem Biophys Res Commun,* 530**,** 367-373.

MA, Y., ASHANDER, L. M., APPUKUTTAN, B., RYAN, F. J., TAN, A. C. R., MATTHEWS, J. M., MICHAEL, M. Z., LYNN, D. J. & SMITH, J. R. 2023. Selective Transcription

Factor Blockade Reduces Human Retinal Endothelial Cell Expression of Intercellular Adhesion Molecule-1 and Leukocyte Binding. *Int J Mol Sci,* 24.

MACFARLANE, S. & MACFARLANE, G. T. 2003. Regulation of short-chain fatty acid production. *Proc Nutr Soc,* 62**,** 67-72.

MADEIRA, M. H., RASHID, K., AMBROSIO, A. F., SANTIAGO, A. R. & LANGMANN, T. 2018. Blockade of microglial adenosine A2A receptor impacts inflammatory mechanisms, reduces ARPE-19 cell dysfunction and prevents photoreceptor loss in vitro. *Sci Rep,* 8**,** 2272.

MARIN, A. I., POPPELAARS, F., WAGNER, B. D., PALESTINE, A. G., PATNAIK, J. L., HOLERS, V. M., FRAZER-ABEL, A. A., MATHIAS, M. T., MANOHARAN, N., FONTEH, C. N., MANDAVA, N., LYNCH, A. M. & UNIVERSITY OF COLORADO RETINA RESEARCH, G. 2022. Sex and Age-Related Differences in Complement Factors Among Patients With Intermediate Age-Related Macular Degeneration. *Transl Vis Sci Technol,* 11**,** 22.

MASLOWSKI, K. M., VIEIRA, A. T., NG, A., KRANICH, J., SIERRO, F., YU, D., SCHILTER, H. C., ROLPH, M. S., MACKAY, F., ARTIS, D., XAVIER, R. J., TEIXEIRA, M. M. & MACKAY, C. R. 2009. Regulation of inflammatory responses by gut microbiota and chemoattractant receptor GPR43. *Nature,* 461**,** 1282-6.

MATCOVITCH-NATAN, O., WINTER, D. R., GILADI, A., VARGAS AGUILAR, S., SPINRAD, A., SARRAZIN, S., BEN-YEHUDA, H., DAVID, E., ZELADA GONZALEZ, F., PERRIN, P., KEREN-SHAUL, H., GURY, M., LARA-ASTAISO, D., THAISS, C. A., COHEN, M., BAHAR HALPERN, K., BARUCH, K., DECZKOWSKA, A., LORENZO-VIVAS, E., ITZKOVITZ, S., ELINAV, E., SIEWEKE, M. H., SCHWARTZ, M. & AMIT, I. 2016. Microglia development follows a stepwise program to regulate brain homeostasis. *Science,* 353**,** aad8670.

MISHRA, S. P., JAIN, S., WANG, B., WANG, S., MILLER, B. C., LEE, J. Y., BORLONGAN, C. V., JIANG, L., POLLAK, J., TARAPHDER, S., LAYDEN, B. T., RANE, S. G. & YADAV, H. 2024. Abnormalities in microbiota/butyrate/FFAR3 signaling in aging gut impair brain function. *JCI Insight,* 9.

MORALES-ROPERO, J. M., ARROYO-UREA, S., NEUBRAND, V. E., MARTIN-OLIVA, D., MARIN-TEVA, J. L., CUADROS, M. A., VANGHELUWE, P., NAVASCUES, J., MATA, A. M. & SEPULVEDA, M. R. 2021. The endoplasmic reticulum Ca(2+) - ATPase SERCA2b is upregulated in activated microglia and its inhibition causes opposite effects on migration and phagocytosis. *Glia,* 69**,** 842-857.

NAGINENI, C. N., KOMMINENI, V. K., WILLIAM, A., DETRICK, B. & HOOKS, J. J. 2012. Regulation of VEGF expression in human retinal cells by cytokines: implications for the role of inflammation in age-related macular degeneration. *J Cell Physiol,* 227**,** 116-26.

NEBEL, C., ASLANIDIS, A., RASHID, K. & LANGMANN, T. 2017. Activated microglia trigger inflammasome activation and lysosomal destabilization in human RPE cells. *Biochem Biophys Res Commun,* 484**,** 681-686.

NOHR, M. K., EGEROD, K. L., CHRISTIANSEN, S. H., GILLE, A., OFFERMANNS, S., SCHWARTZ, T. W. & MOLLER, M. 2015. Expression of the short chain fatty acid receptor GPR41/FFAR3 in autonomic and somatic sensory ganglia. *Neuroscience,* 290**,** 126-37.

NURNBERG, C., KOCIOK, N., BROCKMANN, C., LISCHKE, T., CRESPO-GARCIA, S., REICHHART, N., WOLF, S., BAUMGRASS, R., EMING, S. A., BEER-HAMMER, S. & JOUSSEN, A. M. 2018. Myeloid cells contribute indirectly to VEGF expression upon hypoxia via activation of Muller cells. *Exp Eye Res,* 166**,** 56-69.

OKUNUKI, Y., MUKAI, R., PEARSALL, E. A., KLOKMAN, G., HUSAIN, D., PARK, D. H., KOROBKINA, E., WEINER, H. L., BUTOVSKY, O., KSANDER, B. R., MILLER, J. W. & CONNOR, K. M. 2018. Microglia inhibit photoreceptor cell death and regulate immune cell infiltration in response to retinal detachment. *Proc Natl Acad Sci U S A,* 115**,** E6264-E6273.

PAPADOPOULOS, Z. 2020. Recent Developments in the Treatment of Wet Age-related Macular Degeneration. *Curr Med Sci,* 40**,** 851-857.

PATNALA, R., ARUMUGAM, T. V., GUPTA, N. & DHEEN, S. T. 2017. HDAC Inhibitor Sodium Butyrate-Mediated Epigenetic Regulation Enhances Neuroprotective Function of Microglia During Ischemic Stroke. *Mol Neurobiol,* 54**,** 6391-6411.

PENNESI, M. E., NEURINGER, M. & COURTNEY, R. J. 2012. Animal models of age related macular degeneration. *Mol Aspects Med,* 33**,** 487-509.

POMARE, E. W., BRANCH, W. J. & CUMMINGS, J. H. 1985. Carbohydrate fermentation in the human colon and its relation to acetate concentrations in venous blood. *J Clin Invest,* 75**,** 1448-54.

POZAROWSKA, D. & POZAROWSKI, P. 2016. The era of anti-vascular endothelial growth factor (VEGF) drugs in ophthalmology, VEGF and anti-VEGF therapy. *Cent Eur J Immunol,* 41**,** 311-316.

PROVIS, J. M., PENFOLD, P. L., CORNISH, E. E., SANDERCOE, T. M. & MADIGAN, M. C. 2005. Anatomy and development of the macula: specialisation and the vulnerability to macular degeneration. *Clin Exp Optom,* 88**,** 269-81.

RASHID, K., AKHTAR-SCHAEFER, I. & LANGMANN, T. 2019. Microglia in Retinal Degeneration. *Front Immunol,* 10**,** 1975.

ROWAN, S., JIANG, S., KOREM, T., SZYMANSKI, J., CHANG, M. L., SZELOG, J., CASSALMAN, C., DASURI, K., MCGUIRE, C., NAGAI, R., DU, X. L., BROWNLEE, M., RABBANI, N., THORNALLEY, P. J., BALEJA, J. D., DEIK, A. A., PIERCE, K. A., SCOTT, J. M., CLISH, C. B., SMITH, D. E., WEINBERGER, A., AVNIT-SAGI, T., LOTAN-POMPAN, M., SEGAL, E. & TAYLOR, A. 2017. Involvement of a gut-retina axis in protection against dietary glycemia-induced age-related macular degeneration. *Proc Natl Acad Sci U S A,* 114**,** E4472-E4481.

RUDNICKA, A. R., JARRAR, Z., WORMALD, R., COOK, D. G., FLETCHER, A. & OWEN, C. G. 2012. Age and gender variations in age-related macular degeneration prevalence in populations of European ancestry: a meta-analysis. *Ophthalmology,* 119**,** 571-80.

RYAN, S. J. 1979. The development of an experimental model of subretinal neovascularization in disciform macular degeneration. *Trans Am Ophthalmol Soc,* 77**,** 707-45.

SALAS, A., BADIA, A., FONTRODONA, L., ZAPATA, M., GARCIA-ARUMI, J. & DUARRI, A. 2023. Neovascular Progression and Retinal Dysfunction in the Laser-Induced Choroidal Neovascularization Mouse Model. *Biomedicines,* 11.

SANFORD, J. A., ZHANG, L. J., WILLIAMS, M. R., GANGOITI, J. A., HUANG, C. M. & GALLO, R. L. 2016. Inhibition of HDAC8 and HDAC9 by microbial short-chain fatty acids breaks immune tolerance of the epidermis to TLR ligands. *Sci Immunol,* 1.

SANTOS, A. M., CALVENTE, R., TASSI, M., CARRASCO, M. C., MARTIN-OLIVA, D., MARIN-TEVA, J. L., NAVASCUES, J. & CUADROS, M. A. 2008. Embryonic and postnatal development of microglial cells in the mouse retina. *J Comp Neurol,* 506**,** 224-39.

SATROM, K. M., ENNIS, K., SWEIS, B. M., MATVEEVA, T. M., CHEN, J., HANSON, L., MAHESHWARI, A. & RAO, R. 2018. Neonatal hyperglycemia induces CXCL10/CXCR3 signaling and microglial activation and impairs long-term synaptogenesis in the hippocampus and alters behavior in rats. *J Neuroinflammation,* 15**,** 82.

SCHAEFER, L., HERNANDEZ, H., COATS, R. A., YU, Z., PFLUGFELDER, S. C., BRITTON, R. A. & DE PAIVA, C. S. 2022. Gut-derived butyrate suppresses ocular surface inflammation. *Sci Rep,* 12**,** 4512.

SCHILDERINK, R., VERSEIJDEN, C. & DE JONGE, W. J. 2013. Dietary inhibitors of histone deacetylases in intestinal immunity and homeostasis. *Front Immunol,* 4**,** 226.

SCHLATTERER, K., PESCHEL, A. & KRETSCHMER, D. 2021. Short-Chain Fatty Acid and FFAR2 Activation - A New Option for Treating Infections? *Front Cell Infect Microbiol,* 11**,** 785833.

SCHUETZ, E. & THANOS, S. 2004. Neuro-glial interactions in the adult rat retina after reaxotomy of ganglion cells: examination of neuron survival and phagocytic microglia using fluorescent tracers. *Brain Res Bull,* 62**,** 391-6.

SHAH, A. V., BIRDSEY, G. M. & RANDI, A. M. 2016. Regulation of endothelial homeostasis, vascular development and angiogenesis by the transcription factor ERG. *Vascul Pharmacol,* 86**,** 3-13.

SHAH, S., FILLIER, T., PHAM, T. H., THOMAS, R. & CHEEMA, S. K. 2021. Intraperitoneal Administration of Short-Chain Fatty Acids Improves Lipid Metabolism of Long-Evans Rats in a Sex-Specific Manner. *Nutrients,* 13.

SHEN, Q., ZHANG, R. & BHAT, N. R. 2006. MAP kinase regulation of IP10/CXCL10 chemokine gene expression in microglial cells. *Brain Res,* 1086**,** 9-16.

SHI, D., ZHOU, X. & WANG, H. 2021a. S14G-humanin (HNG) protects retinal endothelial cells from UV-B-induced NLRP3 inflammation activation through inhibiting Egr-1. *Inflamm Res,* 70**,** 1141-1150.

SHI, H., GE, X., MA, X., ZHENG, M., CUI, X., PAN, W., ZHENG, P., YANG, X., ZHANG, P., HU, M., HU, T., TANG, R., ZHENG, K., HUANG, X. F. & YU, Y. 2021b. A fiber-deprived diet causes cognitive impairment and hippocampal microglia-mediated synaptic loss through the gut microbiota and metabolites. *Microbiome,* 9**,** 223.

SHIBUYA, M. 2011. Vascular Endothelial Growth Factor (VEGF) and Its Receptor (VEGFR) Signaling in Angiogenesis: A Crucial Target for Anti- and Pro-Angiogenic Therapies. *Genes Cancer,* 2**,** 1097-105.

SILVA, L. G., FERGUSON, B. S., AVILA, A. S. & FACIOLA, A. P. 2018. Sodium propionate and sodium butyrate effects on histone deacetylase (HDAC) activity, histone acetylation, and inflammatory gene expression in bovine mammary epithelial cells. *J Anim Sci,* 96**,** 5244-5252.

SILVERMAN, S. M. & WONG, W. T. 2018. Microglia in the Retina: Roles in Development, Maturity, and Disease. *Annu Rev Vis Sci,* 4**,** 45-77.

SINGH, N., BENOIT, M. R., ZHOU, J., DAS, B., DAVILA-VELDERRAIN, J., KELLIS, M., TSAI, L. H., HU, X. & YAN, R. 2022. BACE-1 inhibition facilitates the transition from homeostatic microglia to DAM-1. *Sci Adv,* 8**,** eabo1286.

SIVAKUMAR, V., FOULDS, W. S., LUU, C. D., LING, E. A. & KAUR, C. 2011. Retinal ganglion cell death is induced by microglia derived pro-inflammatory cytokines in the hypoxic neonatal retina. *J Pathol,* 224**,** 245-60.

SMITH, P. M., HOWITT, M. R., PANIKOV, N., MICHAUD, M., GALLINI, C. A., BOHLOOLY, Y. M., GLICKMAN, J. N. & GARRETT, W. S. 2013. The microbial metabolites, short-chain fatty acids, regulate colonic Treg cell homeostasis. *Science,* 341**,** 569-73.

SPICHAK, S., DONOSO, F., MOLONEY, G. M., GUNNIGLE, E., BROWN, J. M., CODAGNONE, M., DINAN, T. G. & CRYAN, J. F. 2021. Microbially-derived short-chain fatty acids impact astrocyte gene expression in a sex-specific manner. *Brain Behav Immun Health,* 16**,** 100318.

STRAUSS, O. 2005. The retinal pigment epithelium in visual function. *Physiol Rev,* 85**,** 845-81.

STRIETER, R. M., POLVERINI, P. J., KUNKEL, S. L., ARENBERG, D. A., BURDICK, M. D., KASPER, J., DZUIBA, J., VAN DAMME, J., WALZ, A., MARRIOTT, D. & ET AL. 1995. The functional role of the ELR motif in CXC chemokine-mediated angiogenesis. *J Biol Chem,* 270**,** 27348-57.

SUN, Q. H., LIU, Z. J., ZHANG, L., WEI, H., SONG, L. J., ZHU, S. W., HE, M. B. & DUAN, L. P. 2021. Sex-based differences in fecal short-chain fatty acid and gut microbiota in irritable bowel syndrome patients. *J Dig Dis,* 22**,** 246-255.

SUN, Y., LIN, Z., LIU, C. H., GONG, Y., LIEGL, R., FREDRICK, T. W., MENG, S. S., BURNIM, S. B., WANG, Z., AKULA, J. D., PU, W. T., CHEN, J. & SMITH, L. E. H. 2017. Inflammatory signals from photoreceptor modulate pathological retinal angiogenesis via c-Fos. *J Exp Med,* 214**,** 1753-1767.

SUNKARIA, A., BHARDWAJ, S., HALDER, A., YADAV, A. & SANDHIR, R. 2016. Migration and Phagocytic Ability of Activated Microglia During Post-natal Development is Mediated by Calcium-Dependent Purinergic Signalling. *Mol Neurobiol,* 53**,** 944-954.

TANG, D., CHEN, M., HUANG, X., ZHANG, G., ZENG, L., ZHANG, G., WU, S. & WANG, Y. 2023. SRplot: A free online platform for data visualization and graphing. *PLoS One,* 18**,** e0294236.

TATAR, O., YOERUEK, E., SZURMAN, P., BARTZ-SCHMIDT, K. U., TUBINGEN BEVACIZUMAB STUDY, G., ADAM, A., SHINODA, K., ECKARDT, C., BOEYDEN, V., CLAES, C., PERTILE, G., SCHARIOTH, G. B. & GRISANTI, S. 2008. Effect of bevacizumab on inflammation and proliferation in human choroidal neovascularization. *Arch Ophthalmol,* 126**,** 782-90.

TAUB, D. D., LLOYD, A. R., CONLON, K., WANG, J. M., ORTALDO, J. R., HARADA, A., MATSUSHIMA, K., KELVIN, D. J. & OPPENHEIM, J. J. 1993. Recombinant human interferon-inducible protein 10 is a chemoattractant for human monocytes and T lymphocytes and promotes T cell adhesion to endothelial cells. *J Exp Med,* 177**,** 1809-14.

THAMMAYON, N., WONGDEE, K., TEERAPORNPUNTAKIT, J., PANMANEE, J., CHANPAISAENG, K., CHAROENSETAKUL, N., SRIMONGKOLPITHAK, N., SUNTORNSARATOON, P. & CHAROENPHANDHU, N. 2024. Enhancement of intestinal calcium transport by short-chain fatty acids: roles of Na(+)/H(+) exchanger 3 and transient receptor potential vanilloid subfamily 6. *Am J Physiol Cell Physiol,* 326**,** C317-C330.

THANOS, S. 1991. The Relationship of Microglial Cells to Dying Neurons During Natural Neuronal Cell Death and Axotomy-induced Degeneration of the Rat Retina. *Eur J Neurosci,* 3**,** 1189-1207.

THOMAS, C. J., MIRZA, R. G. & GILL, M. K. 2021. Age-Related Macular Degeneration. *Med Clin North Am,* 105**,** 473-491.

TOBE, T., ORTEGA, S., LUNA, J. D., OZAKI, H., OKAMOTO, N., DEREVJANIK, N. L., VINORES, S. A., BASILICO, C. & CAMPOCHIARO, P. A. 1998. Targeted disruption of the FGF2 gene does not prevent choroidal neovascularization in a murine model. *Am J Pathol,* 153**,** 1641-6.

VECINO, E., RODRIGUEZ, F. D., RUZAFA, N., PEREIRO, X. & SHARMA, S. C. 2016. Glia-neuron interactions in the mammalian retina. *Prog Retin Eye Res,* 51**,** 1-40.

VED, N., HULSE, R. P., BESTALL, S. M., DONALDSON, L. F., BAINBRIDGE, J. W. & BATES, D. O. 2017. Vascular endothelial growth factor-A(165)b ameliorates outer-retinal barrier and vascular dysfunction in the diabetic retina. *Clin Sci (Lond),* 131**,** 1225-1243.

VELILLA, S., GARCIA-MEDINA, J. J., GARCIA-LAYANA, A., DOLZ-MARCO, R., PONS-VAZQUEZ, S., PINAZO-DURAN, M. D., GOMEZ-ULLA, F., AREVALO, J. F., DIAZ-LLOPIS, M. & GALLEGO-PINAZO, R. 2013. Smoking and age-related macular degeneration: review and update. *J Ophthalmol,* 2013**,** 895147.

VINGERLING, J. R., DIELEMANS, I., WITTEMAN, J. C., HOFMAN, A., GROBBEE, D. E. & DE JONG, P. T. 1995. Macular degeneration and early menopause: a case-control study. *BMJ,* 310**,** 1570-1.

WAGNER, N., REINEHR, S., PALMHOF, M., SCHUSCHEL, D., TSAI, T., SOMMER, E., FRANK, V., STUTE, G., DICK, H. B. & JOACHIM, S. C. 2021. Microglia Activation in Retinal Ischemia Triggers Cytokine and Toll-Like Receptor Response. *J Mol Neurosci,* 71**,** 527-544.

WANG, F., RENDAHL, K. G., MANNING, W. C., QUIROZ, D., COYNE, M. & MILLER, S. S. 2003. AAV-mediated expression of vascular endothelial growth factor induces choroidal neovascularization in rat. *Invest Ophthalmol Vis Sci,* 44**,** 781-90.

WANG, X., YU, C., LIU, X., YANG, J., FENG, Y., WU, Y., XU, Y., ZHU, Y. & LI, W. 2022. Fenofibrate Ameliorated Systemic and Retinal Inflammation and Modulated Gut Microbiota in High-Fat Diet-Induced Mice. *Front Cell Infect Microbiol,* 12**,** 839592.

WANG, Y. J., MONTEAGUDO, A., DOWNEY, M. A., ASHTON-RICKARDT, P. G. & ELMALEH, D. R. 2021. Cromolyn inhibits the secretion of inflammatory cytokines by human microglia (HMC3). *Sci Rep,* 11**,** 8054.

WEI, X., ZHANG, T., YAO, Y., ZENG, S., LI, M., XIANG, H., ZHAO, C., CAO, G., LI, M., WAN, R., YANG, P. & YANG, J. 2018. Efficacy of Lenvatinib, a multitargeted tyrosine kinase inhibitor, on laser-induced CNV mouse model of neovascular AMD. *Exp Eye Res,* 168**,** 2-11.

WENZEL, T. J., GATES, E. J., RANGER, A. L. & KLEGERIS, A. 2020. Short-chain fatty acids (SCFAs) alone or in combination regulate select immune functions of microglia-like cells. *Mol Cell Neurosci,* 105**,** 103493.

WONG, W. L., SU, X., LI, X., CHEUNG, C. M., KLEIN, R., CHENG, C. Y. & WONG, T. Y. 2014. Global prevalence of age-related macular degeneration and disease burden projection for 2020 and 2040: a systematic review and meta-analysis. *Lancet Glob Health,* 2**,** e106-16.

WU, J., CHEN, N., GRAU, E., JOHNSON, L., LIU, Y., LI, C., SCOTT, P. A., KIM, C., SUN, D., KAPLAN, H. J. & SHAO, H. 2024. Short chain fatty acids inhibit corneal inflammatory responses to TLR ligands via the ocular G-protein coupled receptor 43. *Ocul Surf,* 32**,** 48-57.

XIAO, X., CHEN, M., XU, Y., HUANG, S., LIANG, J., CAO, Y. & CHEN, H. 2020. Sodium Butyrate Inhibits Neovascularization Partially via TNXIP/VEGFR2 Pathway. *Oxid Med Cell Longev,* 2020**,** 6415671.

XU, C., LIU, G., LIU, X. & WANG, F. 2014. O-GlcNAcylation under hypoxic conditions and its effects on the blood-retinal barrier in diabetic retinopathy. *Int J Mol Med,* 33**,** 624-32.

XU, H., CHEN, M. & FORRESTER, J. V. 2009. Para-inflammation in the aging retina. *Prog Retin Eye Res,* 28**,** 348-68.

XU, M., JIANG, Z., WANG, C., LI, N., BO, L., ZHA, Y., BIAN, J., ZHANG, Y. & DENG, X. 2019. Acetate attenuates inflammasome activation through GPR43-mediated Ca(2+)-dependent NLRP3 ubiquitination. *Exp Mol Med,* 51**,** 1-13.

YANAGIDA, K., ENGELBRECHT, E., NIAUDET, C., JUNG, B., GAENGEL, K., HOLTON, K., SWENDEMAN, S., LIU, C. H., LEVESQUE, M. V., KUO, A., FU, Z., SMITH, L. E. H., BETSHOLTZ, C. & HLA, T. 2020. Sphingosine 1-Phosphate Receptor Signaling Establishes AP-1 Gradients to Allow for Retinal Endothelial Cell Specialization. *Dev Cell,* 52**,** 779-793 e7.

YOSHITOMI, Y., IKEDA, T., SAITO-TAKATSUJI, H. & YONEKURA, H. 2021. Emerging Role of AP-1 Transcription Factor JunB in Angiogenesis and Vascular Development. *Int J Mol Sci,* 22.

YOU, J. J., YANG, C. M., CHEN, M. S. & YANG, C. H. 2010. Regulation of Cyr61/CCN1 expression by hypoxia through cooperation of c-Jun/AP-1 and HIF-1alpha in retinal vascular endothelial cells. *Exp Eye Res,* 91**,** 825-36.

ZABEL, M. K., ZHAO, L., ZHANG, Y., GONZALEZ, S. R., MA, W., WANG, X., FARISS, R. N. & WONG, W. T. 2016. Microglial phagocytosis and activation underlying photoreceptor degeneration is regulated by CX3CL1-CX3CR1 signaling in a mouse model of retinitis pigmentosa. *Glia,* 64**,** 1479-91.

ZAMIRI, P., MASLI, S., STREILEIN, J. W. & TAYLOR, A. W. 2006. Pigment epithelial growth factor suppresses inflammation by modulating macrophage activation. *Invest Ophthalmol Vis Sci,* 47**,** 3912-8.

ZAMIRI, P., SUGITA, S. & STREILEIN, J. W. 2007. Immunosuppressive properties of the pigmented epithelial cells and the subretinal space. *Chem Immunol Allergy,* 92**,** 86-93.

ZHANG, H. & MO, Y. 2023. The gut-retina axis: a new perspective in the prevention and treatment of diabetic retinopathy. *Front Endocrinol (Lausanne),* 14**,** 1205846.

ZHANG, J. Y., XIAO, J., XIE, B., BARBA, H., BOACHIE-MENSAH, M., SHAH, R. N., NADEEM, U., SPEDALE, M., DYLLA, N., LIN, H., SIDEBOTTOM, A. M., D'SOUZA, M., THERIAULT, B., SULAKHE, D., CHANG, E. B. & SKONDRA, D. 2023. Oral Metformin Inhibits Choroidal Neovascularization by Modulating the Gut-Retina Axis. *Invest Ophthalmol Vis Sci,* 64**,** 21.

ZHANG, L., TAN, J., JIANG, X., QIAN, W., YANG, T., SUN, X., CHEN, Z. & ZHU, Q. 2017. Neuron-derived CCL2 contributes to microglia activation and neurological decline in hepatic encephalopathy. *Biol Res,* 50**,** 26.

ZHAO, L., FENG, Z., ZOU, X., CAO, K., XU, J. & LIU, J. 2014. Aging leads to elevation of O-GlcNAcylation and disruption of mitochondrial homeostasis in retina. *Oxid Med Cell Longev,* 2014**,** 425705.

ZHAO, L., ZABEL, M. K., WANG, X., MA, W., SHAH, P., FARISS, R. N., QIAN, H., PARKHURST, C. N., GAN, W. B. & WONG, W. T. 2015. Microglial phagocytosis of living photoreceptors contributes to inherited retinal degeneration. *EMBO Mol Med,* 7**,** 1179-97.

ZHAO, M., REN, K., XIONG, X., CHENG, M., ZHANG, Z., HUANG, Z., HAN, X., YANG, X., ALEJANDRO, E. U. & RUAN, H. B. 2020. Protein O-GlcNAc Modification Links Dietary and Gut Microbial Cues to the Differentiation of Enteroendocrine L Cells. *Cell Rep,* 32**,** 108013.

ZHOU, P., CHANG, W. Y., GONG, D. A., XIA, J., CHEN, W., HUANG, L. Y., LIU, R., LIU, Y., CHEN, C., WANG, K., TANG, N. & HUANG, A. L. 2023. High dietary fructose promotes hepatocellular carcinoma progression by enhancing O-GlcNAcylation via microbiota-derived acetate. *Cell Metab,* 35**,** 1961-1975 e6.

ZIPFEL, P. F., LAUER, N. & SKERKA, C. 2010. The role of complement in AMD. *Adv Exp Med Biol,* 703**,** 9-24.

ZIPFEL, P. F. & SKERKA, C. 2009. Complement regulators and inhibitory proteins. *Nat Rev Immunol,* 9**,** 729-40.

ZLOTNIK, A. & YOSHIE, O. 2000. Chemokines: a new classification system and their role in immunity. *Immunity,* 12**,** 121-7.

Statutory Declaration

“I, Chufan Yan, by personally signing this document in lieu of an oath, hereby affirm that I prepared the submitted dissertation on the topic [SCFA has a preventative effect in a mouse model with relevance for age-related macular degeneration; Untersuchung zur präventiven Wirkung von SCFA in einem Mausmo-dell für altersbedingte Makuladegeneration.], independently and without the support of third parties, and that I used no other sources and aids than those stated.

All parts which are based on the publications or presentations of other authors, either in letter or in spirit, are specified as such in accordance with the citing guidelines. The sections on methodology (in particular regarding practical work, laboratory regulations, statistical processing) and results (in particular regarding figures, charts and tables) are exclusively my responsibility.

Furthermore, I declare that I have correctly marked all of the data, the analyses, and the conclusions generated from data obtained in collaboration with other persons, and that I have correctly marked my own contribution and the contributions of other persons (cf. declaration of contribution). I have correctly marked all texts or parts of texts that were generated in collaboration with other persons.

My contributions to any publications to this dissertation correspond to those stated in the below joint declaration made together with the supervisor. All publications created within the scope of the dissertation comply with the guidelines of the ICMJE (International Committee of Medical Journal Editors; www.icmje.org) on authorship. In addition, I declare that I shall comply with the regulations of Charité – Universitätsmedizin Berlin on ensuring good scientific practice.

I declare that I have not yet submitted this dissertation in identical or similar form to another Faculty.

The significance of this statutory declaration and the consequences of a false statutory declaration under criminal law (Sections 156, 161 of the German Criminal Code) are known to me.”

27. June. 2024

Date Signature

Curriculum vitae

My CV will not be published in the electronic version of my work for data protection reasons.

Acknowledgement

Time flies, and it feels like I've only just begun my PhD journey not too long ago. Yet, in the blink of an eye, nearly four years have passed, and I finally reach the stage of submitting my thesis. These four years have been unforgettable and profoundly meaningful to me. Challenging as it was, it has also been a period of immense personal growth for me. I am immensely grateful to everyone who has provided me with guidance, assistance, and encouragement throughout this journey.

I would like to express my sincere gratitude to Dr. Susanne Wolf, my supervisor, for giving me the opportunity to work in her lab, learn many interesting new skills and expand my research horizons. Her guidance, support, and encouragement throughout this research journey really means a lot to me.

I would like to thank Professor Antonia Joussen for giving me the opportunity to pursue my PhD in the first place and allow me to work in her lab. I would like to thank Professor Olaf Strauβ, whose professionalism and meticulousness dramatically improved my thesis and taught me many writing skills.

I am also deeply thankful to Dr. Inga-Marie Pompös and Paula Arribas-Lange, who conducted the in vivo part of the project, to Dr. Sergej Skosysrki who helped with the laser induction, and Regina Piske, who prepared the isolated microglial cells for me. I would like to thank Dr. Bilge Ugursu, Dr. Marcus Semtner and Dr. Caio Andreeta Figueiredo, who taught me a lot and always could solve my problems. I learned so much from them. I would like to thank Edyta Motta and Yuxuan Jiang, who were always there to comfort and encourage me. I want to express my gratitude to all the members in Wolf lab in MDC and in ophthalmology lab in CVK, for your company and support.

Furthermore, I would like to express my gratitude to my friends, Xuqing Feng, Yue Li and Wenchun Yang. Even miles apart, across time zones, you were always there to company me through the tough times, comforting me and listening to me, I can always share my feelings with you at any moments. I want to thank Fang Yang and my flat mate Bin Zeng, we came here on the same day during pandemic, it is so great to have you during the entire doctoral journey.

In the end, I would like to thank the most important person in my life, my mother and my father, for their unwavering love, understanding and encouragement during all these

years. I can share every detail in my life with them without even thinking, because I know that they are always there and can always hold my back. They tolerate all my instabilities and emotions with endless love. I truly wish that they can be healthy and happy forever.

I am eternally grateful to each and every of you.

Chufan